Title
The Development of Semiconducting Materials for Organic Photovoltaics

Author
Douglas, Jessica D.

Publication Date
2013

Peer reviewed|Thesis/dissertation

The Development of Semiconducting Materials for Organic Photovoltaics

By

Jessica Dakotah Douglas

A dissertation submitted in partial satisfaction of the

requirements for the degree of

Doctor of Philosophy

in

Chemistry

in the

Graduate Division

of the

University of California, Berkeley

Committee in Charge:
Professor Jean M. J. Fréchet (Chair)
Professor K. Peter C. Vollhardt
Professor Ali Javey

Spring 2013

The Development of Semiconducting Materials for Organic Photovoltaics

By

Jessica Dakotah Douglas

Abstract

The Development of Semiconducting Materials for Organic Photovoltaics

By

Jessica Dakotah Douglas

Doctor of Philosophy in Chemistry

University of California, Berkeley

Professor Jean M. J. Fréchet (Chair)

The chemical structure of conjugated semiconducting materials strongly influences the performance of organic photovoltaic (OPV) devices. Thus a good understanding of the structure-function relationships that govern the optoelectronic and physical properties of OPV materials is necessary. In this dissertation, organic polymers and small molecules are evaluated in terms of OPV device output parameters, and molecular design rules are elucidated.

The development of molecules with alternating electron-rich and electron-deficient backbone units provides materials with suitable optoelectronic properties for OPVs and favorable modularity for organic semiconductor design. The choice of specific aromatic units and side chains for conjugated materials are shown to modulate the energy levels and architecture of OPV devices, affecting each of the four mechanistic steps of OPV operation.

In Chapter 2, the relationship between molecular packing parameters and the bulkiness of aliphatic solubilizing group extending away from a polymer backbone is elucidated, and high-performance OPV devices are achieved. In Chapter 3, the inclusion of a post-processing functionality on a polymer side chain is found to have a positive effect on the bulk morphology and overall performance of OPV devices. In Chapter 4, the influence of electron-withdrawing and quinoidal monomers on the optoelectronic properties of conjugated polymers is established, and energy level modulation is shown to affect the electron accepting and donating capabilities of OPV materials in a blended device. In Chapter 5, small molecules are designed with complementary light absorption properties in order to investigate a rarely observed charge generation mechanism.

Table of Contents

Acknowledgements

My four years at Berkeley have been filled with fun, learning, and personal growth. I sincerely cherish the time that I have had in Berkeley and the people that I have met on my journey. I will hold onto all of the good times and the bad, and fondly remember my graduate school experience.

I gratefully acknowledge Professor Fréchet for providing me the opportunity to work in his lab and for his continuing guidance. Professor Fréchet built and maintained an exciting and supportive research lab that helped me to become a scientist, and I am honored to have been a part of his group.

The members of the Fréchet group have been a second family for me, and I appreciate all of the help that I have received from my lab mates over the years. I would especially like to thank my mentor Tom Holcombe for being patient with me as I learned how to work in lab. Tom was always good for a laugh and he helped me build a solid foundation for my graduate career. I would also like to thank Olivia Lee for all of the advice, support, and snacks that she has provided me. Graduate school would have been unbearable without Olivia and I am so lucky that we got to share our Berkeley chemistry experience together. I would also like to acknowledge the rest of the organic electronics team within the Fréchet group: Pierre Beaujuge, Mark Chen, Gianmarco Griffini, Jeremy Niskala, Claudia Piliego, David Unruh, Claire Woo, Alan Yiu, and Eric Young. Together we accomplished much more than we would have individually. I could not have asked for a better or more capable group of people to work with. Thank you! Of course, I also thank Paul Kierstead for filling-in Olivia and me on lab gossip, and Chona and Cezar for taking care of all messy, behind-the-scenes work of running the lab.

I thankfully acknowledge my collaborators from Stanford, UC Santa Barbara, and KAUST. The expertise gained from talking and working with members of the Beaujuge, Chabinyc, McGehee, Sellinger, and Salleo groups greatly helped me with my research.

Beyond lab, teaching, and classes, I have made some outstanding friends that share my love of running, eating, and relaxing. Rebecca Murphy and Tiffany Pham have been unstoppable workout partners and I am going to really miss running and chatting with them daily. Our afternoon runs were a constant in our evolving graduate school experience, and I feel as though we helped each other grow and survive the rough days by releasing our energy running. I am also grateful for the friendships that I have made with Jane Wang, Katherine Mackenzie, Colleen Kellenberger, and Chandra Richards. Each of these girls has a fun-loving attitude and we shared a lot of great times.

Finally, I am thankful for the opportunity that I had at Berkeley to spend more time with my family in Los Gatos. My mom, Brad, and Ken have gone out of their way to spend as much time as possible as a family, and I am going to dearly miss seeing them nearly every week. I wish that I had more time in California so that we could play a few more games of pinochle and dominoes. Hopefully we will all be in the Bay Area again one day. You three are so special to me and I am going to really miss you! I also thank Matt for coming into my life and bringing me unbelievable amounts of happiness. This last year has been amazing, and I look forward to many more.

Everyone that I have worked or played with has had an impact on me during my time at Berkeley, and I thank you all for sharing your life with me. Thank you!

Chapter 1. Overview of Organic Photovoltaics

Motivation and Current Technology

Recent increases in global energy consumption and concerns about our environmental impact have motivated research efforts toward the development of clean and renewable energy. Solar power is a particularly promising technology with the potential to satisfy the world's energy needs from just a fraction of the daily incident sunlight. Existing commercial technologies utilize polycrystalline silicon, which can obtain power conversion efficiencies (PCEs) between 20-25%.[1] Although silicon-based solar cells have relatively high PCEs, organic photovoltaics (OPVs) are an emerging technology that have the potential to be inexpensive, lightweight, flexible, and solution processable (Figure 1.1).[2–4] With further research into the operation of OPVs and the development on new materials, these organic-based excitonic solar cells stand to compete with conventional silicon-based devices as a source of renewable energy.

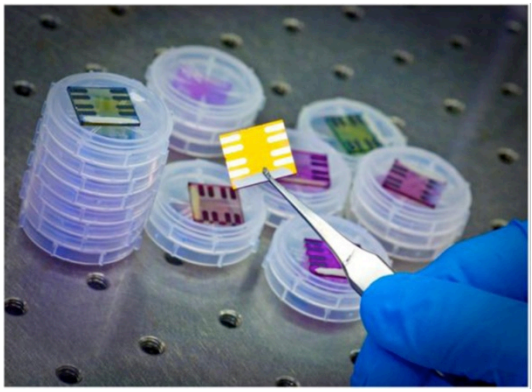

Figure 1.1. Organic photovoltaic devices.

The performance of organic photovoltaics has rapidly increased since the introduction of a two-component active layer device in 1986.[5] Current high performing OPVs are similar to the seminal device in that their active layer contains an electron-donating p-type material and an electron-accepting n-type material; however, high efficiency OPVs are now frequently based on a bulk heterojunction (BHJ)[6,7] blend of the p- and n-type materials instead of a bilayer morphology. When work on this dissertation began in 2009, homopolymer poly(3-hexylthiophene) (P3HT) was the benchmark p-type material, and fullerene derivatives such as [6,6]-phenyl-C_{61}-butyric acid methyl ester ($PC_{61}BM$) were the ubiquitous n-type material (Figure 1.2). Although P3HT:$PC_{61}BM$ blend devices achieved efficiencies of 4-5%,[8–10] the development of a new class of p-type polymers (donor-acceptor copolymers)[11–13] let to the reporting of devices with 6.1% PCE in early 2009.[14,15] OPVs based on donor-acceptor copolymers have now reached efficiencies of 8%,[16–20] and devices that contain p-type small molecules that mimic the donor-acceptor approach have recorded efficiencies as high as 7.0%.[21] Although recent advances have greatly improved upon the 0.95% PCE reported in 1986,[5] more research into the structure-property relationship of OPV materials is needed. This dissertation focuses on the development, synthesis, and performance of new electroactive p- and n-type polymers and small molecules with specific properties that affect OPV light absorption, charge generation, blend morphology, and device lifetime.

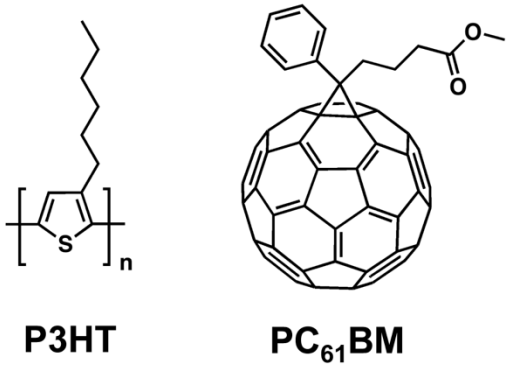

Figure 1.2. The chemical structures of poly(3-hexylthiophene) (P3HT) and [6,6]-phenyl-C_{61}-butyric acid methyl ester ($PC_{61}BM$).

Organic Photovoltaic Device Operation and Structure

Solar cells operate by absorbing light (in the form of photons) and converting the harvested energy into an electrical current (consisting of charge carriers). Despite their identical application, conventional inorganic silicon solar cells and organic photovoltaics use fundamentally different mechanisms for charge generation and free charge carrier formation. In silicon devices, free charge carriers are formed upon photoexcitation, and the individual holes and electrons are pulled apart toward separate electrodes as a result of the internal electric field generated by a p-n junction. The processes of charge generation and charge separation occur sequentially in inorganic devices and can happen throughout the bulk active layer.[22] Conversely, in organic-based excitonic devices, hole and electron generation occurs simultaneously with charge separation, and is limited to a heterointerface.[22,23] In organic photovoltaics, light absorption does not spontaneously create free charge carries, but instead produces a Coulomb-bound electron-hole pair (or exciton), which must migrate to a p-n interface to generate free charges across the heterojunction.

Organic solar cells operate through this excitonic mechanism because they cannot spontaneously generate free charge carriers upon photoexcitation, like inorganic-based photovoltaics, and instead form bound excitons.[22,23] The strong Coulomb attraction of excitons prevents spontaneous charge generation in OPVs and is a result of 1) conjugated organic materials having weak intermolecular forces that localize charge carriers,[24] and 2) carbon-based molecules having valence electrons that are tightly bound to the nucleus, giving them low dielectric constants ($\varepsilon \approx 2\text{-}4$).[25] To effectively dissociate an exciton into free charge carriers, a thermodynamic driving force within the OPV that is greater than the exciton binding energy must exist. In the case of a heterojunction device, the energy level offset between two dissimilar active layer materials can provide a sufficient driving force for exciton dissociation, provided the exciton reaches an interface.[26] This mechanism of charge generation requires that OPVs contain more than one active layer component and have numerous interfacial junctions. Current OPVs achieve these requirements by combining two photoactive materials into a bulk heterojunction blend, which is sandwiched between a transparent top electrode and a metal bottom contact that is typically composed of indium-tin oxide (ITO) and aluminum (Al), respectively (Figure 1.3).

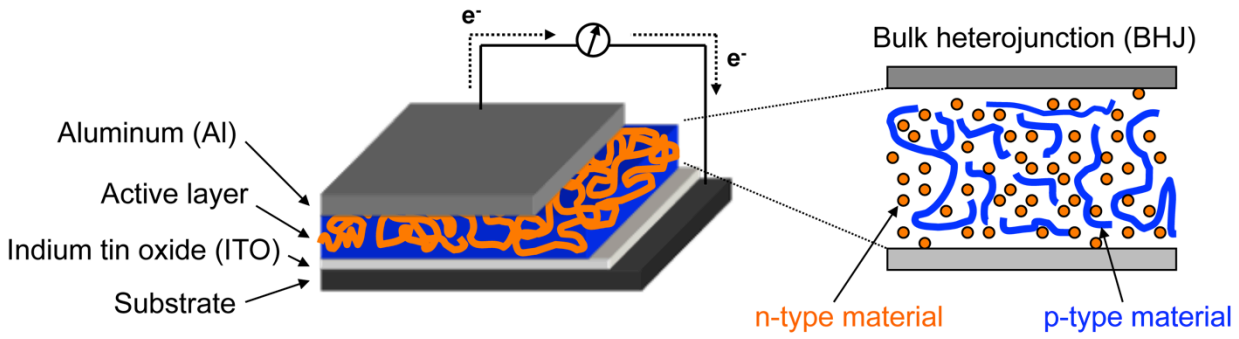

Figure 1.3. Organic photovoltaics have a layered structure where the BHJ active layer is sandwiched between the device electrodes.

The full photo energy conversion process in excitonic, organic solar cells occurs within the active layer and can be described in four steps: 1) light absorption, 2) exciton diffusion, 3) exciton dissociation/charge separation, and 4) charge transport/charge extraction (Figure 1.4). In the first step, photon absorption by the active layer causes excitation of an electron from the

highest occupied molecular orbital (HOMO) to the lowest unoccupied molecular orbital (LUMO) level, forming a bound exciton (Figure 1.4a). This process can occur within either of the semiconducting blend components, but the p-type material is commonly the principle absorber in OPVs because fullerene-based n-type materials often have lower extinction coefficients than conjugated polymers.[27] For simplicity, the process of energy conversion will be described here assuming that excitons are predominately formed within the p-type material. Chapter 5 of this dissertation will describe the less common but analogous process that begins with light absorption by the n-type material.

In the second step of the OPV energy conversion process, photogenerated excitons diffuse within the active layer and must reach a heterointerface to successfully dissociate into free charges (Figure 1.4b). Since organic materials have localized excited states, bound excitons have a short diffusion length (10-20 nm) and a short lifetime (nanoseconds).[28] Effective exciton dissociation requires nanometer scale phase separation and a large amount of interfacial surface area within the device active layer, which is currently best achieved with an interconnected and interpenetrating bulk heterojunction morphology.

Once an exciton successfully reaches a heterojunction, dissociation via electron transfer from the LUMO of the p-type material to the LUMO of the n-type material converts the neutral exciton into free charge carriers, resulting in the localization of the hole on the p-type material and the electron on the n-type material (Figure 1.4c). This charge separation requires the driving force for electron transfer to be energetically more favorable than exciton binding, and it is thought that a LUMO-LUMO offset of 0.3 eV between the p- and n-type materials is sufficient for exciton dissociation.[29] Although charge generation at a BHJ interface is generally assumed to occur in one step, an intermediate charge transfer state (CT state) has been documented in some OPV blends and can be described as a Coulomb-bound charge separated state, or an electron-hole pair.[30,31] The consequence of creating CT state species within an OPV is the topic of some current research,[32,33] but is beyond the scope of this dissertation. For the purpose of this thesis, we will consider exciton dissociation into free charge carriers as a process that occurs directly.

In the final step of the OPV charge generation mechanism, holes and electrons at the BHJ interface must travel to the device electrodes to enable current extraction (Figure 1.4d). The free charge carriers migrate in opposite directions from the heterointerface, with holes moving through the semiconducting p-type phase toward the cathode (usually ITO), and electrons moving through the n-type phase toward the anode (usually Al). This transport within each active layer material proceeds via charge hopping between localized states (intermolecular

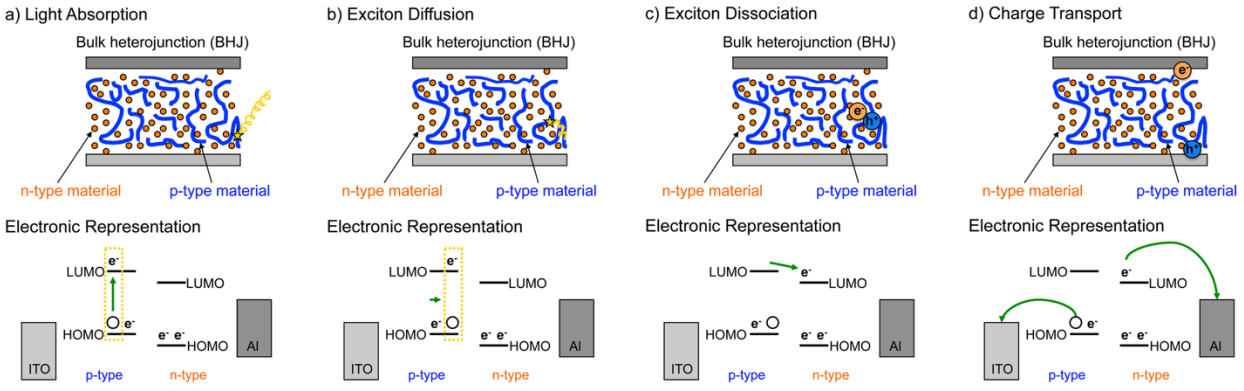

Figure 1.4. The four-step photo energy conversion process in OPVs includes a) light absorption, b) exciton diffusion, c) exciton diffusion, and d) charge transport.

transport) or from band-like conduction through conjugated regions (eg. intramolecular movement along a polymer backbone).[34] The local concentration gradient of charges at the interface and the internal electric field that is generated from the energy level difference between the p- and n-type materials both help to pull free charges toward the device electrodes.[35] While these driving forces direct holes and electrons away from material junctions, the mobility of the active layer components strongly affects the overall charge transport in devices. Parameters such as intrinsic mobility, crystallinity, packing direction relative to the substrate, blend morphology, and impurity concentration contribute to the overall mobility of a material in an OPV blend, and thus affect the charge transport within a device.[36]

Characterization of Organic Photovoltaic Device Efficiency

The efficiency at which an OPV generates photocurrent depends on the wavelength and intensity of device illumination. Standard testing conditions replicate the solar spectrum within the continental United States, which is defined as the solar flux that hits the Earth at an incident angle of 48.2° and a tilt angle of 37° from horizontal (Figure 1.5).[37,38] These standard conditions are set to have an overall intensity of 100 mW/cm^2 and can be described as the air mass 1.5 global (AM 1.5 G) spectrum.

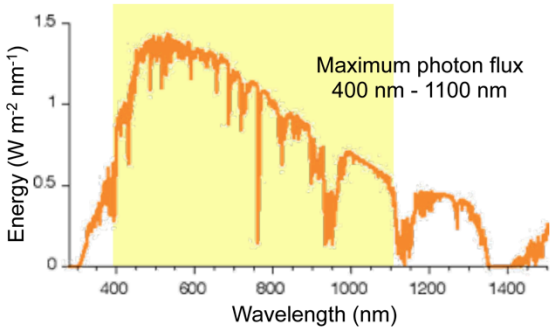

Figure 1.5. The AM 1.5 G spectrum simulates solar irradiation and is used for OPVtesting.

The output characteristics of an illuminated OPV are evaluated with a current-voltage (*J-V*) plot, and a few key performance parameters can be identified from an experimental *J-V* curve (Figure 1.6). In particular, the short-circuit current density (J_{sc}) describes the current generated from a device without an applied external bias (V = 0 V), and the open-circuit voltage (V_{oc}) represents the applied voltage that is required to balance the internal field and stop charge carrier drift (J = 0 mA/cm^2). The fill factor (*FF*) is an ideality value that accounts for loss mechanisms such as recombination within a device and is described as the ratio of the max power point (P_{max}) on the *J-V* curve to the absolute power point ($P_{abs} = J_{sc}$ x V_{oc}). The overall device efficiency (η) is a function of the power output from the OPV (P_{out}) at a known incident illumination intensity (P_{in}), and is described by the equation below.[39]

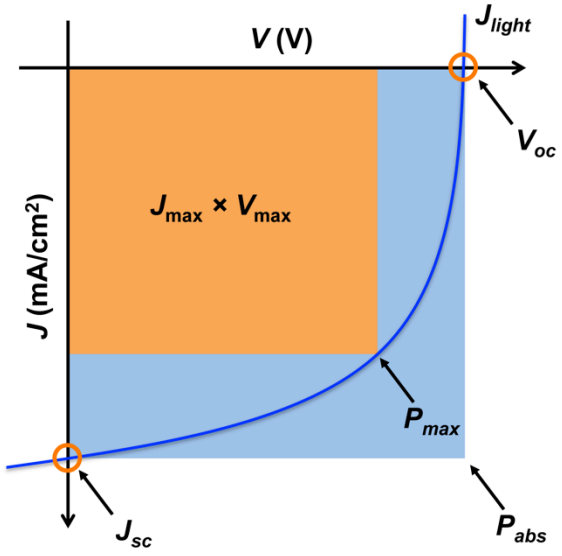

Figure 1.6. A typical *J-V* curve for a solar cell device under illumination (J_{light}). The open-circuit voltage (V_{oc}), short-circuit current density (J_{sc}), max power point (P_{max}), and the absolute power point (P_{abs}) are labeled.

$$\eta = \frac{P_{\text{out}}}{P_{\text{in}}} = \frac{P_{\text{max}}}{P_{\text{in}}} = \frac{J_{\text{sc}} \times V_{\text{oc}} \times FF}{P_{\text{in}}} \text{ where } FF = \frac{P_{\text{max}}}{P_{\text{abs}}} = \frac{P_{\text{max}}}{J_{\text{sc}} \times V_{\text{oc}}}$$

Conjugated Material Design

Organic photovoltaic semiconductors are designed to facilitate the four-step photo energy conversion process, and the development of new electroactive materials is the focus of this dissertation. Consideration of the molecular structure of OPV materials is critical because the chemical properties of conjugated polymers and small molecules influence the optoelectronics and the morphology of the active layer. In particular, the band gap and the energy level offset between the p- and n-type materials can be optimized though molecular design to improve light absorption and charge separation, respectively. Physical characteristics of the active layer components such as solvent solubility, microstructural order, and miscibility can also be synthetically modulated and are significant parameters that affect the BHJ morphology, exciton diffusion, and charge transport. There are still many design principles that are yet to be discovered in our effort to fully control the optoelectronic and morphological properties of OPVs. As a foundation for the work in this dissertation, some established structure-property relationships are described herein.

A discussion of molecular orbital theory is necessary to understand how the optoelectronic properties of organic semiconductors are modulated. When two small molecules covalently bond, new bonding and anti-bonding orbitals are formed from hybridization of the individual molecular orbitals. For conjugated molecules, this means that the π electrons from each original molecule become delocalized over the new conjugated system, and the HOMO and LUMO of the dimer move closer in energy. Through the sequential addition of aromatic and conjugated small molecule units, OPV materials experience a decrease in their HOMO-LUMO energy gap until the conjugation length is reached (Figure 1.7). In most polymers, a conjugation length of about 10 repeat units is observed.[40] The hybridization limit imposed by the conjugation length means that organic molecules cannot obtain a metallic band-like structure, and instead have a energy gap (or band gap) between their HOMO and LUMO. This band gap determines

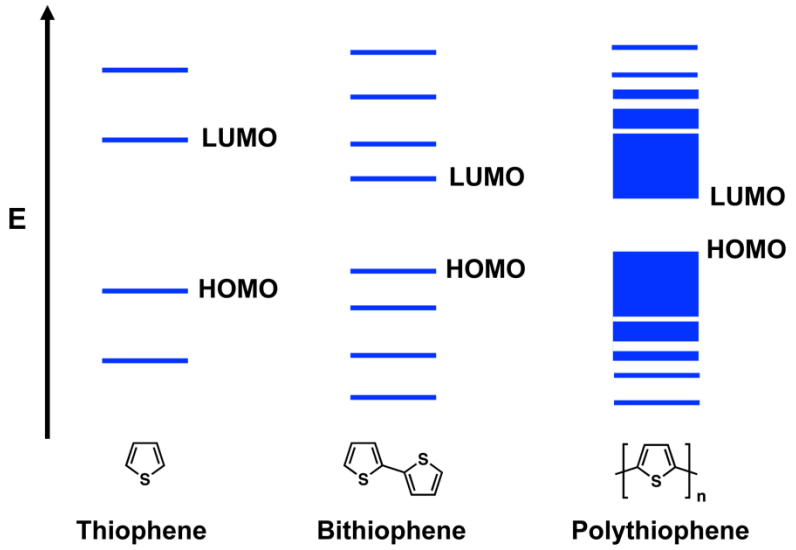

Figure 1.7. Extending molecular conjugation through covalent bonding causes hybridization of the molecular energy levels and a reduction in the HOMO-LUMO energy gap (band gap) until the polymer reaches its conjugation length.

the absorption properties of a semiconducting molecule and mandates that a photon must have enough energy to photoexcite an electron from the material HOMO to the LUMO in order to be successfully absorbed. Although the band gap is an energetic material property, the physical environment and conformation of a molecule can affect its energy levels. In fact, the onset of absorption of OPV materials in solution commonly "red-shifts" (moves to higher wavelengths, or lower energies) upon thin film formation due to increased intermolecular interactions.

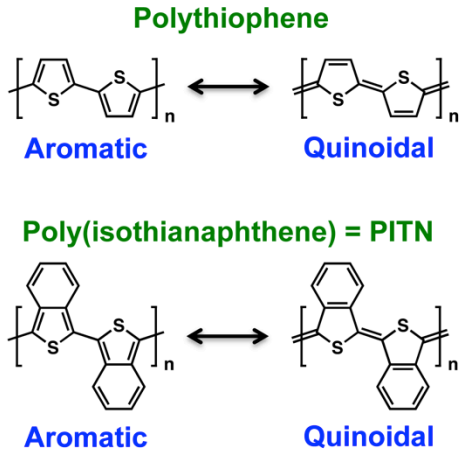

Figure 1.8. The aromatic and quinoidal resonance structures of polythiophene and poly(isothianaphthene) (PITN). Polythiophene favors its aromatic form because thiophene is aromatized, but PITN has been designed to favor its quinoidal form, which has the phenyl ring aromatized.

Toward engineering polymers and small molecules with low band gaps capable of absorbing in the near IR, two methods to decrease bond length alternation and improve electron delocalization are commonly invoked. The first approach involves alternating electron-rich and electron-deficient units along the molecular backbone in the so-called donor-acceptor (D-A) approach. This design strategy works though a "push-pull" mechanism where π electrons on the electron-rich donor monomers are drawn toward the neighboring electron-deficient monomers, thereby increasing electron delocalization and inducing the formation of quinoid mesomeric structures (D−A → D^{+}=A^{-}).[41] The second method for decreasing bond length alternation is similar to the mesomeric effect of the D-A approach and works by creating competing resonance structures that have a significant influence on the overall molecular backbone. With this so-called quinoidal effect, aromatic building blocks are designed to have substantial quinoidal character, rather than just aromatic character, thereby creating two molecular resonance structures and increasing the overall electron delocalization along a conjugated material (Figure 1.8).[42]

The decrease in material band gap induced by the D-A approach or the quinoidal effect can be rationalized with molecular orbital theory. In the case of D-A hybridized materials, electron-rich substituents raise the energy levels of the donor unit while electron-deficient functionalities lower the energy levels of the acceptor unit. This slight energy level mismatch between the donor and acceptor building blocks causes the molecular LUMO to resemble the acceptor, which has a low LUMO, and the molecular HOMO to resemble the donor, which had a raised HOMO (Figure 1.9a). The quinoidal effect decreases the molecular band gap of standard aromatic materials by destabilizing the material energy levels, since organic molecules with significant quinoidal character inherently have less aromatic character and resultantly less aromatic stabilization energy (Figure 1.9b).

In addition to modulating the band gap of semiconducting materials, the D-A approach and the quinoidal effect can be used to tune molecular energy levels and optimize the offset between the p- and n-type materials in an OPV. As mentioned previously, the LUMO-LUMO energy gap between the active layer components drives exciton dissociation. Thus p- and n-type materials should be designed to have a 0.3 eV offset. A larger energy level difference between the LUMOs does not improve charge separation and wastes potential photovoltage.[43] The offset between the p-type HOMO and the n-type LUMO also requires engineering since it dictates the internal electric field of the device and is related to the V_{oc}.[44] A large HOMO-LUMO difference

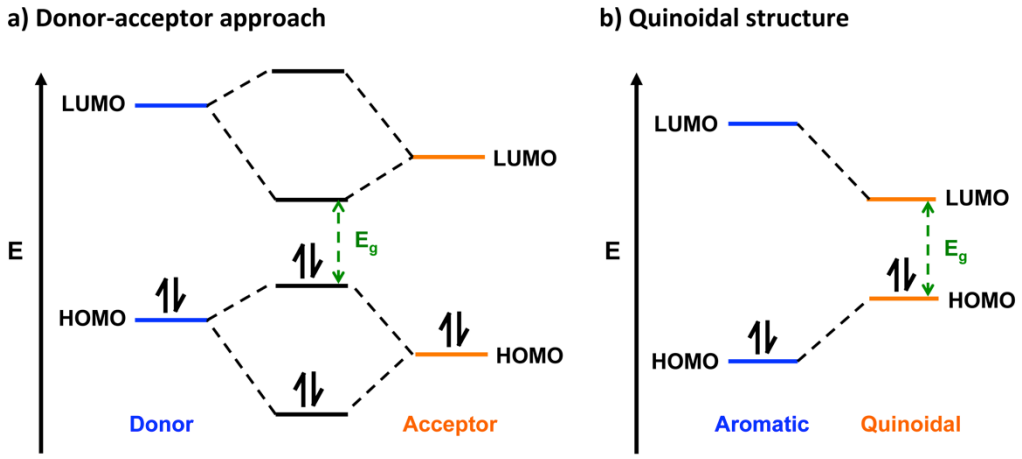

Figure 1.9. a) The electron donating and withdrawing properties of donor and acceptor building blocks decrease the molecular band gap through the donor-acceptor hybridization approach. b) The incorporation of significant quinoidal character into a molecular backbone energetically destabilizes a material and reduces its band gap relative to standard aromatic materials.

allows for high photovoltage output and potentially improved device efficiency. These energy level considerations, in combination with band gap modulation, and are significant optoelectronic parameters that affect OPV operation and performance and require careful molecular design.

Beyond optoelectronic properties, the solid-state structure of OPV active layers also affects device efficiency. In particular, the OPV processes of exciton diffusion, exciton dissociation, and charge transport are sensitive to the blend morphology on length scales that extend from individual crystallites to the bulk active layer. One parameter that specifically influences charge transport and can be modified through synthetic design is charge carrier mobility. The movement of holes and electrons along an active layer material requires molecular interconnectivity and is strongly affected by the crystallinity of material domains.[45] Toward improving interconnectivity between ordered material phases, OPVs are often fabricated with long-chain, high molecular weight (M_n) polymers,[46] or carefully designed small molecules that have specific self-assembly properties.[47] The microstructural order and orientation of the active layer materials also affect the charge carrier mobility, where "face-on" molecular packing with the substrate is advantageous for charge transport.[48] Polymers designed to have a kinked or wavy backbone structure are thought to promote this "face-on" packing orientation, while more linear polymers such as P3HT pack "edge-on" with the OPV substrate.[49]

From a macrostructural perspective, the bulk heterojunction architecture of a device influences charge carrier transport, exciton diffusion, and exciton dissociation. The development of semiconducting materials should therefore consider p- and n-type domain size and the interconnected and interpenetrating nature of BHJs. Although device fabrication conditions are often the strongest influencer of overall BHJ morphology,[45] molecular parameters such as solvent solubility and material miscibility can be synthetically tuned to optimize OPV performance. Conjugated materials should be designed to self-assemble into domains that are compatible with an exciton diffusion length of 4-20 nm.[50] Recently, a material design principle was implemented to prevent long-term thermal phase segregation of the metastable BHJ, thereby preserving favorable domain lengths within the active layer over an extended period of time.[51] The chemical structure of an OPV material should also be optimized to ensure that the active

layer has sufficient interfacial junctions and interconnectivity to promote charge separation and diffusion, respectively. For example, if BHJ domains are not fully interconnected, morphological traps (islands) can limit charge transport and increase bimolecular recombination.[52]

In this dissertation, new structure-function relationships for OPV materials are developed and applied to the four steps of the OPV photoenergy conversion process. In Chapter 2, thienopyrroledione-based polymers are synthesized and the influence of alkyl side chains on molecular packing, charge carrier transport, and device performance is explored. In Chapter 3, the effect of long-term thermal annealing on the BHJ morphology is investigated in terms of domain size, exciton dissociation, and device performance. In Chapter 4, the quinoidal character and electron-withdrawing strength of polymeric monomers is evaluated in order to further understand the relationship between material design and OPV light absorbing properties. In Chapter 5, photoactive n-type small molecules are developed and free charge carrier generation is studied.

References

(1) Green, M. A.; Emery, K.; Hishikawa, Y.; Warta, W.; Dunlop, E. D. *Prog. Photovolt: Res. Appl.* **2012**, *20*, 12–20.
(2) Brabec, C. J.; Sariciftci, N. S.; Hummelen, J. C. *Adv. Funct. Mater.* **2001**, *11*, 15–26.
(3) Thompson, B. C.; Fréchet, J. M. J. *Angew. Chem. Int. Ed.* **2008**, *47*, 58–77.
(4) Brabec, C. J.; Gowrisanker, S.; Halls, J. J. M.; Laird, D.; Jia, S.; Williams, S. P. *Adv. Mater.* **2010**, *22*, 3839–3856.
(5) Tang, C. W. *Appl. Phys. Lett.* **1986**, *48*, 183–185.
(6) Yu, G.; Gao, J.; Hummelen, J. C.; Wudl, F.; Heeger, A. J. *Science* **1995**, *270*, 1789–1791.
(7) Yu, G.; Heeger, A. J. *J. Appl. Phys.* **1995**, *78*, 4510–4515.
(8) Li, G.; Shrotriya, V.; Huang, J.; Yao, Y.; Moriarty, T.; Emery, K.; Yang, Y. *Nat. Mater.* **2005**, *4*, 864–868.
(9) Ma, W.; Yang, C.; Gong, X.; Lee, K.; Heeger, A. J. *Adv. Funct. Mater.* **2005**, *15*, 1617–1622.
(10) Kim, Y.; Cook, S.; Tuladhar, S. M.; Choulis, S. a.; Nelson, J.; Durrant, J. R.; Bradley, D. D. C.; Giles, M.; McCulloch, I.; Ha, C.-S.; Ree, M. *Nat. Mater.* **2006**, *5*, 197–203.
(11) Havinga, E. E.; ten Hoeve, W.; Wynberg, H. *Polym. Bull.* **1992**, *126*, 119–126.
(12) Havinga, E. E.; ten Hoeve, W.; Wynberg, H. *Synt. Met.* **1993**, *57*, 299–306.
(13) Mühlbacher, D.; Scharber, M.; Morana, M.; Zhu, Z.; Waller, D.; Gaudiana, R.; Brabec, C. *Adv. Mater.* **2006**, *18*, 2884–2889.
(14) Park, S. H.; Roy, A.; Beaupré, S.; Cho, S.; Coates, N.; Moon, J. S.; Moses, D.; Leclerc, M.; Lee, K.; Heeger, A. J. *Nat. Photon.* **2009**, *3*, 297–303.
(15) Liang, Y.; Feng, D.; Wu, Y.; Tsai, S.-T.; Li, G.; Ray, C.; Yu, L. *J. Am. Chem. Soc.* **2009**, *131*, 7792–7799.
(16) He, Z.; Zhong, C.; Huang, X.; Wong, W.-Y.; Wu, H.; Chen, L.; Su, S.; Cao, Y. *Adv. Mater.* **2011**, *23*, 4636–4643.
(17) Small, C. E.; Chen, S.; Subbiah, J.; Amb, C. M.; Tsang, S.-W.; Lai, T.-H.; Reynolds, J. R.; So, F. *Nat. Photon.* **2012**, *6*, 115–120.
(18) He, Z.; Zhong, C.; Su, S.; Xu, M.; Wu, H.; Cao, Y. *Nat. Photon.* **2012**, *6*, 591–595.
(19) Lu, L.; Luo, Z.; Xu, T.; Yu, L. *Nano Lett.* **2013**, *13*, 59–64.
(20) Cabanetos, C.; El Labban, A.; Bartelt, J. A.; Douglas, J. D.; Mateker, W. R.; Fréchet, J. M. J.; McGehee, M. D.; Beaujuge, P. M. *J. Am. Chem. Soc.* **2013**, *135*, 4656–4659.
(21) Van der Poll, T. S.; Love, J. A.; Nguyen, T.-Q.; Bazan, G. C. *Adv. Mater.* **2012**, *24*, 3646–3649.
(22) Gregg, B. A. *J. Phys. Chem. B* **2003**, *107*, 4688–4698.
(23) Gregg, B. A.; Hanna, M. C. *J. Appl. Phys.* **2003**, *93*, 3605–3714.
(24) Blom, P. W. M.; Mihailetchi, V. D.; Koster, L. J. A.; Markov, D. E. *Adv. Mater.* **2007**, *19*, 1551–1566.
(25) Hains, A. W.; Liang, Z.; Woodhouse, M. A.; Gregg, B. A. *Chem. Rev.* **2010**, *110*, 6689–6735.
(26) Clarke, T. M.; Durrant, J. R. *Chem. Rev.* **2010**, *110*, 6736–6767.
(27) Hesse, H. C.; Weickert, J.; Hundschell, C.; Feng, X.; Müllen, K.; Nickel, B.; Mozer, A. J.; Schmidt-Mende, L. *Adv. Energy Mater.* **2011**, *1*, 861–869.
(28) Hoppe, H.; Sariciftci, N. S. *J. Mater. Chem.* **2006**, *16*, 45–61.

(29) Scharber, M. C.; Mühlbacher, D.; Koppe, M.; Denk, P.; Waldauf, C.; Heeger, A. J.; Brabec, C. J. *Adv. Mater.* **2006**, *18*, 789–794.
(30) Loi, M. A.; Toffanin, S.; Muccini, M.; Forster, M.; Scherf, U.; Scharber, M. *Adv. Funct. Mater.* **2007**, *17*, 2111–2116.
(31) Muntwiler, M.; Yang, Q.; Tisdale, W. A.; Zhu, X.-Y. *Phys. Rev. Lett.* **2008**, *101*, 196403.
(32) Holcombe, T. W.; Norton, J. E.; Rivnay, J.; Woo, C. H.; Goris, L.; Piliego, C.; Griffini, G.; Sellinger, A.; Brédas, J. L.; Salleo, A.; Fréchet, J. M. J. *J. Am. Chem. Soc.* **2011**, *133*, 12106–12114.
(33) Faist, M. A.; Kirchartz, T.; Gong, W.; Ashraf, R. S.; McCulloch, I.; De Mello, J. C.; Ekins-Daukes, N. J.; Bradley, D. D. C.; Nelson, J. *J. Am. Chem. Soc.* **2012**, *134*, 685–692.
(34) Hertel, D.; Bässler, H.; Scherf, U.; Hörhold, H. H. *J. Chem. Phys.* **1999**, *110*, 9214–9222.
(35) Günes, S.; Neugebauer, H.; Sariciftci, N. S. *Chem. Rev.* **2007**, *107*, 1324–1338.
(36) Rivnay, J.; Mannsfeld, S. C. B.; Miller, C. E.; Salleo, A.; Toney, M. F. *Chem. Rev.* **2012**, *112*, 5488–5519.
(37) Hulstrom, R.; Bird, R.; Riordan, C. *Sol. Cells* **1985**, *15*, 365–391.
(38) Rostalski, J.; Meissner, D. *Sol. Energy Mater. Sol. Cells* **2000**, *61*, 87–95.
(39) Hoppe, H.; Sariciftci, N. S. *J. Mater. Res.* **2004**, *19*, 1924–1945.
(40) Kersting, R.; Lemmer, U.; Mahrt, R. F.; Leo, K.; Kurz, H.; Bässler, H.; Göbel, E. O. *Phys. Rev. Lett.* **1993**, *70*, 3820–3823.
(41) Cheng, Y.-J.; Yang, S.-H.; Hsu, C.-S. *Chem. Rev.* **2009**, *109*, 5868–5923.
(42) Li, G.; Zhu, R.; Yang, Y. *Nat. Photon.* **2012**, *6*, 153–161.
(43) Koster, L. J. A.; Mihailetchi, V. D.; Blom, P. W. M. *Appl. Phys. Lett.* **2006**, *88*, 93511.
(44) Perez, M. D.; Borek, C.; Forrest, S. R.; Thompson, M. E. *J. Am. Chem. Soc.* **2009**, *131*, 9281–9286.
(45) Salleo, A.; Kline, R. J.; DeLongchamp, D. M.; Chabinyc, M. L. *Adv. Mater.* **2010**, *22*, 3812–3838.
(46) Kline, R. J.; McGehee, M. D.; Kadnikova, E. N.; Liu, J. S.; Fréchet, J. M. J.; Toney, M. F. *Macromolecules* **2005**, *38*, 3312–3319.
(47) Lee, O. P.; Yiu, A. T.; Beaujuge, P. M.; Woo, C. H.; Holcombe, T. W.; Millstone, J. E.; Douglas, J. D.; Chen, M. S.; Fréchet, J. M. J. *Adv. Mater.* **2011**, *23*, 5359–5363.
(48) Guo, J.; Liang, Y.; Szarko, J.; Lee, B.; Son, H. J.; Rolczynski, B. S.; Yu, L.; Chen, L. X. *J. Phys. Chem. B* **2010**, *114*, 742–748.
(49) Szarko, J. M.; Guo, J.; Liang, Y.; Lee, B.; Rolczynski, B. S.; Strzalka, J.; Xu, T.; Loser, S.; Marks, T. J.; Yu, L.; Chen, L. X. *Adv. Mater.* **2010**, *22*, 5468–5472.
(50) Coakley, K. M.; McGehee, M. D. *Chem. Mater.* **2004**, *16*, 4533–4542.
(51) Kim, B. J.; Miyamoto, Y.; Ma, B.; Fréchet, J. M. J. *Adv. Funct. Mater.* **2009**, *19*, 2273–2281.
(52) Bartelt, J. A.; Beiley, Z. M.; Hoke, E. T.; Mateker, W. R.; Douglas, J. D.; Collins, B. A.; Tumbleston, J. R.; Graham, K. R.; Amassian, A.; Ade, H.; Fréchet, J. M. J.; Toney, M. F.; McGehee, M. D. *Adv. Energy Mater.* **2013**, *3*, 364–374.

Chapter 2. Synthetic Control of Structural Order in *N*-Alkylthieno[3,4-*c*]-4,6-dione-Based Polymers*

Abstract

The correlation between the nature of alkyl substituents on *N*-alkylthieno[3,4-*c*]pyrrole-4,6-dione (TPD)-based polymers and solar cell device performance has been investigated. After optimizing device parameters, our TPD-based polymers provided photovoltaic responses ranging from 4.0% to 6.8% in bulk heterojunction blends with $PC_{61}BM$, depending on the size and shape of the alkyl solubilizing groups. Further, we have correlated the effect of alkyl side chains on the structural order and orientation of the polymer backbone using grazing incidence X-ray diffraction analysis, and we have demonstrated how fine-tuning the polymer solubilizing groups can improve the power conversion efficiency of organic photovoltaic devices.

Introduction

Intense interdisciplinary research in the field of organic photovoltaics (OPVs) has led to a significant increase in their power conversion efficiencies (PCEs) over the last decade.[1–6] One of the most important advances in OPVs has been the introduction of the bulk heterojunction (BHJ) architecture,[7,8] in which the photoactive thin film consists of an interpenetrating blend of electron donor and electron acceptor components. Extensive research efforts have focused on improving the polymeric electron donor component of the BHJ, while retaining fullerene derivatives as the electron acceptor.[9–11] Key developments have involved narrowing the polymer bandgap, in order to better match the optical absorption with the solar spectrum, and optimization of the energy level offsets with fullerene to achieve maximum open-circuit voltage (V_{oc}).[12–17] For the design of new polymers, non-energetic parameters such as those that influence the physical interaction between the bulk polymer and fullerene are also important.[18–20] In particular, the choice of solubilizing groups is a critical factor, yet reports that directly correlate solubilizing patterns with device performance have been limited.[21–25] Herein, we investigate the correlation between different alkyl substituents on *N*-alkylthieno[3,4-*c*]pyrrole-4,6-dione (TPD)-based polymers and BHJ device performance, reaching PCEs over 6.5%.

Results and Discussion

During the preparation of our manuscript,[26] Leclerc *et al.* reported on a linear alkyl substituted TPD-based polymer showing PCEs on the order of 5.5%.[27] We independently synthesized a series of high molecular weight TPD-based polymers (**P1**-**P3**), and identified device configurations yielding PCEs between 4% and 6.8%. By preserving the π-conjugated backbone structure, while modulating the size and branching of the alkyl substituent appended to TPD, we were able to maintain consistent electronic properties among the polymers. This allowed us to focus on the specific influence of solubilizing groups on OPV performance.

In order to ensure that polymers **P1**-**P3** had comparable electronic backbone structures, our 2-ethylhexyl-, 3,7-dimethyloctyl- and *n*-octyl-substituted TPD monomers were Stille cross-coupled with the same electron-rich donor monomer, 4,8-bis((2-ethylhexyl)oxy)benzo[1,2-*b*:4,5-*b*']dithiophene (BDT-EH) (Scheme 2.1c). The TPD and BDT monomers were readily

* Reproduced in part with permission from Piliego, C.; Holcombe, T. W.; Douglas, J. D.; Woo, C. H.; Beaujuge, P. M.; Fréchet, J. M. J. *J. Am. Chem. Soc.*, **2010**, *132*, 7595-7597.

synthesized with dibromide and distannyl functionalities, respectively, to enable palladium-catalyzed polymerization (Scheme 2.1a and 2.1b). Synthesis of TPD began with bromination of thieno-3,4-dicarboxylic acid, and proceeded through anhydride **3**. The three different alkyl-functionalized TPD monomers were formed via ring-opening of the anhydride by an alkyl-substituted amine, and ring-closure with thionyl chloride. The BDT monomer was synthesized from thiophene-3-carboxylic acid, which was readily converted to amide **6** through an acid chloride intermediate. Two molecules of **6** were then deprotonated with *n*-butyllithium and allowed to intermolecularly react to form benzo[1,2-*b*:4,5-*b*']dithiophene-4,8-dione (**7**). Reduction and alkylation of quinone **7**, followed by stannylation, provided the BDT monomer with 2-ethylhexyl side chains and trimethyltin functionalities.

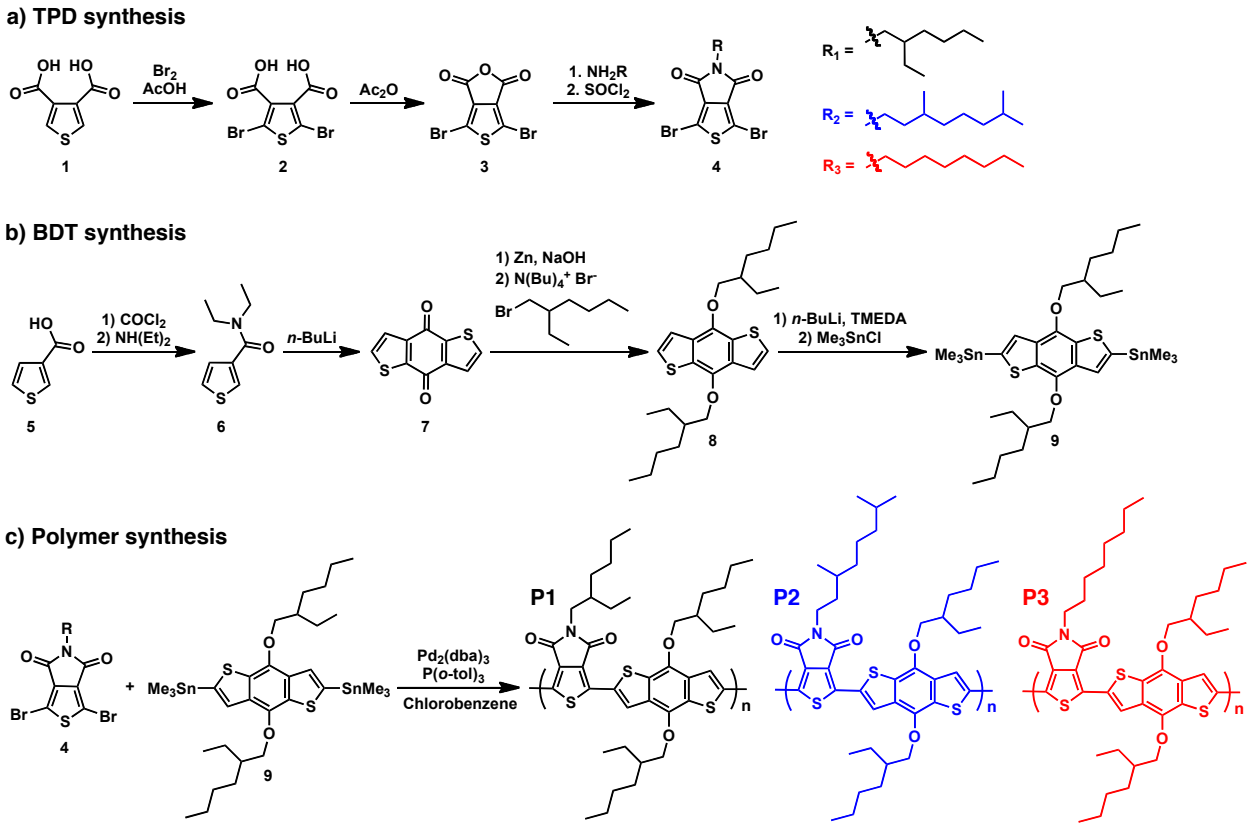

Scheme 2.1. Synthetic routes toward a) the TPD monomer, b) the BDT monomer, and c) polymers **P1**, **P2**, and **P3**.

Polymers **P1**-**P3** were obtained with similar molecular weights (M_n) in the range of 35 to 42 kDa. Very recently, we have synthesized PBDTTPD polymers with slightly higher M_n by using a monomer ratio other than 1:1 during Stille cross-coupling. A monomer imbalance that favors the halogenated monomer by about 3% provides polymers with higher M_n and improved device performance (above 7% PCE).[28,29] A full study about the effect of polymer molecular weight on OPV device morphology and performance is the subject of current collaborative work.

The thin-film optical absorption spectra of the polymers display three maxima in the 400-700 nm range (Figure 2.1a). By replacing the shorter but bulkier ethylhexyl chains in **P1** with the longer but less bulky octyl side chains in **P2** and **P3**, broader and red-shifted absorption spectra with more defined vibronic structure are obtained. This is indicative of a planarization of the conjugated backbone and more efficient packing of the polymer.[30] From the onset of the

absorption spectra, an optical bandgap value of about 1.73 eV was estimated for all three polymers. Cyclic voltammetry (CV) was carried out to determine the electrochemical HOMO levels of **P1**-**P3**. Similar values (**P1** 5.81 eV, **P2** 5.90 eV, **P3** 5.73 eV) were found for all three materials.

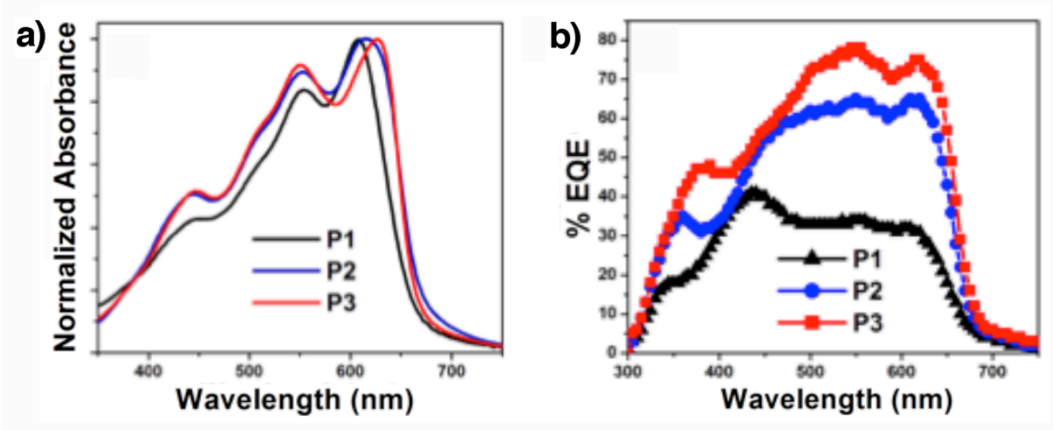

Figure 2.1. a) The thin-film UV-vis absorption spectra and b) the external quantum efficiency (EQE) of **P1**-**P3**.

The photovoltaic properties of **P1**-**P3** were investigated in the device structure ITO/PEDOT:PSS/polymer:[6,6]-phenyl-C61-butyric acid methyl ester ($PC_{61}BM$)/Ca/Al. The active layers were spin-coated from chlorobenzene (CB), and in some cases a small amount of the high boiling point additive 1,8-diiodooctane (DIO)[31] was used in order to optimize the morphology. The solubility of all three polymers in CB is high enough to allow for extensive characterization. The best *J-V* curves are reported in Figure 2.2a, and the average device parameters are listed in Table 2.1. When comparing **P1** and **P2**, it is clear that decreasing the branch length from two carbons to one and moving the branching point from the 2-position to the 3-position leads to an improvement in device performance. In optimized devices, the PCE increases from 3.9% for **P1**, which possesses an ethylhexyl side chain, to 5.4% for **P2**, which possesses a dimethyloctyl side chain. The elimination of branching on the TPD side chain in **P3** further enhances performance. We obtained a maximum PCE value of 6.8% in our best device with a short-circuit current of 11.5 mA/cm^2, an open-circuit voltage of 0.85 V and a fill factor of

Table 2.1. Polymer and optoelectronic properties of **P1**-**P3**, and photovoltaic performance of **P1**-**P3** based devices

	Polymer Properties		Optoelectronic Properties		Photovoltaic Performance				
	M_n (kDa)	PDI	HOMO[a] (eV)	E_g[b] (eV)	Additive	V_{oc} (V)	J_{sc} (mA/cm^2)	*FF*	PCE (%)
P1[c]	42	2.5	5.81	1.75	--	0.89	-5.5	55	2.7 (2.8)
					2% DIO	0.87	-8.1	56	3.9 (4.0)
P2[d]	39	3.0	5.90	1.70	--	0.82	-7.3	62	3.7 (3.9)
					1% DIO	0.81	-9.7	67	5.4 (5.7)
P3[e]	35	2.7	5.73	1.73	--	0.86	-10.6	68	6.3 (6.4)
					1% DIO	0.85	-11.5	68	6.6 (6.8)

Average device properties are reported with maximum values in parentheses. [a] CV determined HOMO values are reported relative to Fc/Fc^+ at -5.13 eV. [b] Optical band gap in thin films based on onset of absorption. [c] **P1**:$PC_{61}BM$ device blend ratio of 1:2 in chlorobenzene (CB). [d] **P2**:$PC_{61}BM$ device blend ratio of 1:1.5 in CB. [e] **P3**:$PC_{61}BM$ device blend ratio of 1:1.5 in CB.

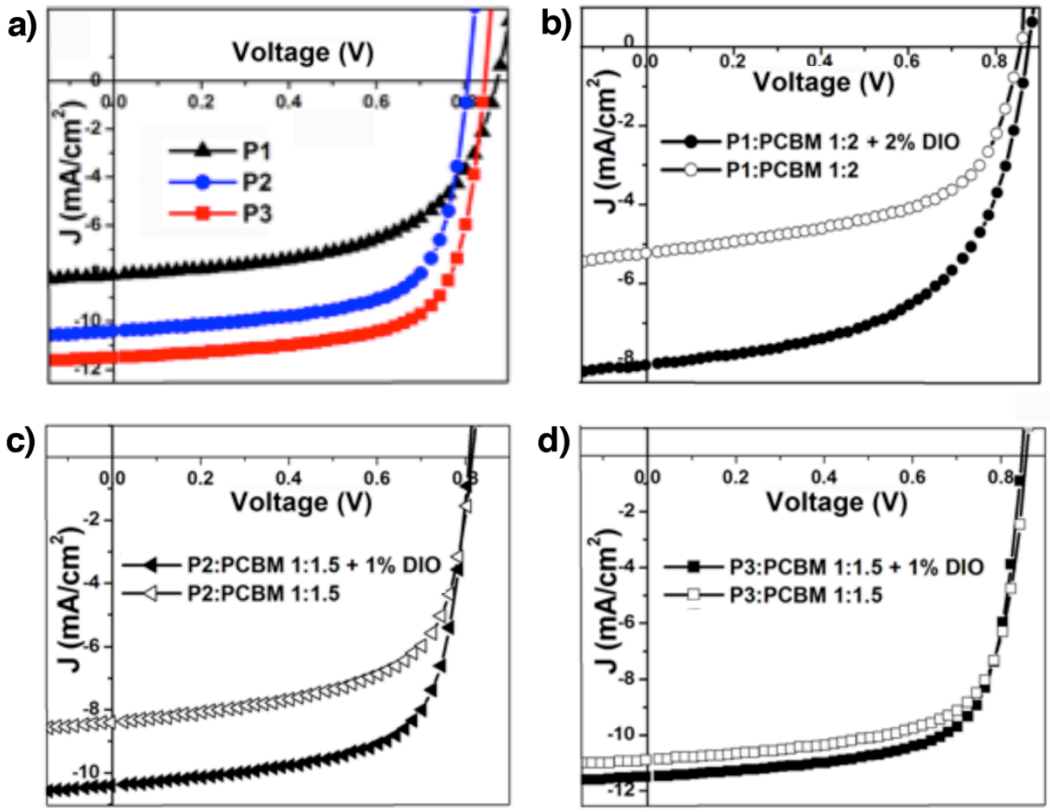

Figure 2.2. Optimized *J-V* curves of solar cells based on BHJ blends with $PC_{61}BM$ and a) **P1**, **P2** and **P3** with DIO additive, b) **P1** with and without DIO additive, c) **P2** with and without DIO additive, d) **P3** with and without DIO additive, under illumination of AM 1.5G, 100mW/cm^2.

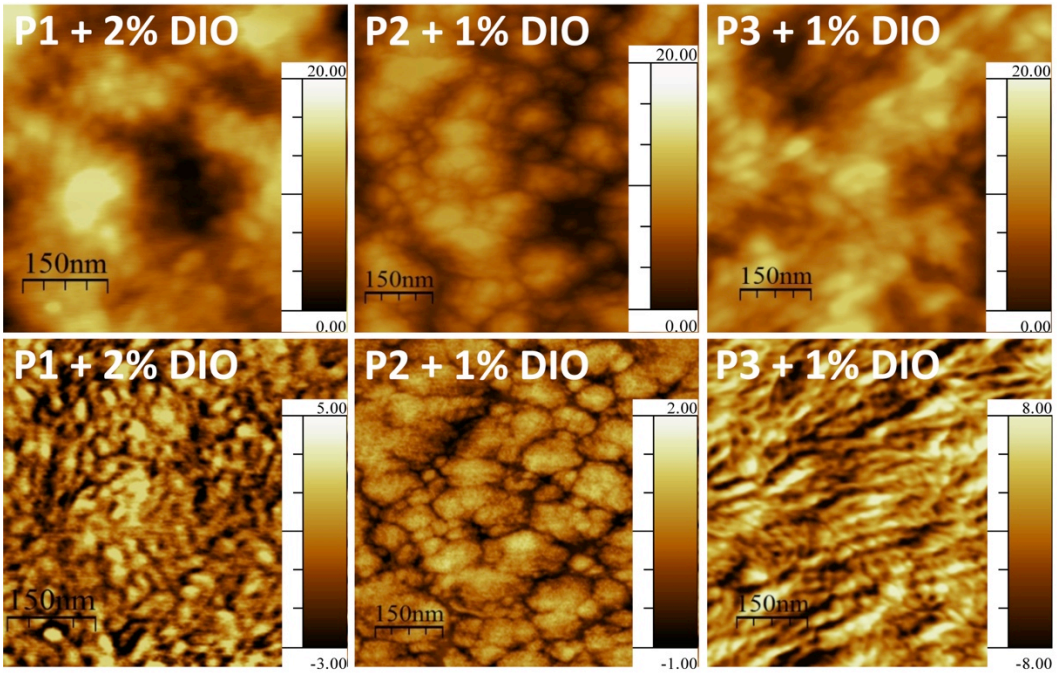

Figure 2.3. Tapping mode atomic force microscopy (AFM) images of optimized polymer:$PC_{61}BM$ blend film containing DIO additive. The top row contains topography images and the bottom row contains phase images.

69.8%. The high *FF* values obtained in the best-performing devices suggest that an optimized morphology was achieved (Figure 2.3 atomic force microscopy images). The external quantum efficiency (EQE) spectra of the optimized devices are shown in Figure 2.1b, and the maximum values are among the highest reported for solar cells based on polymer:$PC_{61}BM$ blends.

In the cases of **P1** and **P2**, the addition of DIO to the blend solution dramatically improved the performances of the devices. The use of high boiling point additives has been shown to promote packing of the polymer by avoiding excessive crystallization of the fullerene.[32] We believe that this mechanism is responsible for the large enhancement in the device performances of **P1** and **P2**. In contrast, for devices realized using **P3**, the addition of DIO only led to slight improvements. These results suggest that **P3** reaches a high level of order in the blend without DIO.

To confirm these hypotheses, we investigated the influence of the different alkyl substituents on the molecular organization in the polymer thin films using grazing incidence X-ray diffraction (GIXD). Polymer blends with $PC_{61}BM$ were also examined to directly correlate microstructural order in the blends with device performance. As shown by the GIXD patterns of **P1**, **P2**, and **P3** (Figure 2.4a), the (010) peak corresponding to π-stacking is more prominent in the out-of-plane direction, which suggests that the polymer backbones are oriented parallel to the substrate (inset, Figure 2.4b). This face-on orientation is beneficial for charge transport in the device, and the effect is enhanced by reducing the distance d_2 (inset, Figure 2.4b) between the backbones. As extracted from the out-of-plane GIXD profile (Figure 2.4b), the value of d_2 is equal to 3.8 Å for **P1** and 3.6 Å for both **P2** and **P3**. Therefore, by replacing the ethylhexyl substituent on **P1** with the dimethyloctyl and *n*-octyl analogs on **P2** and **P3**, respectively, the π-stacking distances are reduced, which correlates well with increased device performance. The stronger intensity of the reflection coming from **P3** compared to **P2** (Figure 2.4a) indicates that a higher fraction of polymer backbones are oriented in the direction parallel to the substrate in the case of the **P3** film. An additional intense peak, corresponding to the reflection from the (100) crystal plane, is present in all pristine polymer films. This peak represents the distance d_1 (inset Figure 2.4b), which corresponds to the lamellar spacing in the plane. Since this distance is likely to be related to the length of the side chain, it is smaller for the hexyl derivative **P1** (d_1 = 18.9 Å) than for the octyl derivatives **P2** (d_1 = 21.6 Å) and **P3** (d_1 = 21.2 Å).

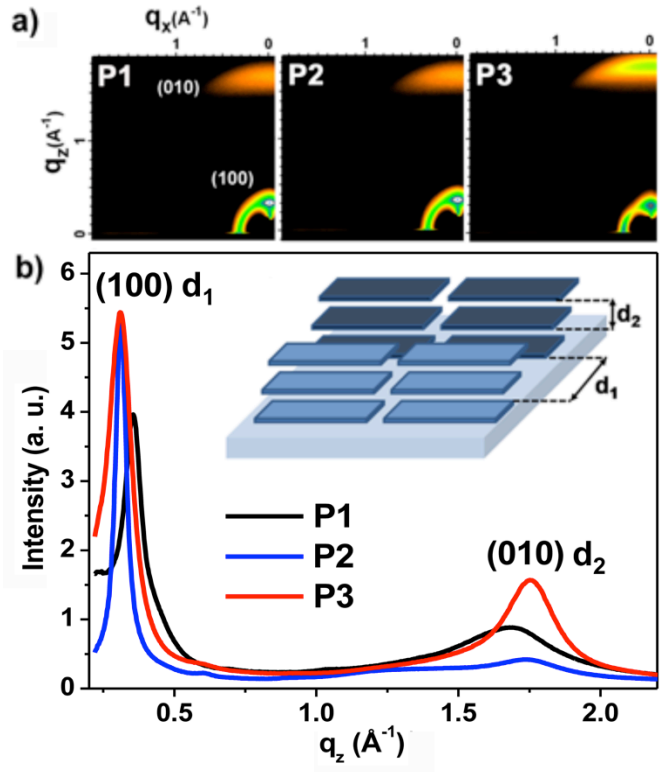

Figure 2.4. a) 2D Grazing Incidence X-ray Diffraction (GIXD) patterns of neat films of **P1**, **P2** and **P3**. b) Out-of-plane linecuts of GIXD. Inset: Schematic illustration of the face-on orientation of polymers with backbones parallel to the substrate. The lamellar spacing and the π-stacking distance are labeled d_1 and d_2 respectively.

Interestingly, the same diffraction peaks of the pristine polymers are still visible in the 2D patterns of the blends with $PC_{61}BM$ together with the characteristic reflection of fullerene. Figure 2.5 shows the 2D GIXD patterns of the polymer:$PC_{61}BM$ films, obtained from the same solutions used for device fabrication. Except for the pattern of the **P1**:$PC_{61}BM$ film without DIO, the π-stacking peak is visible in all samples, indicating that the polymers are able to retain the same face-on orientation when blended with fullerene. Compared to the samples without DIO, GIXD images of the films cast from solutions containing DIO show increased intensity of the π-stacking peak. This enhancement could be attributed to the additive, which likely promotes ordering of the polymer domains. The **P3**:$PC_{61}BM$ blend with DIO solution clearly shows the highest intensity peak, indicating more extended π-stacking with respect to the other samples. The increased ordering in **P3** films is probably due to the reduction of the side chain bulkiness, which allows the polymer to crystallize more easily, even in the presence of $PC_{61}BM$. We believe that this increased order also contributes to the higher device efficiency observed for **P3**.

By extracting the π-stacking distance from the GIXD pattern, we found that blend films containing **P2** and **P3** exhibit the same d_2 value as the pristine films (3.6 Å). From the GIXD analysis, we conclude that these TPD-based polymers are able to maintain a face-on orientation of the backbone, and preserve a small π-stacking distance in the blends with fullerene.

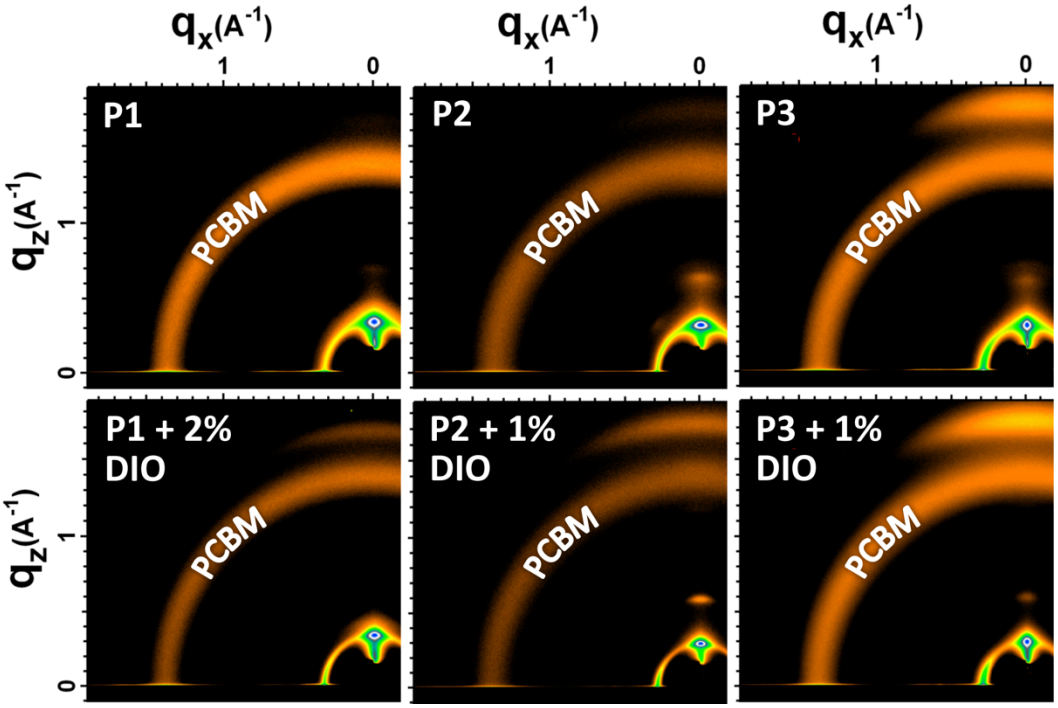

Figure 2.5. 2D GIXD patterns of polymer:$PC_{61}BM$ BHJ blends top) spin-casted from CB without additives and bottom) spin-casted from CB with DIO additive.

These structures provide one of the first reports of face-on oriented polymers for solar cell applications.[33] The unique molecular packing structure is likely one of the main reasons why the TPD-based polymers are able to outperform regioregular poly(3-hexylthiophene), which has an edge-on orientation with respect to the substrate.[34,35] In addition to the face-on orientation of the polymer backbone, the extended microstructural order observed in the blend films of **P3** contributes to the high performance of this polymer.

Conclusions

In conclusion, we report the synthesis and device performance of a series of alkyl-substituted TPD-based polymers with photovoltaic responses ranging from 4.0% to 6.8%, depending on the choice of the alkyl solubilizing group. We demonstrate and rationalize, via GIXD analysis, how variations in the solubilizing groups impact structural order and orientation in polymer backbones, critically affecting device performance. Our results provide important insights for the design of new polymeric and molecular systems to be used in efficient solar cells.

Experimental

Materials.

All commercially available reagents obtained from suppliers were used without further purification. Unless otherwise noted, all reactions were carried out under nitrogen with standard Schlenk techniques, and all glassware used in dry reactions was flame dried under high-vacuum prior to use. Tetrahydrofuran (THF), dichloromethane (DCM), and hexanes were purified and dried by passing through two columns of neutral alumina, under nitrogen, prior to use. Flash chromatography was performed using Silicycle SiliaFlash ® P60 (particle size 40-63 μm, 230-400 mesh) silica gel.

Material Characterization.

All ^{1}H and ^{13}C NMR spectra were obtained with a Bruker AVQ-400, AVB-400 or DRX-500 instrument and ^{13}C spectra were measured with a proton-decoupling pulse program. NMR abbreviations: aq = apparent quartet, bm = broad multiplet, d = doublet, dd= doublet of doublets, m = multiplet, s = singlet, and t = triplet. Elemental analysis (CHN) was performed by the UC Berkeley microanalysis laboratory. Data from high-resolution mass spectrometry (HRMS) using electron impact (EI) were obtained by the UC Berkeley mass spectrometry facility.

For polymer molecular weight determination, polymer solutions (1 mg/mL) were prepared using HPLC grade THF. Samples were briefly heated and then allowed to return to room temperature prior to filtering through a 0.45 μm PVDF filter. Size exclusion chromatography (SEC) was performed by passing HPLC grade THF (1.0 mL/min) through three PLgel columns (7.5 x 300 mm) with pore sizes of 10^5, 10^3, and 500 Å. The particle size in the columns was 5 μm and the columns were thermostated at 35 °C. The SEC system consisted of a Waters 510 pump, a Waters 717 autosampler, and a Waters 486 tunable absorption detector. The apparent molecular weights and polydispersities (M_w/M_n) were determined with a calibration based on linear polystyrene standards using Empower software from Waters.

Thin-film UV-vis absorption spectra were gathered at room temperature using a Varian Cary 50 Conc spectrophotometer. The polymers were spin-coated on quartz substrates from chlorobenzene solutions (15 mg/ml). The thickness of the thin films was about 100 nm and a blank quartz substrate was used as reference.

Cyclic voltammograms (CV) were collected using a Solartron 1285 potentiostat under the control of CorrWare II software. A standard three electrode cell based on a Pt wire working electrode, a silver wire reference electrode (calibrated vs. Fc/Fc^+ at -5.13 eV), and a Pt wire counter electrode was purged with nitrogen and maintained under a nitrogen atmosphere during all measurements. Anhydrous acetonitrile was purchased from Aldrich, and tetrabutylammonium hexafluorophosphate (0.1 M) was used as the supporting electrolyte. Polymer films were drop cast onto a Pt wire working electrode from a 1% (w/w) chloroform solution and dried under nitrogen prior to measurement.

Synthesis.

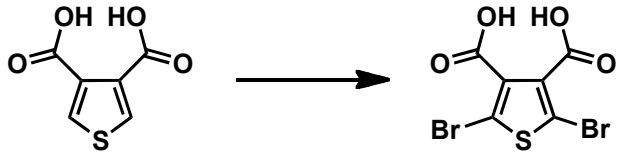

1 **2**

*2,5-Dibromothiophene-3,4-dicarboxylic acid (**2**).* Thiophene-3,4-dicarboxylic acid (**1**) (20.0 g, 116 mmol), glacial acetic acid (120 mL) and bromine (23.9 mL, 74.3 g, 465 mmol) were combined in a 1 L flask and heated to 55 °C for 96 h. After cooling the reaction mixture to almost room temperature, excess bromine was quenched with a saturated solution of $NaHSO_3$ until the reaction contents became nearly clear. The reaction mixture was cooled to 4 °C and flakey beige solids crystallized from solution. The crystals were crushed during filtration and washed with ice water to yield 22.0 g of a beige powder (57 %). ^{13}C (100 MHz, acetone-d_6, δ): 162.5, 135.9, 115.3. EI-MS (*m/z*): $[M]^+$ calculated for $C_6H_2Br_2O_4S$, 329.8020; found, 329.7987.

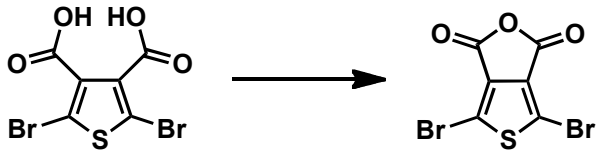

2 **3**

*4,6-Dibromothieno[3,4-c]furan-1,3-dione (**3**).* Compound **2** (13.3 g, 40.3 mmol) was combined with acetic anhydride (110 mL) in a 500 mL flask and stirred at 110 °C for 1 h. After cooling the reaction flask to room temperature, crystallization occurred. The crystals were filtered and washed with hexanes to yield 10.9 g of off-white needles (87 %). ^{13}C NMR (100 MHz, acetone-d_6, δ): 161.7, 135.0, 114.7. EI-MS (*m/z*): $[M]^+$ calculated for $C_6Br_2O_3S$, 311.7914; found, 311.7919.

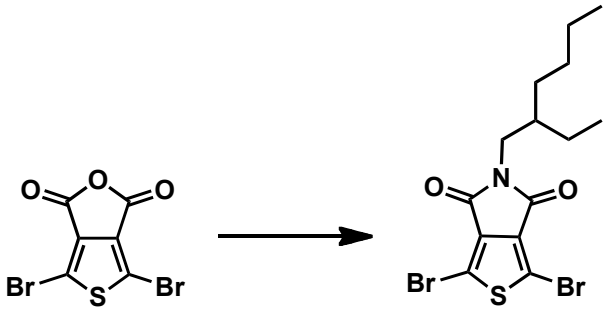

3 **EH-4**

*1,3-Dibromo-5-(2-ethylhexyl)-4H-thieno[3,4-c]pyrrole-4,6(5H)-dione (**EH-4** = **TPD-EH**).* Compound **3** (1.46 g, 4.68 mmol) and 2-ethylhexylamine (633 mg, 4.90 mmol) were combined with THF (12 mL) in a 50 mL flask and heated to 50 °C for 3 h. After cooling the reaction mixture to room temperature, thionyl chloride (5 mL) was added, and the reaction contents were stirred at 55 °C for 4 h. The reaction mixture was then precipitated into methanol (150 mL) and the crude solid was purified by flash chromatography ($CHCl_3$) to yield 1.32 g of white powder (67 %). ^1H NMR (500 MHz, $CDCl_3$, δ): 3.49 (d, J = 7.17 Hz, 2 H), 1.81-1.73 (m, 1 H), 1.37-1.17 (m, 8 H), 0.89 (aq, J = 7.03 Hz, 6 H). ^{13}C NMR (125 MHz, $CDCl_3$, δ): 160.8, 134.8, 113.1, 42.8,

38.3, 30.6, 28.7, 24.0, 23.1, 14.2, 10.5. EI-MS (*m/z*): $[M]^+$ calculated for $C_{14}H_{17}Br_2NO_2S$, 422.9326; found, 422.9320. Anal. calculated for $C_{14}H_{17}Br_2NO_2S$: C, 39.74; H, 4.05; N, 3.31; found: C, 39.51; H, 3.95; N, 3.35.

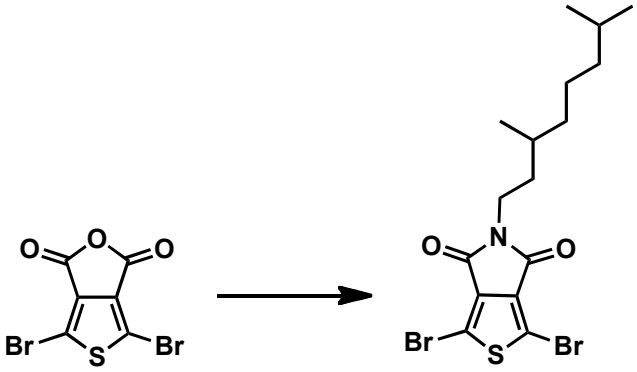

3 **DMO-4**

*1,3-Dibromo-5-(3,7-dimethyloctyl)-4H-thieno[3,4-c]pyrrole-4,6(5H)-dione (**DMO-4** = **TPD-DMO**)*. Compound **3** (1.50 g, 4.81 mmol) and 3,7-dimethyloctylamine (832 mg, 5.29 mmol) were combined with THF (12 mL) in a 50 mL flask and heated to 50 °C for 3 h. After cooling the reaction mixture to room temperature, thionyl chloride (4 mL) was added, and the reaction contents were stirred at 55 °C for 4 h. The reaction mixture was then precipitated into methanol (150 mL) and the crude solid was purified by flash chromatography ($CHCl_3$) to yield 1.52 g of white powder (70 %). ^{1}H NMR (500 MHz, $CDCl_3$, δ): 3.61 (t, *J* = 7.37 Hz, 2 H), 1.69-1.57 (m, 1 H), 1.56-1.48 (m, 1 H), 1.47-1.37 (m, 2 H), 1.34-1.26 (m, 2 H), 1.25-1.18 (m, 1 H), 1.17-1.07 (m, 3 H), 0.94 (d, *J* = 6.29 Hz, 3 H), 0.85 (d, *J* = 6.61 Hz, 6 H). ^{13}C NMR (125 MHz, $CDCl_3$, δ): 160.5, 135.0, 113.0, 39.3, 37.2, 37.1, 35.3, 30.8, 28.1, 24.6, 22.8, 22.7, 19.5. EI-MS (*m/z*): $[M]^+$ calculated for $C_{16}H_{21}Br_2NO_2S$, 450.9639; found, 450.9651. Anal. calculated for $C_{16}H_{21}Br_2NO_2S$: C, 42.59; H, 4.69; N, 3.10; found: C, 42.40; H, 4.81; N, 3.19.

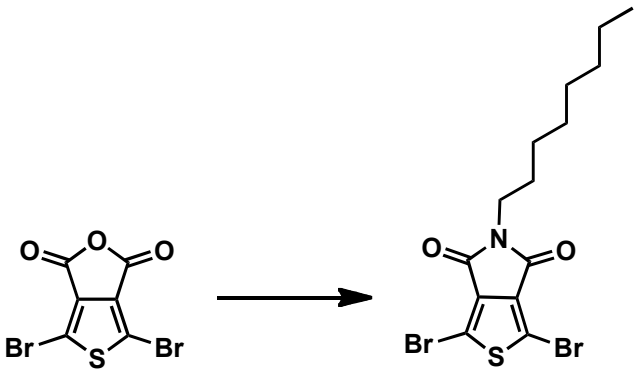

3 ***n*8-4**

*1,3-Dibromo-5-octyl-4H-thieno[3,4-c]pyrrole-4,6(5H)-dione (**n8-4** = **TPD-O**)*. Compound **3** (2.00 g, 6.41 mmol) and octylamine (912 mg, 7.06 mmol) were combined with THF (15 mL) in a 50 mL flask and heated to 60 °C for 1 h. After cooling the reaction mixture to room temperature, thionyl chloride (2.5 mL) was added, and the reaction contents were stirred at 60 °C for 4 h. The reaction mixture was then precipitated into water (100 mL) and the crude solid was purified by flash chromatography (DCM) to yield 2.36 g of white powder (87 %). ^{1}H NMR (400 MHz,

$CDCl_3$, δ): 3.58 (t, *J* = 7.32 Hz, 2 H), 1.67-1.58 (m, 2 H), 1.35-1.19 (m, 10 H), 0.86 (t, *J* = 6.83 Hz, 3 H). ^{13}C NMR (100 MHz, $CDCl_3$, δ): 160.5, 134.9, 113.0, 39.0, 31.9, 29.2, 28.4, 26.9, 22.7, 14.2. EI-MS (*m/z*): $[M]^+$ calculated for $C_{14}H_{17}Br_2NO_2S$, 422.9326; found, 422.9321. Anal. calculated for $C_{14}H_{17}Br_2NO_2S$: C, 39.74; H, 4.05; N, 3.31; found: C, 39.83; H, 3.94; N, 3.31.

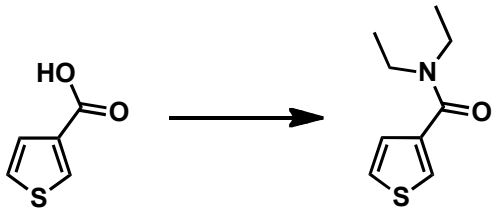

5 **6**

*N,N-diethylthiophene-3-carboxamide (**6**).*[36] Thiophene-3-carboxylic acid (**5**) (25.0 g, 195 mmol) was combined with DCM (40 mL) in a 250 mL flask and chilled to 0 °C for 30 min. Oxalyl chloride (49.5 g, 390 mmol) was added to the reaction mixture, and the reaction contents were stirred at room temperature for 12 h. Volatiles were removed under reduced pressure to yield the crude intermediate (thiophene-3-carbonyl chloride) as a while solid. The intermediate solid was dissolved in DCM (35 mL) and added dropwise to a solution of diethyl amine (28.5 g, 390 mmol) in DCM (40 mL) at 0 °C. After stirring at room temperature for 1 h, the reaction contents were extracted with DCM, washed with water, dried over $MgSO_4$, and filtered. Volatiles were removed under reduced pressure to yield 35.2 g of a clear light yellow oil (98%). The crude product was used without further purification. ^1H NMR (400 MHz, $CDCl_3$, δ): 7.47 (d, *J* = 2.92 Hz, 1 H), 7.32 (dd, *J* = 4.98, 2.95 Hz, 1 H), 7.19 (d, *J* = 4.99 Hz, 1 H), 3.68-3.21 (bm, 4 H), 1.37-1.07 (m, 6 H). ^{13}C NMR (100 MHz, $CDCl_3$, δ): 166.2, 137.0, 126.4, 125.4, 124.6, 41.9, 37.9, 13.6, 12.2. EI-MS (*m/z*): $[M]^+$ calculated for $C_9H_{13}NOS$, 183.0718; found, 183.0722.

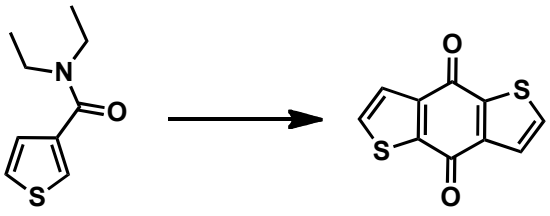

6 **7**

*Benzo[1,2-b:4,5-b']dithiophene-4,8-dione (**7**).*[36] Compound **6** (25.0 g, 136 mmol) was added to a flame-dried 500 mL flask and the reaction vessel was purged with three vacuum/nitrogen cycles before being chilled to 0 °C for 1 h with THF (75 mL). *N*-butyllithium (60.0 mL of a 2.5 M solution in hexanes, 150 mmol) was added to the reaction mixture over 35 min, and the reaction contents were stirred at room temperature for 30 min. The reaction mixture was then poured into an ice water bath (600 g) and stirred at room temperature for 2 h. The crude brown mixture was filtered, and the resulting solids were washed with water (200 mL), methanol (80 mL), and hexanes (100 mL) to yield 11.2 g of green powder (75 %). ^1H NMR (400 MHz, $CDCl_3$, δ): 7.69 (d, *J* = 5.03 Hz, 2 H), 7.65 (d, *J* = 5.03 Hz, 2 H). EI-MS (*m/z*): $[M]^+$ calculated for $C_{10}H_4O_2S_2$, 419.9653; found, 219.9655.

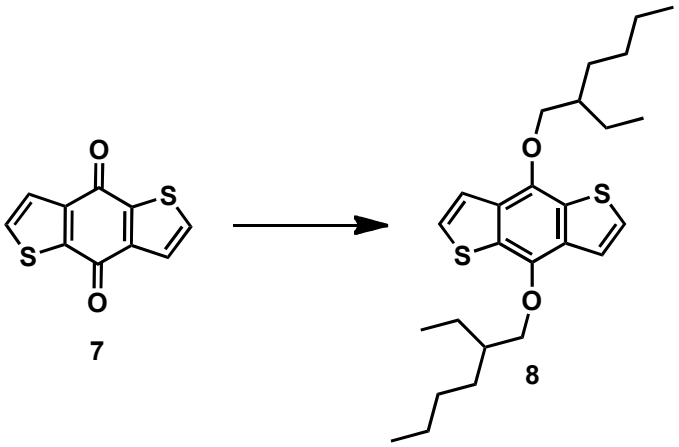

*4,8-Bis((2-ethylhexyl)oxy)benzo[1,2-b:4,5-b']dithiophene (**8**)*. Compound **7** (8.00 g, 36.3 mmol), zinc powder (5.22 g, 79.9 mmol) and water (100 mL) were combined in a 250 mL flask. Sodium hydroxide (21.8 g, 545 mmol) was added to the reaction mixture and the reaction contents were heated at reflux for 3 h. Once the reaction turned bright yellow, the reaction mixture was cooled to room temperature, and 2-ethylhexyl bromide (28.1 g, 146 mmol) and tetrabutylammonium bromide (3.51 g, 10.9 mmol) were added to the flask. The reaction contents were heated again at reflux for 12 h before being cooled to room temperature. The reaction mixture was extracted with diethyl ether, washed with water, dried over $MgSO_4$, and volatiles were removed under reduced pressure. The crude material was purified by flash chromatography (90:10 hexanes: dichloromethane) to yield 11.5 g of a light yellow oil (71 %). ^{1}H NMR (400 MHz, $CDCl_3$, δ): 7.48 (d, *J* = 5.54 Hz, 2 H), 7.37 (d, *J* = 5.53 Hz, 2 H), 4.18 (d, *J* = 5.36 Hz, 4 H), 1.86-1.76 (m, 2 H), 1.75-1.66 (m, 2 H), 1.65-1.55 (m, 4 H), 1.54-1.45 (m, 2 H), 1.44-1.34 (m, 8 H), 1.02 (t, *J* = 7.45 Hz, 6 H), 0.94 (t, *J* = 7.08 Hz, 6 H). ^{13}C NMR (100 MHz, $CDCl_3$, δ): 144.8, 131.6, 130.1, 126.1, 120.4, 76.2, 40.8, 30.6, 29.3, 24.0, 23.3, 14.3, 11.5. EI-MS (*m/z*): $[M]^+$ calculated for $C_{26}H_{38}O_2S_2$, 446.2313; found, 446.2312. Anal. calculated for $C_{26}H_{38}O_2S_2$: C, 69.91; H, 8.57; found: C, 69.56; H, 8.66; N, 0.27.

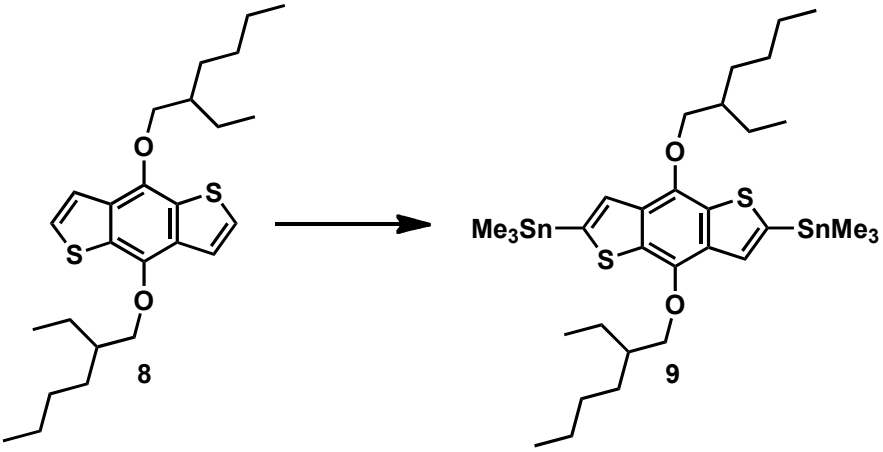

*(4,8-Bis((2-ethylhexyl)oxy)benzo[1,2-b:4,5-b']dithiophene-2,6-diyl)bis(trimethylstannane) (**9** = **BDT-EH**)*. Compound **8** (4.00 g, 8.95 mmol), tetramethylethylenediamine (dried over CaH_2 and vacuum distilled, 3.12 g, 26.9 mmol) and hexanes (115 mL) were combined in a 250 mL flame-dried flask. The reaction contents were cooled to 0 °C and *n*-butyllithium (7.52 mL of a 2.5 M solution in hexanes, 18.8 mmol) was added to the reaction mixture dropwise. After stirring for

2 h on the melting ice bath, the reaction mixture was cooled to 0 °C and trimethyltin chloride (5.35 g, 26.9 mmol) was added. The reaction contents were stirred for another 8 h at room temperature before being quenched with water (50 mL). The reaction mixture was then extracted with diethyl ether, washed with water, dried over $MgSO_4$, and filtered. Volatiles were removed under reduced pressure, and the crude product was recrystallized (isopropyl alcohol) twice to yield 4.71 g of pale yellow crystalline needles (68 %). ^{1}H NMR (400 MHz, $CDCl_3$, δ): 7.51 (s, 2 H), 4.19 (d, J = 5.39 Hz, 4 H), 1.85-1.77 (m, 2 H), 1.76-1.62 (m, 4 H), 1.61-1.47 (m, 4 H), 1.44-1.35 (m, 8 H), 1.02 (t, J = 7.43 Hz, 6 H), 0.94 (t, J = 7.00 Hz, 6 H), 0.44 (s, 18 H). ^{13}C NMR (100 MHz, $CDCl_3$, δ): 143.4, 140.5, 134.0, 133.0, 128.1, 75.8, 40.8, 30.7, 29.4, 24.0, 23.3, 14.4, 11.5, -8.1. EI-MS (*m/z*): $[M]^+$ calculated for $C_{32}H_{54}O_2S_2Sn_2$, 772.1603; found, 772.1599.

Polymer Synthesis.

Copolymer P1. BDT-EH (350 mg, 453 μmol), TPD-EH (192 mg, 453 μmol), tris(dibenzylideneacetone)dipalladium(0) (8.30 mg, 9.06 μmol), and tri-*o*-tolylphosphine (11.0 mg, 36.2 μmol) were dissolved in degassed chlorobenzene (8 mL) and stirred at 110 °C for 36 h. A strong complexing ligand (N,N-diethylphenylazothioformamide) was added to the reaction mixture to remove residual catalyst before precipitating the reaction contents into methanol (200 mL). The precipitate was filtered through a Soxhlet thimble and purified via Soxhlet extraction for 12 h with methanol, 2 h with hexanes, and was finally collected in chloroform. The chloroform solution was then concentrated under reduced pressure, precipitated into methanol (200 mL), and filtered to yield 274 mg of a dark purple solid (85 %). SEC analysis: M_n = 42 kDa, M_w = 105 kDa, PDI = 2.5.

Copolymer P2. Synthesized with the same procedure that was used for **P1** except BDT-EH (171 mg, 221 μmol) and TPD-DMO (93.5 mg, 221 μmol) were copolymerized to yield 109 mg of a dark purple solid (67 %). SEC analysis: M_n = 39 kDa, M_w = 117 kDa, PDI = 3.0.

Copolymer P3. Synthesized with the same procedure that was used for **P1** except BDT-EH (365 mg, 0.473 μmol) and TPD-O (213 mg, 0.473 μmol) were copolymerized to yield 268 mg of a dark purple solid (80 %). SEC analysis: M_n = 35 kDa, M_w = 95 kDa, PDI = 2.7.

Device Fabrication.

All devices were fabricated on ITO-coated glass substrates (pre-patterned, R = 20 Ω/sq, Thin Film Devices, Inc.). A thin layer (30-40 nm) of PEDOT:PSS (Baytron PH) was spin-coated onto UV-ozone treated ITO substrates at 4000 RPM for 40 s and then baked at 140 °C for 15 min in air. The photoactive layer containing the polymers (15 mg/ml) and $PC_{61}BM$ (40 mg/ml) in different ratios was spun cast from chlorobenzene solution after passing through a 0.45 μm polytetrafluoroethylene filter. Different concentrations for the blend solutions were tested in order to obtain the optimized thicknesses. 1,8-Diiodooctane (purchased from Sigma Aldrich, used as received) with 2% volume ratio for **P1** and 1% volume ratio for **P2** and **P3** was then added to the solution and stirred overnight before spin-coating. The active layers were spin-coated inside a glove-box at 1200 rpm for 40 sec. The cathode, consisting of Ca (20nm) and Al (100 nm), was then thermally evaporated under vacuum (~10-7 torr) through a shadow mask defining an active device area of ~ 0.03 cm^2. In order to optimize the various parameters for all three polymers (concentration, blend ratio and DIO percentage) more than 300 devices were tested and experiments were repeated multiple times in order to check the reproducibility of the data.

Device Characterization.

Solar cell devices were tested under AM 1.5 G solar illumination at 100 mW/cm^2 (1 sun) using a Thermal-Oriel 150W solar simulator. Current-voltage (*J-V*) curves were measured using a Keithley 2400 source-measure unit.

External quantum efficiency (EQE) values were obtained with a monochromator and calibrated with a silicon photodiode.

Tapping-mode atomic force microscopy (AFM) was performed on a Veeco Nanoscope V scanning probe microscope.

Grazing-Incidence X-ray Diffraction (GIXD) experiments were conducted at the Stanford Synchrotron Radiation Laboratory on beamline 11-3. The sample was irradiated at a fixed incident angle on the order of 0.1° and the GIXD patterns were recorded with a 2D image detector (MAR345 image plate detector). GIXD patterns were recorded with an X-ray energy of 12.72 keV (λ = 0.975 Å). To maximize the intensity from the polymer sample, the incident angle (~0.1°-0.12°) was carefully chosen such that the X-ray beam penetrates the polymer sample completely but does not interact with the silicon substrate. Typical exposure times were 30-180 s. To produce identical surface condition for samples as those used for device fabrication, a thin layer (~40 nm) of PEDOT:PSS was cast onto silicon substrates that were pretreated with UV-ozone for 30 min. Then the GIXD samples were prepared by spin-coating the same polymer solutions used for fabricating devices onto the silicon substrates at 1200 RPM for 40 s.

References

(1) Thompson, B. C.; Fréchet, J. M. J. *Angew. Chem. Int. Ed.* **2008**, *47*, 58–77.
(2) Kippelen, B.; Brédas, J.-L. *Energy Environ. Sci.* **2009**, *2*, 251–261.
(3) Dennler, G.; Scharber, M. C.; Brabec, C. J. *Adv. Mater.* **2009**, *21*, 1323–1338.
(4) Helgesen, M.; Søndergaard, R.; Krebs, F. C. *J. Mater. Chem.* **2010**, *20*, 36–60.
(5) Park, S. H.; Roy, A.; Beaupré, S.; Cho, S.; Coates, N.; Moon, J. S.; Moses, D.; Leclerc, M.; Lee, K.; Heeger, A. J. *Nat. Photon.* **2009**, *3*, 297–303.
(6) Liang, Y.; Xu, Z.; Xia, J.; Tsai, S.-T.; Wu, Y.; Li, G.; Ray, C.; Yu, L. *Adv. Mater.* **2010**, *22*, E135–E138.
(7) Yu, G.; Heeger, A. J. *J. Appl. Phys.* **1995**, *78*, 4510–4515.
(8) Yu, G.; Gao, J.; Hummelen, J. C.; Wudl, F.; Heeger, A. J. *Science* **1995**, *270*, 1789–1791.
(9) Blouin, N.; Michaud, A.; Leclerc, M. *Adv. Mater.* **2007**, *19*, 2295–2300.
(10) Hou, J.; Chen, H.-Y.; Zhang, S.; Li, G.; Yang, Y. *J. Am. Chem. Soc.* **2008**, *130*, 16144–16145.
(11) Huo, L.; Hou, J.; Zhang, S.; Chen, H.-Y.; Yang, Y. *Angew. Chem. Int. Ed.* **2010**, *49*, 1500–1503.
(12) Scharber, M. C.; Mühlbacher, D.; Koppe, M.; Denk, P.; Waldauf, C.; Heeger, A. J.; Brabec, C. J. *Adv. Mater.* **2006**, *18*, 789–794.
(13) Blouin, N.; Michaud, A.; Gendron, D.; Wakim, S.; Blair, E.; Neagu-Plesu, R.; Belletête, M.; Durocher, G.; Tao, Y.; Leclerc, M. *J. Am. Chem. Soc.* **2008**, *130*, 732–742.
(14) Huo, L.; Hou, J.; Chen, H.-Y.; Zhang, S.; Jiang, Y.; Chen, T. L.; Yang, Y. *Macromolecules* **2009**, *42*, 6564–6571.
(15) Liang, Y.; Feng, D.; Wu, Y.; Tsai, S.-T.; Li, G.; Ray, C.; Yu, L. *J. Am. Chem. Soc.* **2009**, *131*, 7792–7799.
(16) Mondal, R.; Ko, S.; Norton, J. E.; Miyaki, N.; Becerril, H. A.; Verploegen, E.; Toney, M. F.; Brédas, J.-L.; McGehee, M. D.; Bao, Z. *J. Mater. Chem.* **2009**, *19*, 7195–7197.
(17) Zoombelt, A. P.; Fonrodona, M.; Wienk, M. M.; Sieval, A. B.; Hummelen, J. C.; Janssen, R. A. J. *Org. Lett.* **2009**, *11*, 903–906.
(18) Ma, W.; Yang, C.; Gong, X.; Lee, K.; Heeger, A. J. *Adv. Funct. Mater.* **2005**, *15*, 1617–1622.
(19) Mayer, A. C.; Toney, M. F.; Scully, S. R.; Rivnay, J.; Brabec, C. J.; Scharber, M.; Koppe, M.; Heeney, M.; McCulloch, I.; McGehee, M. D. *Adv. Funct. Mater.* **2009**, *19*, 1173–1179.
(20) Cates, N. C.; Gysel, R.; Beiley, Z.; Miller, C. E.; Toney, M. F.; Heeney, M.; McCulloch, I.; McGehee, M. D. *Nano Lett.* **2009**, *9*, 4153–4157.
(21) Inganäs, O.; Svensson, M.; Zhang, F.; Gadisa, A.; Persson, N. K.; Wang, X.; Andersson, M. R. *Appl. Phys. A* **2004**, *79*, 31–35.

(22) Thompson, B. C.; Kim, B. J.; Kavulak, D. F.; Sivula, K.; Mauldin, C.; Fréchet, J. M. J. *Macromolecules* **2007**, *40*, 7425–7428.
(23) Chen, M.-H.; Hou, J.; Hong, Z.; Yang, G.; Sista, S.; Chen, L.-M.; Yang, Y. *Adv. Mater.* **2009**, *21*, 4238–4242.
(24) Zoombelt, A. P.; Leenen, M. A. M.; Fonrodona, M.; Nicolas, Y.; Wienk, M. M.; Janssen, R. A. J. *Polymer* **2009**, *50*, 4564–4570.
(25) Wu, P.-T.; Ren, G.; Jenekhe, S. A. *Macromolecules* **2010**, *43*, 3306–3313.
(26) Piliego, C.; Holcombe, T. W.; Douglas, J. D.; Woo, C. H.; Beaujuge, P. M.; Fréchet, J. M. J. *J. Am. Chem. Soc.* **2010**, *132*, 7595–7597.
(27) Zou, Y.; Najari, A.; Berrouard, P.; Beaupré, S.; Aïch, B. R.; Tao, Y.; Leclerc, M. *J. Am. Chem. Soc.* **2010**, *132*, 5330–5311.
(28) Bartelt, J. A.; Beiley, Z. M.; Hoke, E. T.; Mateker, W. R.; Douglas, J. D.; Collins, B. A.; Tumbleston, J. R.; Graham, K. R.; Amassian, A.; Ade, H.; Fréchet, J. M. J.; Toney, M. F.; McGehee, M. D. *Adv. Energy Mater.* **2013**, *3*, 364–374.
(29) Cabanetos, C.; El Labban, A.; Bartelt, J. A.; Douglas, J. D.; Mateker, W. R.; Fréchet, J. M. J.; McGehee, M. D.; Beaujuge, P. M. *J. Am. Chem. Soc.* **2013**, *135*, 4656–4659.
(30) Koeckelberghs, G.; De Cremer, L.; Persoons, A.; Verbiest, T. *Macromolecules* **2007**, *40*, 4173–4181.
(31) Peet, J.; Senatore, M. L.; Heeger, A. J.; Bazan, G. C. *Adv. Mater.* **2009**, *21*, 1521–1527.
(32) Peet, J.; Cho, N. S.; Lee, S. K.; Bazan, G. C. *Macromolecules* **2008**, *41*, 8655–8659.
(33) Guo, J.; Liang, Y.; Szarko, J.; Lee, B.; Son, H. J.; Rolczynski, B. S.; Yu, L.; Chen, L. X. *J. Phys. Chem. B* **2010**, *114*, 742–748.
(34) Salleo, A. *Mater. Today* **2007**, *10*, 38–45.
(35) Woo, C. H.; Thompson, B. C.; Kim, B. J.; Toney, M. F.; Fréchet, J. M. J. *J. Am. Chem. Soc.* **2008**, *130*, 16324–16329.
(36) Hou, J.; Park, M.-H.; Zhang, S.; Yao, Y.; Chen, L.-M.; Li, J.-H.; Yang, Y. *Macromolecules* **2008**, *41*, 6012–6018.

Chapter 3. Long-Term Thermal Stability of High-Efficiency Polymer Solar Cells Based on Photocrosslinkable Donor-Acceptor Conjugated Polymers[†]

Abstract

Highly-efficient polymer solar cells based on novel photocrosslinkable donor-acceptor conjugated polymers are fabricated and their long-term thermal stability is reported. After 72 h of thermal annealing at 150 °C, a stable power conversion efficiency as high as 4.7% is maintained. The control of active layer morphology and device performance through annealing is correlated with the synthetic design of the photocrosslinkable polymer.

Introduction

Solution processable polymer-based organic photovoltaics (OPVs) have attracted considerable attention over the past two decades because of the many advantages they can provide: low-cost fabrication, flexible devices, and light-weight construction.[1–6] In the most successful OPV device architectures, the photoactive layer is composed of a blend of a p-type conjugated polymer and an n-type fullerene derivative, forming the so-called donor-acceptor bulk heterojunction (BHJ).[7,8]

Recently, the long-term stability of OPV devices has been recognized as an important area of research, both in academia and industry.[9] Concerning this issue, a number of studies have demonstrated the detrimental effects of oxygen and moisture on device operation,[10–13] and attempts have been made to elucidate the degradation mechanism of the photoactive organic layer.[14–16] In addition to chemical degradation pathways, achieving and maintaining an effective BHJ morphology within the active layer is critical for sustaining high OPV performance. In optimized BHJs, phase separation of the electron donor and the electron acceptor domains should be on the same length-scale as the exciton diffusion length, facilitating efficient exciton harvesting.[17] Furthermore, a 3D bicontinuous network of the donor and acceptor materials is necessary for productive charge extraction from the device.[18,19]

Although an optimized BHJ morphology can be attained by means of several processing techniques,[20] the peak-performance morphology only represents a metastable state, which cannot usually be maintained over long operation times. In fact, most BHJ systems show poor stability and often undergo macrophase segregation of the blend components, especially after prolonged exposure to heat.[21,22] Considering that normal OPV device operation may subject the active layer to large temperature fluctuations, improving the robustness of the BHJ with respect to thermal stability is critical.[23,24]

Several studies have reported on the morphological evolution and thermal stability of the active layer in standard BHJ systems such as blends of poly(3-hexylthiophene) (P3HT):[6,6]-phenyl-C_{61}-butyric acid methyl ester ($PC_{61}BM$) or poly[2-methoxy-5-(3',7'-dimethyloctyloxy)-1,4-phenylenevinylene] (MDMO-PPV):$PC_{61}BM$. In such systems, phase segregation in the active layer occurs upon thermal annealing, resulting first in an improvement followed by a quick decline in device performance, particularly at high temperatures.[25–28] In order to improve the thermal stability of these OPV devices, different strategies have been presented, which

[†] Reproduced in part with permission from Griffini, G.; Douglas, J. D.; Piliego, C.; Holcombe, T. W.; Turri, S.; Fréchet, J. M. J.; Mynar, J. L. *Adv. Mater.*, **2011**, *23*, 1660-1664. Copyright 2011 Jon Wiley & Sons, Inc.

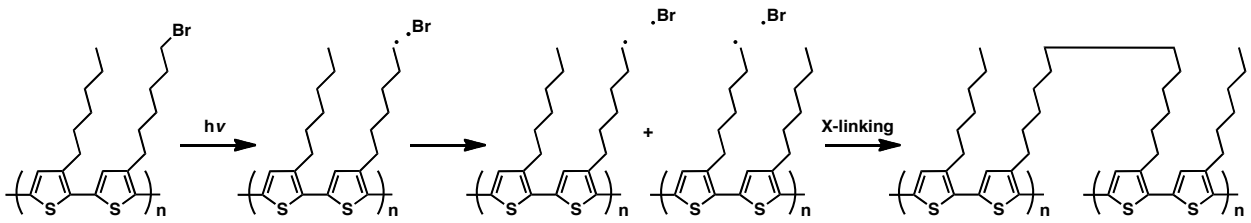

Figure 3.1. A proposed method of photocrosslinking in bromide-containing P3HT.

include the use of diblock copolymer compatibilizers,[29] the use of fullerene-attached diblock copolymers,[30] and the use of both thermally crosslinkable acceptor[31] and donor[32] materials within the active layer. Recently, our group synthesized a library of photocrosslinkable P3HT copolymers containing some light-sensitive bromoalkyl substituents for use as p-type materials in BHJ devices (Figure 3.1). Utilizing these materials, it was shown that even after two days of annealing at an elevated temperature of 150 °C, the devices containing the photocrosslinked polymer within the active layer were able to retain their initial power conversion efficiency (PCE). This result was attributed to the stabilizing effect of the photocrosslinked polymer on the nanoscale morphology of the active layer.[33] In contrast to thermal crosslinking, photocrosslinking does not interfere with the thermal treatments that are often needed during device optimization; thus, this process allows for morphology optimization with independent control of crosslinking and thermal annealing.

Although BHJ devices based on the P3HT:$PC_{61}BM$ blend represent a benchmark in OPV literature, new p-type polymers have been synthesized in an effort to improve device efficiencies.[34–36] In particular, the copolymerization of electron-rich and electron-poor monomers, constituting the so-called donor-acceptor (D-A) approach, has proven to be an effective strategy to obtain low band-gap polymers with optical and electronic properties that can be tuned via synthetic control of the electron-rich and electron-poor units. Using this strategy, reports have demonstrated PCEs approaching 7-8%, after systematic optimization of appropriate device parameters.[37–41] However, the thermal stability of OPVs based on D-A polymers has yet to be investigated in detail: no example of long-term thermally stable devices based on this class of high efficiency p-type polymers has been reported to date.

Herein, we report the first study on the thermal stability of OPV devices based on D-A copolymers. Through a new synthetic pathway, we have developed a photocrosslinkable derivative of the thieno[3,4-*c*]pyrrole-4,6-dione (TPD)-based polymer that was recently reported.[39,41] The new polymer contains TPD repeat units with a terminal, primary bromide functionality appended to the octyl solubilizing group (TPD-Br), thereby allowing for photocrosslinking of the polymer in devices. By synthetically tuning the amount of Br units in the polymer and by employing UV-mediated photocrosslinking, OPV devices with high PCE and excellent thermal stability were fabricated. Devices employing copolymers with varying amounts of Br units were tested: 0% Br units (**TPD-Br0**), 16% Br units (**TPD-Br16**) and 33% Br units (**TPD-Br33**). The best OPV performance after annealing was obtained with photocrosslinked **TPD-Br16**. In contrast to the sharp PCE decrease observed for **TPD-Br0** devices, the annealed OPVs based on photocrosslinked **TPD-Br16** demonstrated remarkable long-term thermal stability. After 72 h of thermal annealing at 150 °C, an average PCE of 4.6% ± 0.1 % was obtained with a short-circuit current density (J_{sc}) of 10.1 mA/cm^2, an open-circuit voltage (V_{oc}) of 0.85 V, and a fill factor (*FF*) of 54%. The maximum PCE obtained was as high as 4.7%. To the best of our knowledge, this represents the highest PCE reported thus far for OPV systems subjected to long-term thermal annealing at high temperature.

Results and Discussion

Our photocrosslinkable D-A copolymer was deigned to contain the TPD and benzodithiophene (BDT) monomers that were developed for **P3** in Chapter 2, and a new alkyl-bromide-containing TPD monomer, TPD-Br. The photocleavable TPD-Br monomer and TPD were synthesized with the same two initial steps, but diverged at anhydride **3** (Scheme 3.1a). Instead of directly installing an alkyl solubilizing group onto the anhydride, as was done for the TPD monomer, the TPD-Br synthesis proceeded by converting anhydride **3** into an unsubstituted imide (**5**). Deprotonation of imide **5**, followed by an S_N2 attack on 1,8-dibromooctane quickly provided the alkyl-bromide-functionalized TPD-Br monomer. Stille cross-coupling with BDT and varying molar ratios of TPD:TPD-Br provided the crosslinkable polymers **TPD-Br16**, and **TPD-Br33**, and non-crosslinkable control polymer **TPD-Br0** (Scheme 3.1b).

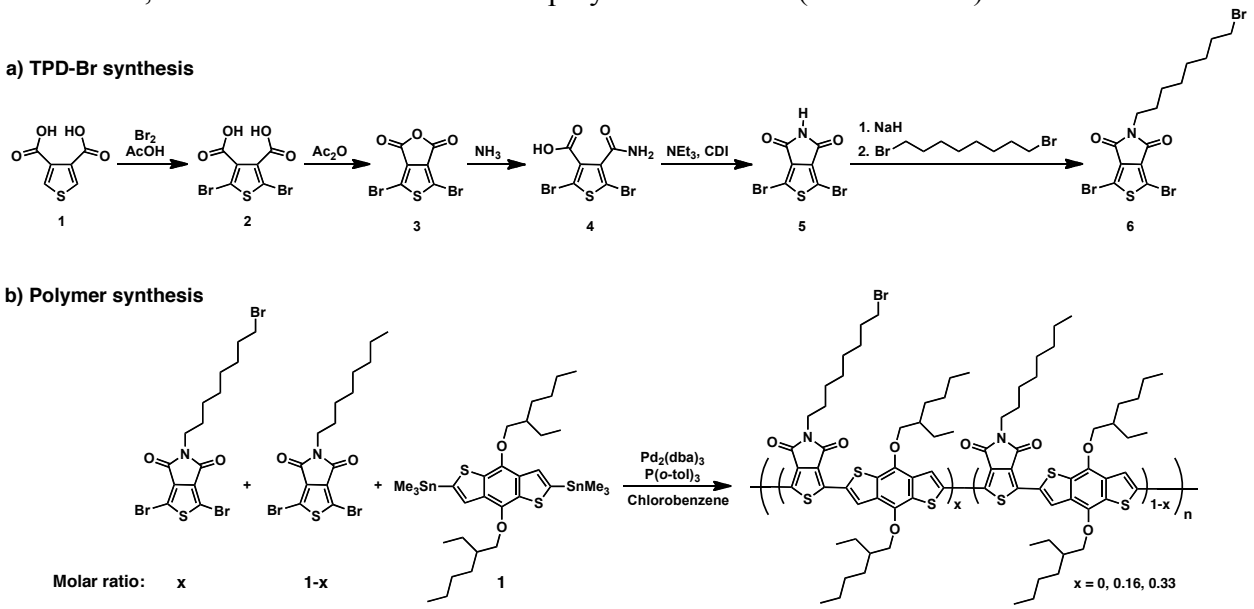

Scheme 3.1. Synthesis of a) the TPD-Br monomer, and b) crosslinkable TPD-Br-containing polymers.

The normalized thin film UV-vis absorption spectra of **TPD-Br16, TPD-Br33**, and **TPD-Br0** show that each of the polymers exhibit three maxima between 400 nm and 700 nm, in accordance with previous reports (Figure 3.2).[39,41] Furthermore, no major differences can be observed between the absorption spectra of the two polymers, indicating that the addition of Br units to the polymer does not significantly affect its optical properties. Figure 3.3a shows the UV-vis absorption spectra of **TPD-Br16** films as-cast and after photocrosslinking. Crosslinking for 45 min under UV-irradiation provides the polymer films with resistance to solvent washing, whereas thermal annealing does not provide solvent resistance (not pictured).[33] The absorption intensity at 550 nm differs by less than 4% between the as-cast film and the UV-irradiated and solvent washed film, indicating that

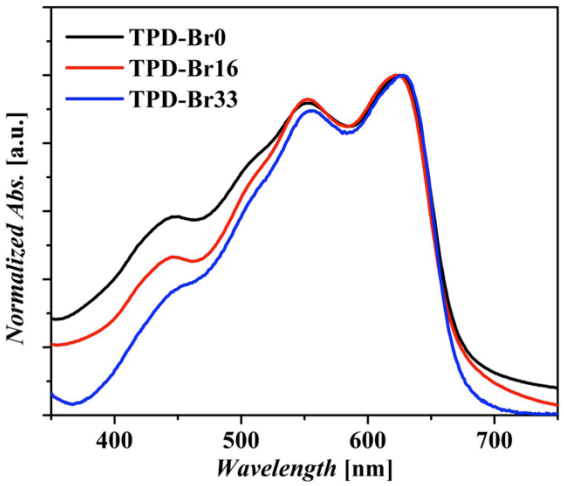

Figure 3.2. The thin-film UV-vis absorption spectra of **TPD-Br0**, **TPD-Br16**, and **TPD-Br33**

photocrosslinking has occurred with the UV-irradiated film. In addition, no major differences between the absorption spectra of as-cast and photocrosslinked films are observed, indicating that the photocrosslinking process does not significantly affect the optical properties of the solid state polymer. A similar trend was observed for **TPD-Br33** thin films (Figure 3.3b), but not for **TPD-Br0**, as evidenced by the solubility of UV-irradiated **TPD-Br0** thin films in chlorobenzene.

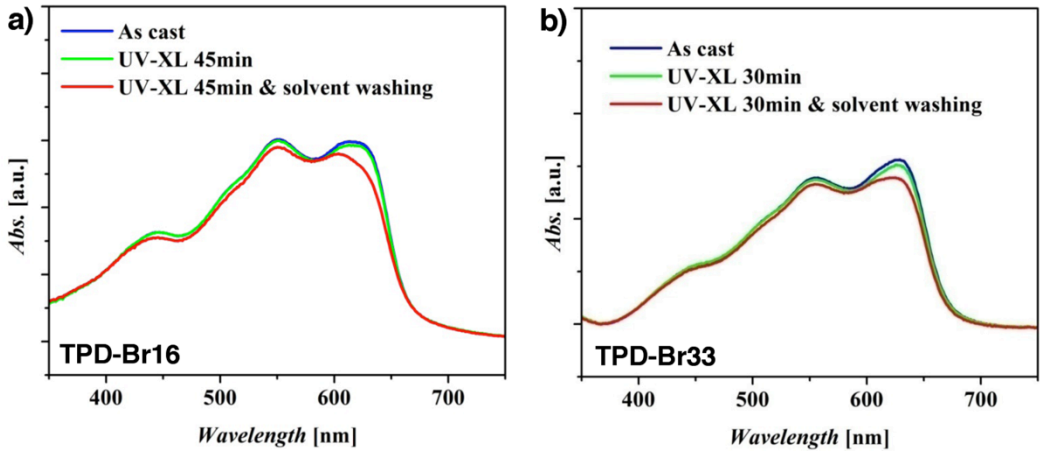

Figure 3.3. The UV-vis absorption spectra of as-cast, UV-irradiated (XL), and UV-irradiated and solvent washed thin films of a) **TPD-Br16** and b) **TPD-Br33**. Complete photocrosslinking and thin-film solvent resistance is obtained after UV-irradiation for 45 min with **TPD-Br16**, and after 30 min with **TPD-Br33**.

The performance of the corresponding OPV devices was investigated using the ITO/PEDOT:PSS/polymer:[6,6]-phenyl-C_{71}-butyric acid methyl ester ($PC_{71}BM$)/Ca/Al device architecture. After optimization of **TPD-Br16** and **TPD-Br33** device parameters, *ortho*-dichlorobenzene (*o*-DCB) was chosen as the solvent for the active layer blend deposition. The blends also do not contain high boiling point solvent additives,[42,43] as they did not improve the performance of **TPD-Br16** and **TPD-Br33** OPV devices. $PC_{71}BM$ was employed as the n-type material because it was found to yield higher device performance compared to $PC_{61}BM$ during device optimization.

The thermal stability of **TPD-Br16** devices is shown in Figure 3.4a, where the performances of both photocrosslinked (**TPD-Br16** XL) and non-photocrosslinked (**TPD-Br16** no XL) devices are shown. For comparison, the thermal stability of **TPD-Br0** devices is also shown. The average device parameters at 0 h and 72 h annealing are listed in Table 3.1. An optimal polymer:$PC_{71}BM$ weight ratio of 1:2 was found for both **TPD-Br0** and **TPD-Br16** polymer systems. The initial performance of **TPD-Br16** no XL devices (5.6% PCE) is comparable to that of **TPD-Br0** devices (5.2% PCE), suggesting that the introduction of a terminal alkyl-bromine functionality on the solubilizing group of TPD does not detrimentally affect the optical properties of the polymer and the photovoltaic performance of the OPV devices, at this incorporation ratio. On the other hand, **TPD-Br16** XL devices show a significantly lower initial PCE (3.3%) with respect to both **TPD-Br0** and **TPD-Br16** no XL. This can be attributed to the effect of crosslinking on the π-stacking of the polymer chains, affecting the electronic properties of the polymer and the OPV device performance.[39] However, a striking difference is observed between **TPD-Br16** XL and the other two devices upon exposure to heat: while both **TPD-Br0** and **TPD-Br16** no XL devices undergo a sharp decrease in performance upon thermal annealing over time, **TPD-Br16** XL devices show an increase in PCE, which stabilizes after 24 h

of annealing. A PCE as high as 4.6% was obtained for the crosslinked polymer exposed to 72 h of annealing at 150 °C. This represents the first demonstration of long-term thermally stable OPV devices based on a D-A copolymer.

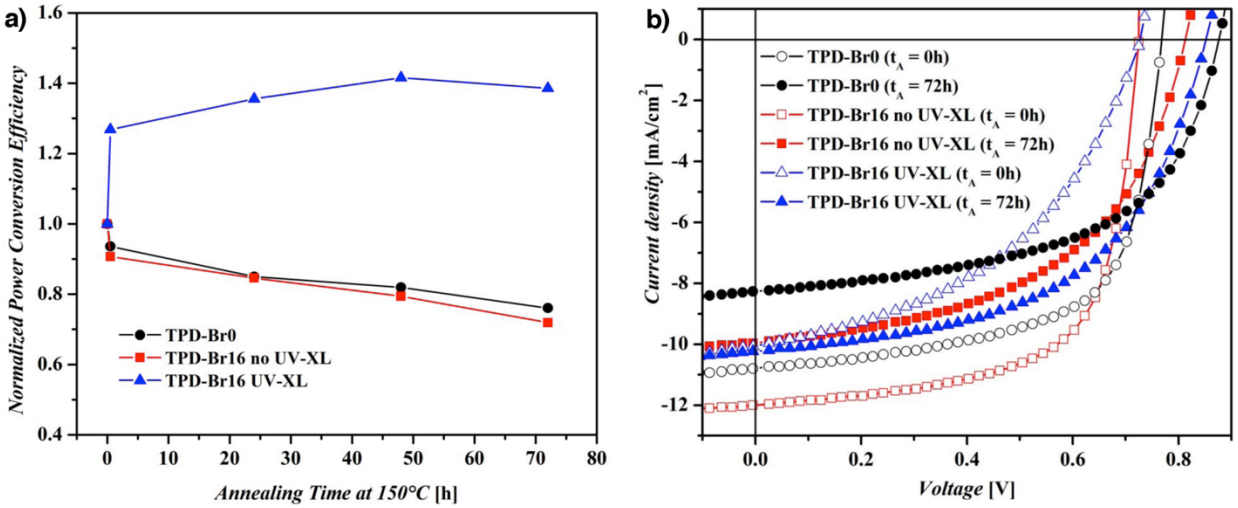

Figure 3.4. a) The normalized power conversion efficiencies of blend devices based on **TPD-Br0**:$PC_{71}BM$ (●), non-photocrosslinked **TPD-Br16**:$PC_{71}BM$ (no UV-XL ■) and photocrosslinked **TPD-Br16**:$PC_{71}BM$ (UV-XL ▲) during long-term thermal annealing at 150 °C. The efficiency of each device was normalized to its initial efficiency (at 0 h). The data shows that photocrosslinked **TPD-Br16**:$PC_{71}BM$ devices do not decrease in performance as significantly as non-crosslinked control devices when subjected to thermal annealing. b) Optimized *J-V* curves of solar cells based on BHJ blends of **TPD-Br0**:$PC_{71}BM$ and **TPD-Br16**:$PC_{71}BM$ before (open symbols, t_A = 0 h) and after (full symbols, t_A = 72 h) long-term thermal annealing (t_A) at 150 °C.

Table 3.1. Photovoltaic performance of **TPD-Br0**:$PC_{71}BM$, **TPD-Br16**:$PC_{71}BM$ and **TPD-Br33**:$PC_{71}BM$ devices

	Film Treatment		Photovoltaic Performance			
	UV-XL[a]	Annealing time (h)	V_{oc} (V)	J_{sc} (mA/cm^2)	*FF*	PCE (%)
TPD-Br0	-	0	0.76	-10.6	64	5.2 (5.3)
	-	72	0.87	-8.2	55	3.9 (4.1)
TPD-Br16	-	0	0.73	-11.7	66	5.6 (5.7)
	-	72	0.81	-9.6	51	4.0 (4.2)
	+	0	0.73	-10.0	45	3.3 (3.3)
	+	72	0.85	-10.1	53	4.6 (4.7)
TPD-Br33	-	0	0.72	-11.6	66	5.5 (5.6)
	-	72	0.80	-8.1	59	3.9 (3.9)
	+	0	0.74	-8.8	45	3.0 (3.1)
	+	72	0.83	-8.7	55	4.0 (4.1)

Average device properties are reported with maximum values in parentheses. [a] Active layers not subjected (-) and subjected (+) to crosslinking under UV-irradiation prior to cathode deposition.

The evolution of device performance with annealing time for the three systems reported in Figure 3.4a can be better understood by analyzing the *J-V* output characteristics recorded at annealing times 0 h and 72 h at 150 °C (Figure 3.4b). An increase in the V_{oc} is observed for all devices after 72 h of annealing at high temperature. This increase may be related to a change in the energy of the interfacial charge-transfer states between polymer and fullerene caused by morphological rearrangement of the fullerene molecules adjacent to the polymer chains after annealing.[44,45] However, both **TPD-Br0** and **TPD-Br16** no XL devices undergo a significant

decrease in their short-circuit current density and fill factor during annealing, which results in a sharp decrease of PCE with respect to the initial values. Conversely, the J_{sc} of **TPD-Br16** XL devices remains constant, even after 72 h of annealing at 150 °C, while the fill factor increases about 18% compared to its initial value. This indicates that photocrosslinking has allowed for an optimal morphology of the active layer to be preserved throughout the entire annealing process, thus leading to remarkable long-term thermal stability of these devices. Similar trends were found for **TPD-Br33** devices, although lower PCEs with respect to **TPD-Br16** were observed for both the non-photocrosslinked and the photocrosslinked systems (Figure 3.5). This indicates that judicious control of the TPD-Br content in the polymer is necessary to ensure optimal photovoltaic performances.

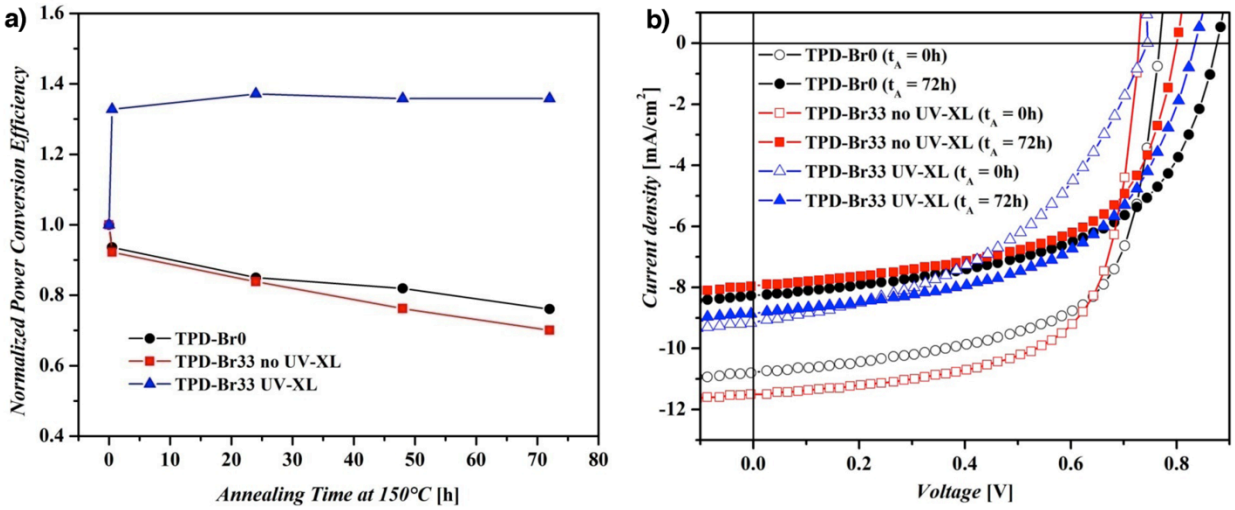

Figure 3.5. a) The normalized power conversion efficiencies of blend devices based on **TPD-Br0**:$PC_{71}BM$ (●), non-photocrosslinked **TPD-Br33**:$PC_{71}BM$ (no UV-XL ■) and photocrosslinked **TPD-Br33**:$PC_{71}BM$ (UV-XL ▲) during long-term thermal annealing at 150 °C. The efficiency of each device was normalized to its initial efficiency (at 0 h). The data shows that photocrosslinked **TPD-Br33**:$PC_{71}BM$ devices do not decrease in performance as significantly as non-crosslinked control devices when subjected to thermal annealing. b) Optimized *J-V* curves of solar cells based on BHJ blends of **TPD-Br0**:$PC_{71}BM$ and **TPD-Br33**:$PC_{71}BM$ before (open symbols, t_A = 0 h) and after (full symbols, t_A = 72 h) long-term thermal annealing (t_A) at 150 °C.

In order to clarify the effect of photocrosslinking on the morphology of the active layer, atomic force microscopy (AFM) was performed on both **TPD-Br16** no XL and **TPD-Br16** UV-XL films (Figure 3.6). Before thermal annealing, the non-photocrosslinked **TPD-Br16** active layer film (Figure 3.6, column 3) shows a well-developed interpenetrating network and similarly fine nanoscale morphology as the photocrosslinked film (Figure 3.6, column 1). The surface root-mean-square (RMS) roughness before annealing is 2.48 nm and 2.08 nm for non-photocrosslinked and photocrosslinked films, respectively. After annealing at 150 °C for 72 h, a very rough surface morphology is observed on the non-photocrosslinked film (Figure 3.6, column 4), resulting in a value of RMS roughness as high as 34.85 nm. This significant morphology change may yield poor contact between the active layer and the electrode, as well as unfavourable conditions for charge separation and transport. Accordingly, a significant decrease in device performance is observed for the **TPD-Br16** no XL device after annealing. On the other hand, a finer morphology is observed for the photocrosslinked film after annealing (Figure 3.6, column 2), which is correlated to the increase in device PCE. Only a slight increase of RMS roughness is observed for this film (up to 3.0 nm), suggesting that photocrosslinking allows for

the preservation of a well-developed, interpenetrating donor-acceptor network that can be maintained, even after 72 h of annealing at 150 °C.

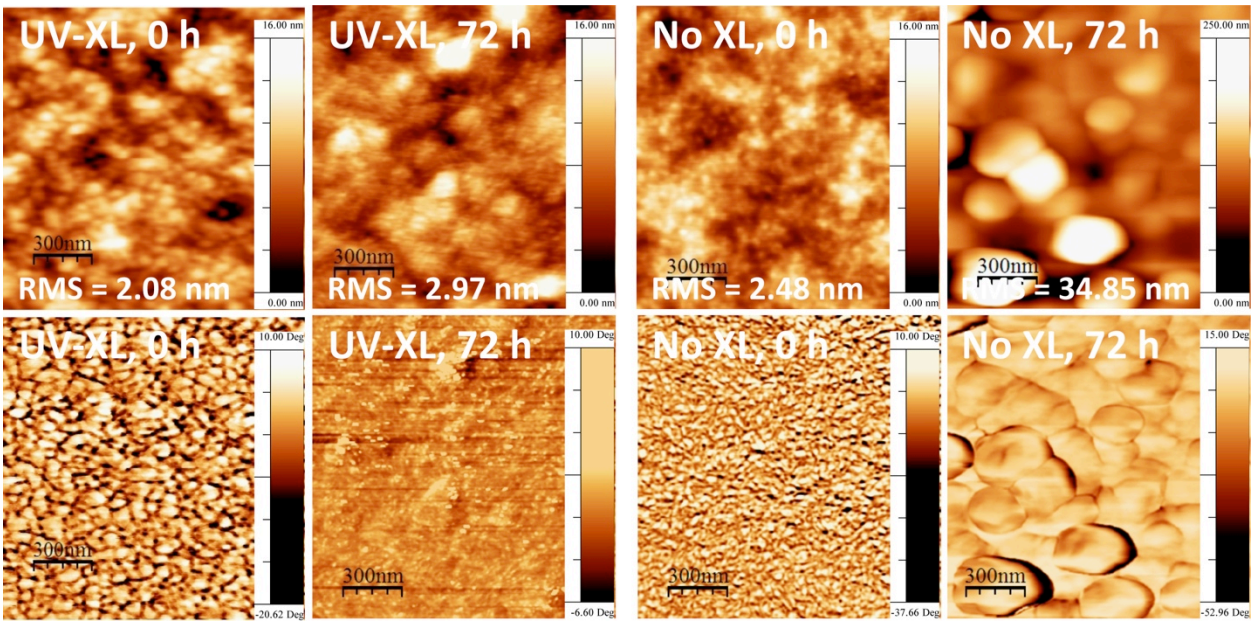

Figure 3.6. Tapping mode atomic force microscopy (AFM) images of **TPD-Br16**:$PC_{71}BM$ active layers. The top row contains topography images and the bottom row contains phase images. The left four images are of the crosslinked films (UV-XL), before and after 72 h of thermal annealing at 150 °C. The right four images are of the non-crosslinked devices (No XL), before and after 72 h of thermal annealing at 150 °C. RMS = root-mean-square roughness of the active layer surface. The images show that photocrosslinked **TPD-Br16**:$PC_{71}BM$ active layers do not phase segregate when subjected to thermal annealing, as compared to non-crosslinked **TPD-Br16**:$PC_{71}BM$ active layers.

It is worth mentioning that during device optimization, each polymer was also tested in BHJ devices with $PC_{61}BM$. As opposed to BHJs containing photocrosslinked polymer and $PC_{71}BM$, devices containing photocrosslinked **TPD-Br16** and $PC_{61}BM$ showed a peak PCE after 30 min annealing at 150 °C that was not maintained after longer annealing times (Figure 3.7). Additionally, AFM analysis revealed the formation of aggregates in both photocrosslinked and non-photocrosslinked active layers after 72 h of annealing at 150 °C, although a rougher surface was found for non-photocrosslinked films (Figure 3.8). We speculate that the different behavior found for **TPD-Br16**:$PC_{61}BM$ blends compared to **TPD-Br16**:$PC_{71}BM$ blends may be related to the different sizes of these fullerene molecules (1.67 vs. 1.92 nm)[46] and their movement during the annealing process. Thermal annealing appears to allow the smaller $PC_{61}BM$ molecules to diffuse within the crosslinked polymer network, initially improving the performance but ultimately leading to formation of larger aggregates, whereas this effect is not observed with $PC_{71}BM$. Due to steric bulkiness, the larger $PC_{71}BM$ molecules may be confined into the polymer network, thus inhibiting the formation of large aggregates. This result may indicate that, in addition to increased light absorption with respect to $PC_{61}BM$, $PC_{71}BM$ is able to provide morphological stability of the active layer at high temperature.

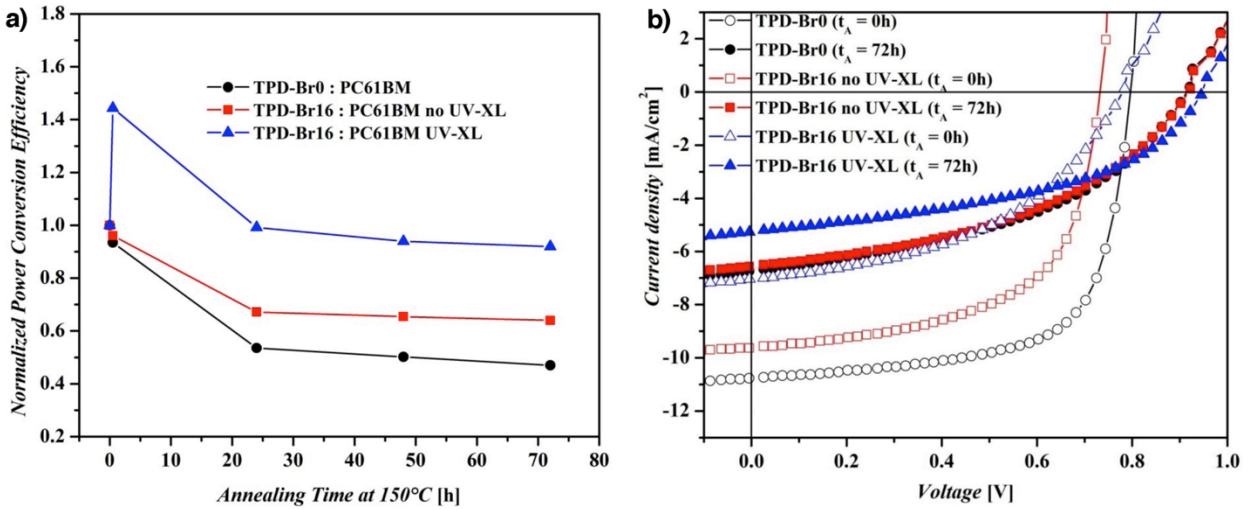

Figure 3.7. a) The normalized power conversion efficiencies of blend devices based on **TPD-Br0**:$PC_{61}BM$ (●), non-photocrosslinked **TPD-Br16**:$PC_{61}BM$ (no UV-XL ■) and photocrosslinked **TPD-Br16**:$PC_{61}BM$ (UV-XL ▲) during long-term thermal annealing at 150 °C. The efficiency of each device was normalized to its initial efficiency (at 0 h). The data shows that photocrosslinked **TPD-Br16**:$PC_{61}BM$ devices and non-crosslinked control devices significantly decrease in performance when subjected to thermal annealing. b) Optimized *J-V* curves of solar cells based on BHJ blends of **TPD-Br0**:$PC_{71}BM$ and **TPD-Br16**:$PC_{71}BM$ before (open symbols, t_A = 0 h) and after (full symbols, t_A = 72 h) long-term thermal annealing (t_A) at 150 °C.

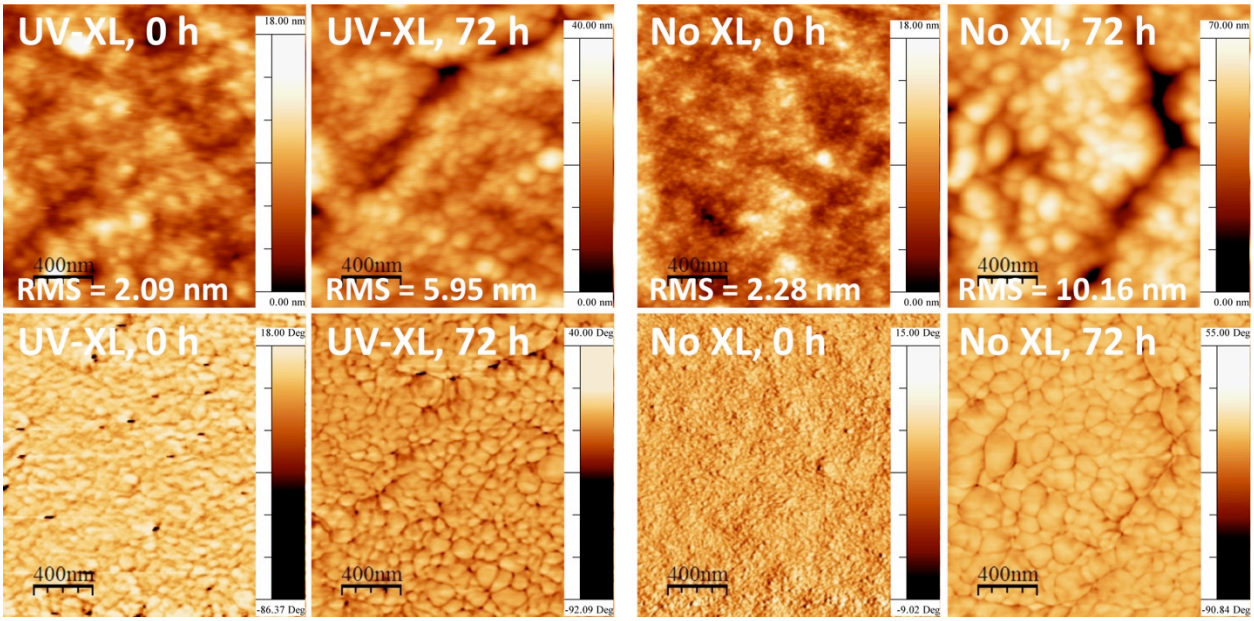

Figure 3.8. Tapping mode atomic force microscopy (AFM) images of **TPD-Br16**:$PC_{61}BM$ active layers. The top row contains topography images and the bottom row contains phase images. The left four images are of the crosslinked films (UV-XL), before and after 72 h of thermal annealing at 150 °C. The right four images are of the non-crosslinked devices (No XL), before and after 72 h of thermal annealing at 150 °C. RMS = root-mean-square roughness of the active layer surface. The images show that photocrosslinked **TPD-Br16**:$PC_{61}BM$ active layers slight phase segregate when subjected to thermal annealing, but not as significantly as non-crosslinked **TPD-Br16**:$PC_{61}BM$ active layers.

Conclusions

In summary, we have developed the first photocrosslinkable donor-acceptor conjugated polymer for use in BHJ organic solar cells. We demonstrated that, after 72 h of thermal annealing at 150 °C, a stable PCE of 4.6% was obtained in devices containing photocrosslinked polymer in the active layer. This represents the highest performance reported thus far for thermally stable OPV devices. Careful control of the crosslinking moiety content in the polymer was found to be critical in order to achieve optimal device performance. The results of our study provide important guidelines for the design and development of OPV materials with long-term thermal stability and high efficiency.

Experimental

Materials.

All commercially available reagents obtained from suppliers were used without further purification. Unless otherwise noted, all reactions were carried out under nitrogen with standard Schlenk techniques, and all glassware used in dry reactions was flame dried under high-vacuum prior to use. Tetrahydrofuran (THF) and dimethylformamide (DMF) were purified and dried by passing through two columns of neutral alumina, under nitrogen, prior to use. Flash chromatography was performed using Silicycle SiliaFlash ® P60 (particle size 40-63 μm, 230-400 mesh) silica gel.

Polymer **TPD-Br0** was synthesized according to the procedure for **P3** in the previous chapter. Building block 4,6-dibromothieno[3,4-*c*]furan-1,3-dione (**3**) and monomers (4,8-bis((2-ethylhexyl)oxy)benzo[1,2-*b*:4,5-*b*']dithiophene-2,6-diyl)bis(trimethylstannane) (BDT-EH) and 1,3-dibromo-5-octyl-4*H*-thieno[3,4-*c*]pyrrole-4,6(5*H*)-dione (TPD-O) were synthesized according to the procedures in the previous chapter.

Material Characterization.

All ^{1}H and ^{13}C NMR spectra were obtained with a Bruker AVQ-400, AVB-400 or AV-500 instrument, and ^{13}C spectra were collected with a proton-decoupling pulse program. NMR abbreviations: bs = broad singlet, m = multiplet, s = singlet, and t = triplet. Data from high-resolution mass spectrometry (HRMS) using electron impact (EI) were obtained by the UC Berkeley mass spectrometry facility.

For polymer molecular weight determination, polymer solutions (1 mg/mL) were prepared using HPLC grade THF. Samples were briefly heated and then allowed to return to room temperature prior to filtering through a 0.45 μm PVDF filter. Size exclusion chromatography (SEC) was performed by passing HPLC grade THF (1.0 mL/min) through three PLgel columns (7.5 x 300 mm) with pore sizes of 10^5, 10^3, and 500 Å. The particle size in the columns was 5 μm and the columns were thermostated at 35 °C. The SEC system consisted of a Waters 510 pump, a Waters 717 autosampler, and a Waters 486 tunable absorption detector. The apparent molecular weights and polydispersities (M_w/M_n) were determined with a calibration based on linear polystyrene standards using Empower software from Waters.

Thin-film UV-vis absorption spectra were gathered at room temperature using a Varian Cary 50 Conc spectrophotometer. Measurements were collected by spincoating an *o*-dichlorobenzene (*o*-DCB) solution (15 mg/mL) of the sample onto ITO-coated glass substrates. The thickness of the thin films was measured by profilometry (Veeco Dektat 150) and determined to be 90±10 nm. A blank ITO-coated glass substrate was used as reference.

Synthesis.

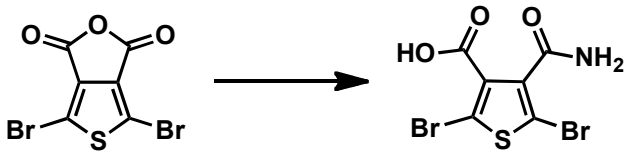

3 **4**

*2,5-Dibromo-4-carbamoylthiophene-3-carboxylic acid (**4**).* Compound **3** (4.00 g, 12.8 mmol) was dissolved in dry THF (12 mL) in a 100 mL flask. Ammonia (7.54 mL of a 5.1 M solution in methanol, 38.5 mmol) was added to the flask and the reaction mixture was stirred at room temperature for 5 minutes. After volatiles were removed from the reaction under reduced pressure, water was added to the flask until the organic residue completely dissolved. The crude product was precipitated by dropwise addition of concentrated hydrochloric acid (3 mL), and then filtered to yield 3.68 g of a white powder (87 %). ^{1}H NMR (400 MHz, DMSO-d_6, δ): 13.46 (bs, 1 H), 7.86 (s, 1 H), 7.62 (s, 1 H). ^{13}C NMR (100 MHz, DMSO-d_6, δ): 163.7, 161.9, 140.9, 133.3, 116.2, 109.8. EI-MS (*m/z*): $[M]^+$ calculated for $C_6H_3Br_2NO_3S$, 328.8180; found, 328.8179.

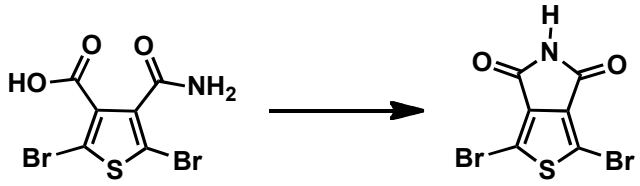

4 **5**

*1,3-Dibromo-4H-thieno[3,4-c]pyrrole-4,6(5H)-dione (**5**).* Triethylamine (2.23 mL, 1.62 g, 16.0 mmol) and then carbonyldiimidazole (2.72 g, 16.8 mmol) were slowly added to a solution of Compound **4** (5.26 g, 16.0 mmol) in dry THF (200 mL) in a 500 mL flask. After stirring for 12 h at room temperature, the reaction mixture was quenched with water, and the reaction contents were extracted with ethyl acetate, washed with a 1.0 M solution of aqueous $NaHSO_4$, dried over $MgSO_4$, and filtered. Volatiles were removed under reduced pressure to yield 4.62 g of a fine white solid (93 %). ^{1}H NMR (500 MHz, DMSO-d_6, δ) 11.57 (s, 1 H). ^{13}C NMR (125 MHz, DMSO-d_6, δ): 161.0, 136.0, 112.5. EI-MS (*m/z*): $[M]^+$ calculated for $C_6HBr_2NO_2S$, 310.8074; found, 310.8080.

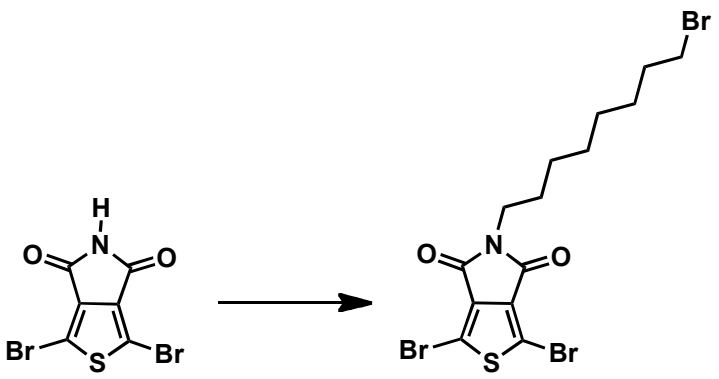

5 **6**

*1,3-Dibromo-5-(8-bromooctyl)-4H-thieno[3,4-c]pyrrole-4,6(5H)-dione (**6** = **TPD-Br**).* Compound **5** (1.00 g, 3.22 mmol) and sodium hydride (0.100 g, 4.18 mmol) were combined in a 50 mL flask, and the reaction vessel was purged with three vacuum/nitrogen cycles before dry DMF (6 mL) was added. The reaction contents were stirred at room temperature for 1 h before being added dropwise to a 50 °C solution of 1,8-dibromooctane (2.62 g, 9.65 mmol) in dry DMF (10 mL). After stirring for 12 h at room temperature, the reaction mixture was quenched with water, and the reaction contents were extracted with diethyl ether, washed with water, dried over $MgSO_4$, and filtered. Volatiles were removed under reduced pressure. The crude material was purified by flash chromatography (80:20 $CHCl_3$:hexanes) and recrystallized (MeOH and $CHCl_3$) to yield 0.534 g of flakey, light yellow crystals (33%). ^{1}H NMR (400 MHz, $CDCl_3$, δ): 3.59 (t, J = 7.25 Hz, 2 H), 3.39 (t, J = 6.84 Hz, 2 H), 1.88-1.79 (m, 2 H), 1.67-1.57 (m, 2 H), 1.46-1.36 (m, 2 H), 1.35-1.26 (m, 6 H). ^{13}C NMR (100 MHz, $CDCl_3$, δ): 160.5, 134.9, 113.1, 38.9, 34.2, 32.8, 29.0, 28.7, 28.3, 28.2, 26.8. EI-MS (*m/z*): $[M]^+$ calculated for $C_{14}H_{16}Br_3NO_2S$, 500.8431; found, 500.8438.

Polymer Synthesis.

TPD-Br16. BDT-EH (200 mg, 259 μmol), TPD-O (91.3 mg, 216 μmol), TPD-Br (21.7 mg, 43.2 μmol), tris(dibenzylideneacetone)dipalladium(0) (7.11 mg, 7.77 μmol), and tri-*o*-tolylphosphine (9.46 mg, 31.1 μmol) were combined in a 50 mL Schlenk flask and the reaction vessel was purged with three vacuum/nitrogen cycles before chlorobenzene (6 mL) was added. The reaction contents stirred at 110 °C for 36 h. A strong complexing ligand (*N*,*N*-diethyl-2-phenyldiazenecarbothioamide, 17.0 mg, 76.8 μmol mmol) was added to the reaction mixture to remove residual catalyst before precipitating the reaction contents into methanol (200 mL). The precipitate was filtered through a Soxhlet thimble and purified via Soxhlet extraction for 2 h with methanol, 2 h with methylene chloride, and was finally collected in chlorobenzene. The chlorobenzene solution was purified by flash chromatography on a mixed column of silica gel, Celite, and neutral alumina (warm chloroform). Volatiles in the eluent were removed under reduced pressure, and the purple solution was precipitated into methanol (200 mL) and filtered to yield 179 mg of a dark purple solid (96 %). SEC analysis: M_n = 28 kDa, M_w = 87 kDa, PDI = 3.1.

TPD-Br33. Synthesized with the same procedure that was used for TPD-Br16 except BDT-EH (200 mg, 259 μmol), TPD-O (73.1 mg, 173 μmol) and TPD-Br (43.3 mg, 86.3 μmol) were copolymerized to yield 188 mg of a dark solid (99 %). SEC analysis: M_n = 28 kDa, M_w = 87 kDa, PDI = 3.1.

Device Fabrication.

All devices were fabricated on ITO-coated glass substrates (pre-patterned,R = 20 Ω/sq, Thin Film Devices, Inc.). The substrates were subjected to successive ultrasonication in de-ionized water (20 min), acetone (20 min) and isopropyl alcohol (20 min). The substrates were then dried under a stream of nitrogen. A thin-layer (40 nm) of filtered PEDOT:PSS (Baytron PH) was spin-coated onto UV-ozone treated ITO substrates at 4000 RPM for 40 s followed by baking at 140 °C for 15 min in air. All substrates were then moved to a nitrogen-filled glove box to perform all the following fabrication steps. Solutions of the polymers (15 mg/mL) and $PC_{71}BM$ (40 mg/mL) in *o*-DCB were prepared separately and stirred overnight at 110 °C. The solutions were passed through a 0.45 μm polytetrafluoroethylene filter, prior to the preparation of the blend solutions. The polymer:$PC_{71}BM$ (**TPD-Br16**:$PC_{71}BM$ = 1:2 wt/wt, **TPD-Br33**:$PC_{71}BM$ = 1:2.5 wt/wt) blend solution (24 mg/mL in *o*-DCB) was spin-coated onto the substrate for 40 sec at 1200 RPM followed by 4 sec at 2000 RPM to produce a film with a thickness of 90-100 nm. UV-mediated photocrosslinking was then performed on the **TPD-Br16** and **TPD-Br33** cast films, by irradiating them with a low-power UV lamp at 254 nm (UV light intensity: 2.1 - 2.4 mW/cm^2). The cathode, consisting of Ca (20nm) and Al (100 nm), was then deposited by thermal evaporation under vacuum (~ 10^{-7} torr) through a shadow mask defining an active device area of 0.03 cm^2. The layout of the shadow mask afforded eight independent devices on each substrate. In order to carry out the thermal stability tests, thermal annealing was performed on complete devices on a temperature-controlled hot plate at 150 °C. Devices were left to cool down to room temperature before testing. During device optimization, different concentrations for the blend solutions and different polymer:$PC_{71}BM$ ratios were tested in order to obtain the optimized process conditions, and the experiments were repeated multiple times to ensure data reproducibility. Eight distinct devices on each substrate were tested.

Device Characterization.

Photocrosslinking was carried out in a nitrogen-filled glove box by irradiating the polymer films with UV light (λ = 254 nm) from a low-power hand-held lamp (2.1 - 2.4 mW/cm^2) with exposure times ranging from 0 to 45 min. To evaluate the extent of photocrosslinking, the irradiated polymer films were immersed in chlorobenzene for 5 min, followed by rinsing with acetone for 3 min, and finally the films were dried under a stream of nitrogen. The UV-vis absorption spectra were then recorded for the polymer films after irradiation and solvent washing, and compared to the UV-vis absorption spectra of the same polymer films prior to irradiation.

Solar cell devices were tested under AM 1.5 G solar illumination at 100 mW/cm^2 (1 sun) using a Thermal-Oriel 150W solar simulator. Current-voltage (*J-V*) curves were measured using a Keithley 2400 source-measure unit.

Tapping-mode atomic force microscopy (AFM) was performed on a Veeco Nanoscope V scanning probe microscope using RTESP tips.

References

(1) Brabec, C. J.; Gowrisanker, S.; Halls, J. J. M.; Laird, D.; Jia, S.; Williams, S. P. *Adv. Mater.* **2010**, *22*, 3839–3856.
(2) Dennler, G.; Scharber, M. C.; Brabec, C. J. *Adv. Mater.* **2009**, *21*, 1323–1338.
(3) Kippelen, B.; Brédas, J.-L. *Energy Environ. Sci.* **2009**, *2*, 251–261.
(4) Thompson, B. C.; Fréchet, J. M. J. *Angew. Chem. Int. Ed.* **2008**, *47*, 58–77.
(5) Krebs, F. C.; Fyenbo, J.; Jørgensen, M. *J. Mater. Chem.* **2010**, *20*, 8994–9001.

(6) Krebs, F. C.; Nielsen, T. D.; Fyenbo, J.; Wadstrøm, M.; Pedersen, M. S. *Energy Environ. Sci.* **2010**, *3*, 512–525.
(7) Yu, G.; Gao, J.; Hummelen, J. C.; Wudl, F.; Heeger, A. J. *Science* **1995**, *270*, 1789–1791.
(8) Yu, G.; Heeger, A. J. *J. Appl. Phys.* **1995**, *78*, 4510–4515.
(9) Jørgensen, M.; Norrman, K.; Krebs, F. C. *Sol. Energy Mater. Sol. Cells* **2008**, *92*, 686–714.
(10) Krebs, F. C.; Spanggaard, H. *Chem. Mater.* **2005**, *17*, 5235–5237.
(11) Krebs, F. C.; Norrman, K. *Prog. Photovoltaics* **2007**, *15*, 697–712.
(12) Reese, M. O.; Morfa, A. J.; White, M. S.; Kopidakis, N.; Shaheen, S. E.; Rumbles, G.; Ginley, D. S. *Sol. Energy Mater. Sol. Cells* **2008**, *92*, 746–752.
(13) Seemann, A.; Egelhaaf, H.-J.; Brabec, C. J.; Hauch, J. A. *Org. Electron.* **2009**, *10*, 1424–1428.
(14) Manceau, M.; Chambon, S.; Rivaton, A.; Gardette, J.-L.; Guillerez, S.; Lemaître, N. *Sol. Energy Mater. Sol. Cells* **2010**, *94*, 1572–1577.
(15) Reese, M. O.; Nardes, A. M.; Rupert, B. L.; Larsen, R. E.; Olson, D. C.; Lloyd, M. T.; Shaheen, S. E.; Ginley, D. S.; Rumbles, G.; Kopidakis, N. *Adv. Funct. Mater.* **2010**, *20*, 3476–3483.
(16) Rivaton, A.; Chambon, S.; Manceau, M.; Gardette, J.-L.; Lemaître, N.; Guillerez, S. *Polym. Degrad. Stab.* **2010**, *95*, 278–284.
(17) Pal, S. K.; Kesti, T.; Maiti, M.; Zhang, F.; Inganäs, O.; Hellström, S.; Andersson, M. R.; Oswald, F.; Langa, F.; Österman, T.; Pascher, T.; Yartsev, A.; Sundström, V. *J. Am. Chem. Soc.* **2010**, *132*, 12440–12451.
(18) Ma, W.; Yang, C.; Gong, X.; Lee, K.; Heeger, A. J. *Adv. Funct. Mater.* **2005**, *15*, 1617–1622.
(19) Yang, X.; Loos, J. *Macromolecules* **2007**, *40*, 1353–1362.
(20) Peet, J.; Senatore, M. L.; Heeger, A. J.; Bazan, G. C. *Adv. Mater.* **2009**, *21*, 1521–1527.
(21) Bertho, S.; Janssen, G.; Cleij, T. J.; Conings, B.; Moons, W.; Gadisa, A.; D'Haen, J.; Goovaerts, E.; Lutsen, L.; Manca, J.; Vanderzande, D. *Sol. Energy Mater. Sol. Cells* **2008**, *92*, 753–760.
(22) Paci, B.; Generosi, A.; Rossi Albertini, V.; Generosi, R.; Perfetti, P.; De Bettignies, R.; Sentein, C. *J. Phys. Chem. C* **2008**, *112*, 9931–9936.
(23) Di Nuzzo, D.; Aguirre, A.; Shahid, M.; Gevaerts, V. S.; Meskers, S. C. J.; Janssen, R. A. J. *Adv. Mater.* **2010**, *22*, 4321–4324.
(24) Helgesen, M.; Bjerring, M.; Nielsen, N. C.; Krebs, F. C. *Chem. Mater.* **2010**, *22*, 5617–5624.
(25) Conings, B.; Bertho, S.; Vandewal, K.; Senes, A.; D'Haen, J.; Manca, J.; Janssen, R. A. J. *Appl. Phys. Lett.* **2010**, *96*, 163301.
(26) Yang, X.; Loos, J.; Veenstra, S. C.; Verhees, W. J. H.; Wienk, M. M.; Kroon, J. M.; Michels, M. A. J.; Janssen, R. A. J. *Nano Lett.* **2005**, *5*, 579–583.
(27) Yang, X.; Van Duren, J. K. J.; Janssen, R. A. J.; Michels, M. A. J.; Loos, J. *Macromolecules* **2004**, *37*, 2151–2158.
(28) Sivula, K.; Luscombe, C. K.; Thompson, B. C.; Fréchet, J. M. J. *J. Am. Chem. Soc.* **2006**, *128*, 13988–13989.
(29) Sivula, K.; Ball, Z. T.; Watanabe, N.; Fréchet, J. M. J. *Adv. Mater.* **2006**, *18*, 206–210.
(30) Miyanishi, S.; Zhang, Y.; Tajima, K.; Hashimoto, K. *Chem. Commun.* **2010**, *46*, 6723–6725.
(31) Drees, M.; Hoppe, H.; Winder, C.; Neugebauer, H.; Sariciftci, N. S.; Schwinger, W.; Schäffler, F.; Topf, C.; Scharber, M. C.; Zhu, Z.; Gaudiana, R. *J. Mater. Chem.* **2005**, *15*, 5158–5163.
(32) Miyanishi, S.; Tajima, K.; Hashimoto, K. *Macromolecules* **2009**, *42*, 1610–1618.
(33) Kim, B. J.; Miyamoto, Y.; Ma, B.; Fréchet, J. M. J. *Adv. Funct. Mater.* **2009**, *19*, 2273–2281.
(34) Bundgaard, E.; Krebs, F. *Solar Energy Materials and Solar Cells* **2007**, *91*, 954–985.
(35) Chen, H.-Y.; Hou, J.; Zhang, S.; Liang, Y.; Yang, G.; Yang, Y.; Yu, L.; Wu, Y.; Li, G. *Nat. Photon.* **2009**, *3*, 649–653.
(36) Li, Y.; Zou, Y. *Adv. Mater.* **2008**, *20*, 2952–2958.
(37) Huo, L.; Hou, J.; Zhang, S.; Chen, H.-Y.; Yang, Y. *Angew. Chem. Int. Ed.* **2010**, *49*, 1500–1503.
(38) Liang, Y.; Xu, Z.; Xia, J.; Tsai, S.-T.; Wu, Y.; Li, G.; Ray, C.; Yu, L. *Adv. Mater.* **2010**, *22*, E135–E138.
(39) Piliego, C.; Holcombe, T. W.; Douglas, J. D.; Woo, C. H.; Beaujuge, P. M.; Fréchet, J. M. J. *J. Am. Chem. Soc.* **2010**, *132*, 7595–7597.
(40) Zhang, Y.; Hau, S. K.; Yip, H.; Sun, Y.; Acton, O.; Jen, A. K. *Chem. Mater.* **2010**, *22*, 2696–2698.
(41) Zou, Y.; Najari, A.; Berrouard, P.; Beaupré, S.; Aïch, B. R.; Tao, Y.; Leclerc, M. *J. Am. Chem. Soc.* **2010**, *132*, 5330–5311.
(42) Hoven, C. V; Dang, X.-D.; Coffin, R. C.; Peet, J.; Nguyen, T.-Q.; Bazan, G. C. *Adv. Mater.* **2010**, *22*, E63–E66.

(43) Lee, J. K.; Ma, W. L.; Brabec, C. J.; Yuen, J.; Moon, J. S.; Kim, J. Y.; Lee, K.; Bazan, G. C.; Heeger, A. J. *J. Am. Chem. Soc.* **2008**, *130*, 3619–3623.
(44) Vandewal, K.; Tvingstedt, K.; Gadisa, A.; Inganäs, O.; Manca, J. V *Phys. Rev. B* **2010**, *81*, 125204.
(45) Perez, M. D.; Borek, C.; Forrest, S. R.; Thompson, M. E. *J. Am. Chem. Soc.* **2009**, *131*, 9281–9286.
(46) Kawauchi, T.; Kumaki, J.; Kitaura, A.; Okoshi, K.; Kusanagi, H.; Kobayashi, K.; Sugai, T.; Shinohara, H.; Yashima, E. *Angew. Chem. Int. Ed.* **2008**, *47*, 515–519.

Chapter 4. Functionalized Isothianaphthene Monomers that Promote Quinoidal Character in Donor-Acceptor Copolymers for Organic Photovoltaics[‡]

Abstract

A series of low band gap isothianaphthene-based (ITN) polymers with various electron-withdrawing substituents and intrinsic quinoidal character were synthesized, characterized and tested in organic photovoltaic (OPV) devices. The three investigated ITN cores contained either ester, imide or nitrile functionalities, and were each synthesized in only four linear steps. The relative electron-withdrawing strength of the three substituents on the ITN moiety was evaluated and correlated to the optical and electronic properties of ITN-based copolymers. The ester- and imide-containing p-type polymers reached device efficiencies as high as 3% in bulk heterojunction blends with phenyl C_{61}-butyric acid methyl ester ($PC_{61}BM$), while the significantly electron-deficient nitrile functionalized polymer behaved as an n-type material with an efficiency of 0.3% in bilayer devices with poly(3-(4-*n*-octyl)-phenylthiophene) (POPT).

Introduction

Organic photovoltaics (OPVs) have attracted considerable attention due to their promise as a flexible and potentially low-cost alternative to commercial silicon-based solar technologies.[1,2] In the highest performing OPVs, the device active layer is comprised of an interpenetrating network of a p-type polymer and an n-type fullerene. To ensure that the polymer absorbs low-energy light and charges are separated at the polymer-fullerene interface, the energy level alignment of both the p- and n-type materials must be considered.[3,4] By designing polymers with alternating electron-rich (donor) and electron-poor (acceptor) backbone components, the HOMO and LUMO of p-type polymers can be modulated to optimize the polymer band gap, energy level offset with a fullerene acceptor, and the open circuit voltage of OPV devices.[5–7] Recently, many performance breakthroughs, with device efficiencies surpassing 7%, have occurred as a result of this donor-acceptor approach.[8–12] In particular, the development of new acceptor monomers with electron-withdrawing substituents has yielded new, high performance polymer backbones.

Alongside substituent effects, polymers with quinoidal character can have favorable electronic properties, including reduced bond length alternation, significant electron delocalization along the polymer backbone, and a narrow band gap.[13,14] One well-known, low band gap polymer with a chemical structure that intrinsically stabilizes its quinoidal state is poly(isothianaphthene) (PITN).[15] The ITN monomer is a bicyclic compound comprised of a phenyl ring fused to the C_3-C_4 bond of thiophene, resulting in competing aromaticity between the two rings. Depending on whether the thiophenyl or phenyl portion of each monomer is aromatized, PITN is stabilized in either its aromatic or quinoidal resonance form, respectively. It has been calculated that the quinoidal form of PITN is 2.4 kcal/mol lower in energy than the aromatic form, as a result of the stronger aromatic stabilization energy of benzene versus thiophene.[16,17] This energy difference imparts significant quinoidal character to the structure of PITN, giving the polymer a uniquely low band gap of about 1.0 eV.[18–20]

[‡] Reproduced in part with permission from Douglas, J. D.; Griffini, G.; Holcombe, T. W.; Young, E. P.; Lee, O. P. Chen, M. S.; Fréchet, J. M. J. *Macromolecules*, **2012**, *45*, 4069-4074. Copyright 2012 American Chemical Society.

PITN, and other low band gap polymers based on ITN, have previously been synthesized by electrochemical or oxidative polymerizations.[21–26] Unfortunately, these polymerization methods produce ITN homo- and copolymers that often have low molecular weights and poor film-forming properties.[27,28] In order to achieve high molecular weight polymers with suitable properties and tunable band gaps, ITN-based copolymers have been synthesized with the donor-acceptor approach, through palladium cross-coupling reactions.[29,30] Synthesis of ITN-based monomers for these copolymers follow the original route, which begins with a substituted benzene that ultimately undergoes a ring closure to form the thiophene portion of isothianaphthene.[22-31] While this route appears short (3 or 4 steps), it requires functional groups and solubilizing chains to be preinstalled on the phenyl ring, decreasing the flexibility of the synthesis.

Herein, we report a new synthetic route toward three functionalized ITN acceptor monomers for donor-acceptor copolymers. In our approach, we construct the ITN core by installing a phenyl ring onto thiophene in a four-step synthesis. This route allows for electron-withdrawing functionality to be added to the monomer in the penultimate step, thereby facilitating the rapid synthesis of a variety of functionalized ITN monomers. By combining the quinoidal character of ITN with electron-withdrawing substituents, we obtain a new class of acceptor monomer for low band gap copolymers that are suitable for OPV applications (Figure 4.1). We further show that ester, imide or nitrile substituents on ITN can control the optoelectronic properties of the resulting donor-acceptor copolymers, including the polymer's OPV performance as a p- or n-type material.

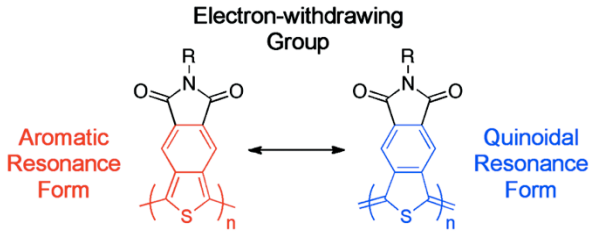

Figure 4.1. Strategy toward ITN-based acceptor monomers.

Results and Discussion

In order to study the effect of different electron-withdrawing substituents on acceptor monomers and conjugated polymers, we investigated 5,6-disubstitued ITN monomers functionalized with either methyl esters (ITN-ME), an alkyl imide (ITN-I) or nitriles (ITN-CN) (Scheme 4.1). Each of the monomers was synthesized in four linear steps and was obtained through a common dialdehyde intermediate (**2**). Thiophene-3,4-dicarbaldehyde (**2**) was synthesized by first reducing thiophene-3,4-dicarboxylic acid with diisobutylaluminium hydride (DIBAL-H) to form diol **1**, which was then oxidized with pyridinium chlorochromate (PCC) to produce **2**. Next, through a one-pot Wittig olefination and Knoevenagel condensation,[32] dialdehyde **2** was reacted with an electron-deficient, disubstituted olefin to yield the functionalized ITN cores: dimethyl maleate was used for ITN-ME, *N*-octylmaleimide for ITN-OI, *N*-(2-ethylhexyl)maleimide for ITN-EHI, and fumaronitrile for ITN-CN. The electron deficiency of these ITN cores was evaluated by the NMR chemical shifts of the two thiophene protons on **3**, **5** and **7**, which appeared at 7.82 ppm, 8.00 ppm and 8.55 ppm, respectively. Because electron-withdrawing functional groups generally deshield adjacent protons, leading to a downfield (higher value) chemical shift, the observed trend confirms that there is increasing electron-deficiency when replacing the diester with an imide, and then with a dinitrile functionality. To complete the comonomer synthesis, the three ITN cores were dibrominated with *N*-bromosuccinimide (NBS) to enable palladium-catalyzed polymerization. Compared to previous

preparations,[21–30] the streamlined synthetic routes presented here offer a new, quick and simple pathway to generate functionalized ITN monomers.

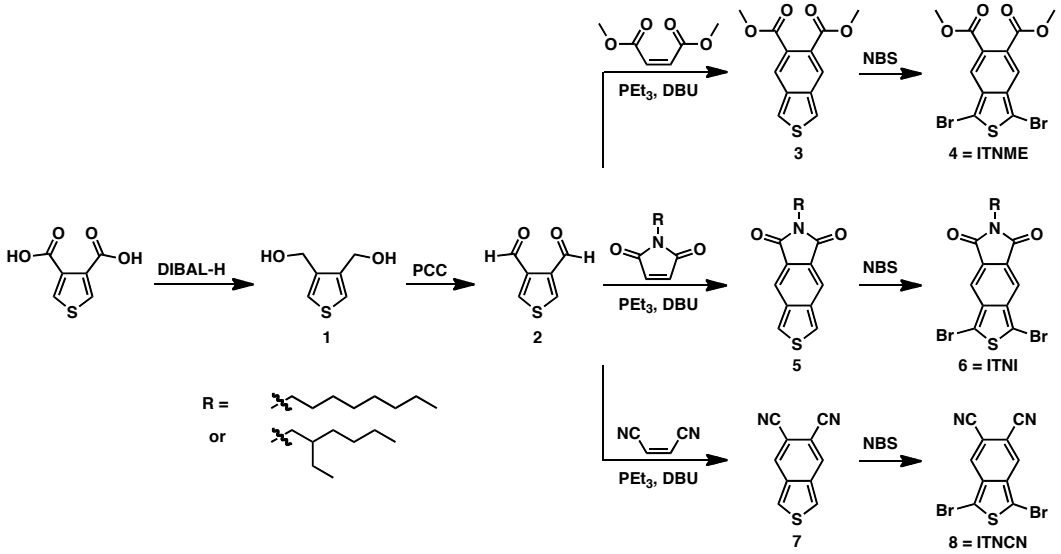

Scheme 4.1. Synthetic route to functionalized ITN monomers ITNME, ITNI, and ITNCN.

It is worth noting that while all three ITN cores were successfully obtained and dibrominated, the ester-functionalized core appeared to be the least oxidatively stable in the series, as **3** became discolored if left at room temperature overnight. The instability of **3** required bromination to be performed immediately upon obtaining the functionalized core; however, despite this precaution, only a small amount of **4** was obtained from the bromination reaction. While this result was disappointing, it was not unexpected, as the unfunctionalized ITN monomer is known to oxidatively polymerize under ambient conditions.[25,31] Interestingly, **5** and **7** can be easily dibrominated with NBS because the electron-withdrawing imide and nitrile functionalities provide increased oxidative stability to the ITN core, leading to a significant improvement in the reaction yield.[26]

ITN monomers **4**, **6** and **8** were Stille cross-coupled with benzodithiophene (BDT) to yield new copolymers. BDT was chosen as the donor monomer because it is known to have a strong propensity to π-stack as a result of its large, planar structure,[33,34] and it has been used in many of the highest performing OPV polymers.[8–10,35,36] For each polymer synthesized, the alkyl side chains on BDT were judiciously chosen to allow for a high level of solution-processability while minimizing excessive side chain length and bulk (Figure 4.2). For **P1** and **P3**, the relatively large 2-butyloctyl (BO) solubilizing group was chosen for BDT because ITN-ME and ITN-CN possess limited solubilizing power. Conversely, for **P2**, smaller side chains were chosen for BDT because ITN-I contains an aliphatic side chain that imparts solubility to the polymer. Additionally, because the size and placement of polymer side chains has been shown to affect OPV device performance,[35,37,38] four different BDT-*co*-ITN-I polymers were synthesized (**P2a-d**). The number-average molecular weight (M_n) and polydispersity index (PDI) of the six new ITN copolymers was measured with size-exclusion chromatography and calibrated with polystyrene standards. All of the polymers reached M_n values between 16 and 43 kDa, with degrees of polymerization above 20, and had PDIs between 2.2 and 4.6 (Table 4.1).

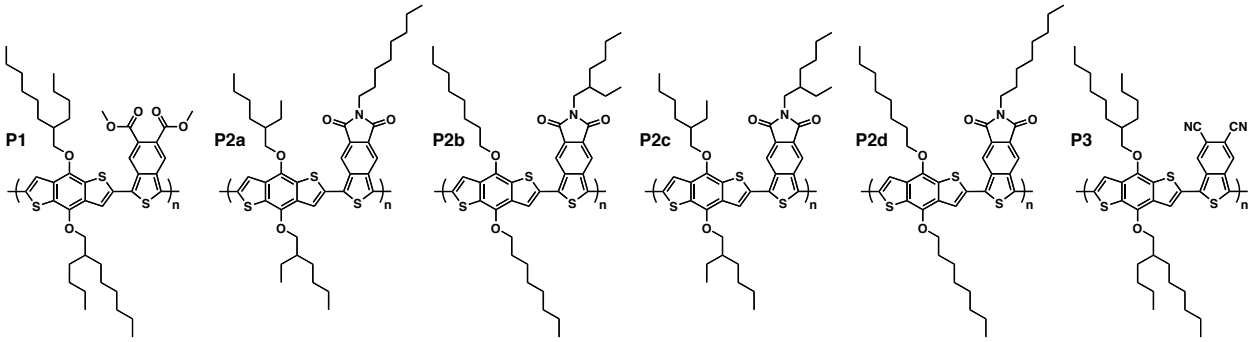

Figure 4.2. Structure of ITN-based polymers **P1**-**P3**.

Toward studying the effect of electron-withdrawing substituents on the synthesized copolymers, the polymer HOMO and LUMO energy levels were determined with cyclic voltammetry (CV) vs. Fc/Fc^{+}, where the half-potential of ferrocene oxidation was set to -5.13 eV vs. vacuum (Figure 4.3). Since electron-withdrawing character is known to lower orbital energy levels,[39,40] it is reasonable that the ITN-ME containing polymer, **P1**, has the highest energy levels in the three-polymer series, whereas the ITN-CN containing polymer, **P3**, has the lowest energy levels (**P1** HOMO = -5.59 eV, LUMO = -3.48 eV; **P3** HOMO = -5.79 eV, LUMO = -4.16 eV). It is worth noting that while the HOMO energy levels of the copolymers experience a slight decrease with increased monomer electron-withdrawing strength, there is a dramatic decrease in LUMO energy levels. This behavior indicates that the electronics of the acceptor monomer has a greater influence on the LUMO of the polymer than on the HOMO.

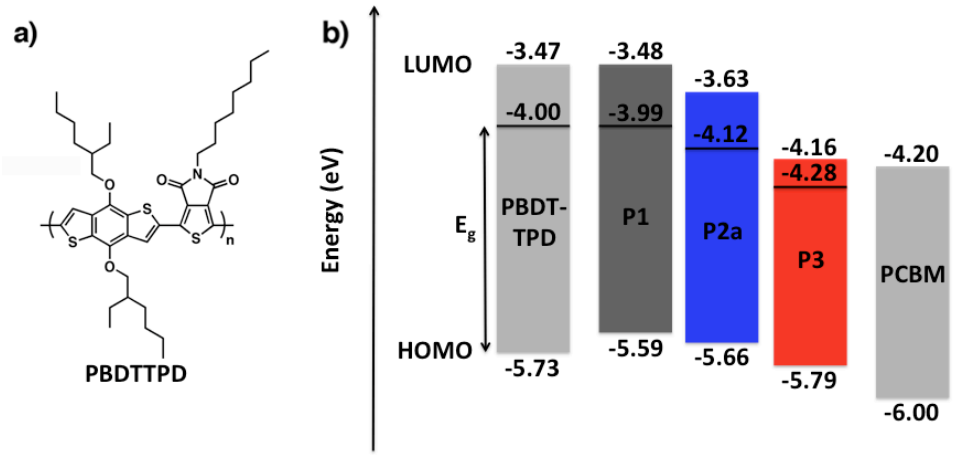

Figure 4.3. a) Structure of **PBDTTPD** and b) energy level alignment of **PBDTTPD**, **P1**, **P2a**, **P3**, and $PC_{61}BM$, where E_g represents the optical band gap.

The effect of quinoidal character on ITN-I was evaluated by comparing the energy levels of **P2a** with **PBDTTPD**, a polymer synthesized by our group that contains a thienopyrroledione (TPD) acceptor monomer and a BDT donor monomer.[35,41,42] Both ITN-I and TPD have imide functionalites, but ITN-I has a quinoidal isothianaphthene core, while TPD has only a thiophene core. With identical solubilizing chains on both **P2a** and **PBDTTPD**, the effect of quinoidal character on the polymer energy levels can be clearly identified. The HOMO of **PBDTTPD** was found to be at a lower oxidation potential (-5.73 eV) than the HOMO of **P2a** (-5.66 eV), showing that quinoidal character destabilizes the polymer HOMO. These data corroborate calculations

that predicted HOMO destabilization and LUMO stabiliziation with increased quinoidal character.[20,43,44]

Solution and thin-film absorption spectra of the ITN copolymers demonstrate favorable overlap with the visible region of the solar emission spectrum (Figure 4.4). In the solid state, the weakly electron-withdrawing ester-containing polymer, **P1**, has an onset of absorption at about 750 nm, making it the material with the largest band gap (E_g) in this series (1.60 eV). Compared to **P1**, the more electron-deficient polymers, **P2a** and **P3**, have considerably red-shifted onsets of absorption and narrower band gaps (1.54 and 1.51 eV, respectively). The strong quinoidal character of ITN contributes to the narrow band gap of these polymers, as revealed by the band gap comparison of **P2a** with **PBDTTPD** (1.73 eV). Although the thin-film band gaps of **P1**, **P2a** and **P3** become narrower with increasing monomer electron-deficiency, the absorption profiles of the polymers in solution do not trend as expected. Nitrile-based polymer, **P3**, has the smallest band gap in thin-films; however, in solution, **P3** has a larger band gap than imide-based polymer **P2a**. While this result is notable, there are physical considerations in addition to electronics that contribute to a material's absorption spectra. For example, in the solid state, increased polymer packing allows for greater electron delocalization though π-π interactions, and a red-shifted

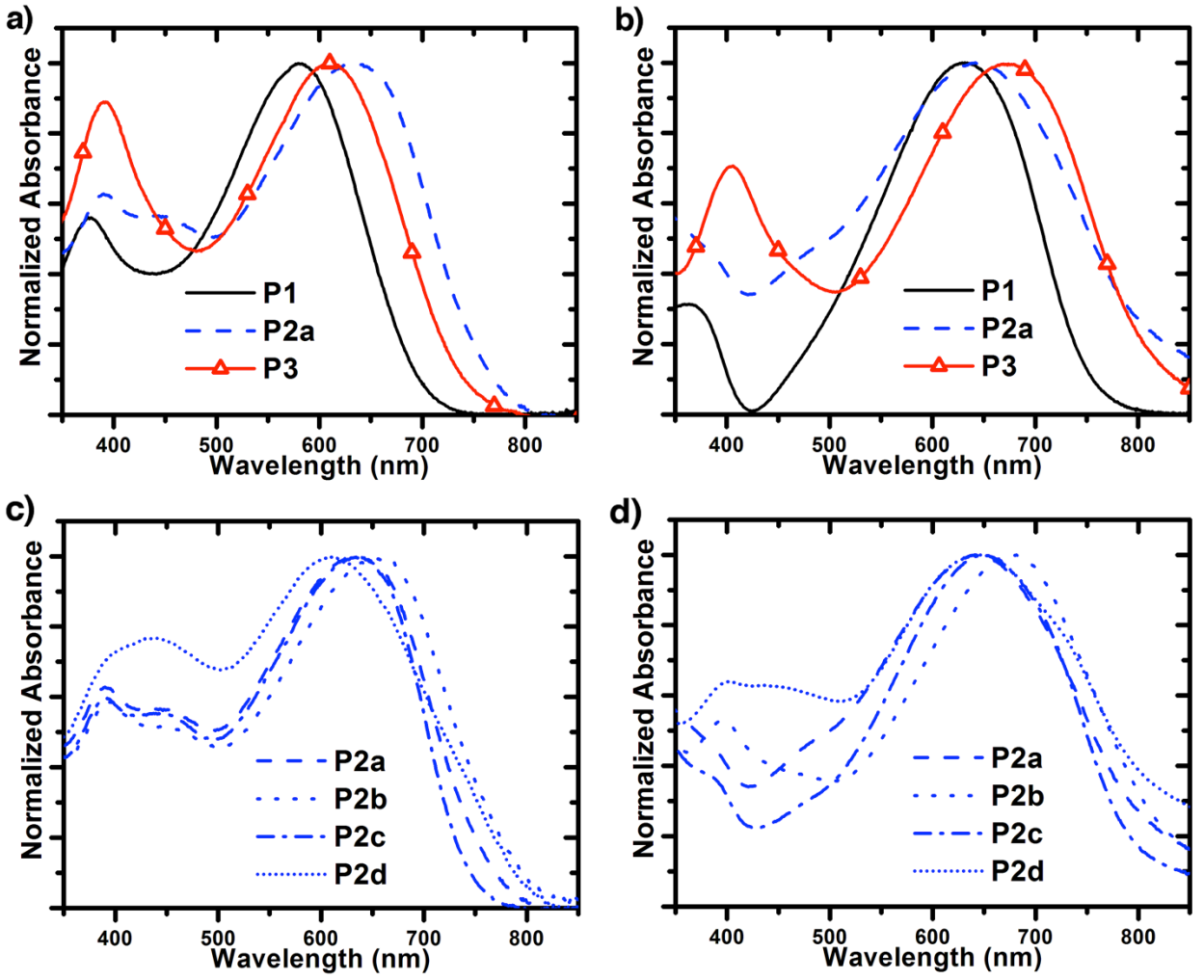

Figure 4.4. UV-vis absorption spectra of ester, imide, and nitrile containing polymers **P1**, **P2a**, and **P3** in a) chloroform solutions and b) thin films. UV-vis absorption spectra of imide-based polymers **P2a-d** in a) chloroform solutions and b) thin films.

absorption may be observed.[45,46] Conversely, in solution, solvent effects may decrease interchain coupling. It is likely that **P3** has less interchain coupling in solution than in thin-films, giving it a larger-than-expected band gap in solution.

The OPV performance of bulk heterojunction (BHJ) devices was investigated with the following device architecture: ITO/PEDOT:PSS/polymer:$PC_{61}BM$/Ca/Al. Each polymer device was individually optimized with processing parameters such as solvents, polymer concentrations, donor-acceptor blend ratios, solvent additives and thermal annealing. With $PC_{61}BM$, **P1** and **P2** have power conversion efficiencies (PCE) between 1.3% and 3.0% (Figure 4.5). Ester-functionalized polymer, **P1**, has an average PCE of 2.7% and does not improve upon addition of solvent additives. With 1,8-diiodooctane or chloronaphthalene as solvent additives, imide-functionalized polymers **P2a**, **P2b** and **P2c** achieve average PCEs between 2.9% and 3.0%, while the less soluble **P2d** polymer reaches an average PCE of 1.3%, which does not improve when employing solvent additives. Interestingly, **P1** has the largest V_{oc} (0.87 V) and the highest HOMO energy level (-5.59 eV) of the polymer series. This result suggests that device V_{oc} is partly influenced by parameters other than the polymer HOMO, and that engineering of the HOMO energy levels alone does not guarantee high V_{oc}.

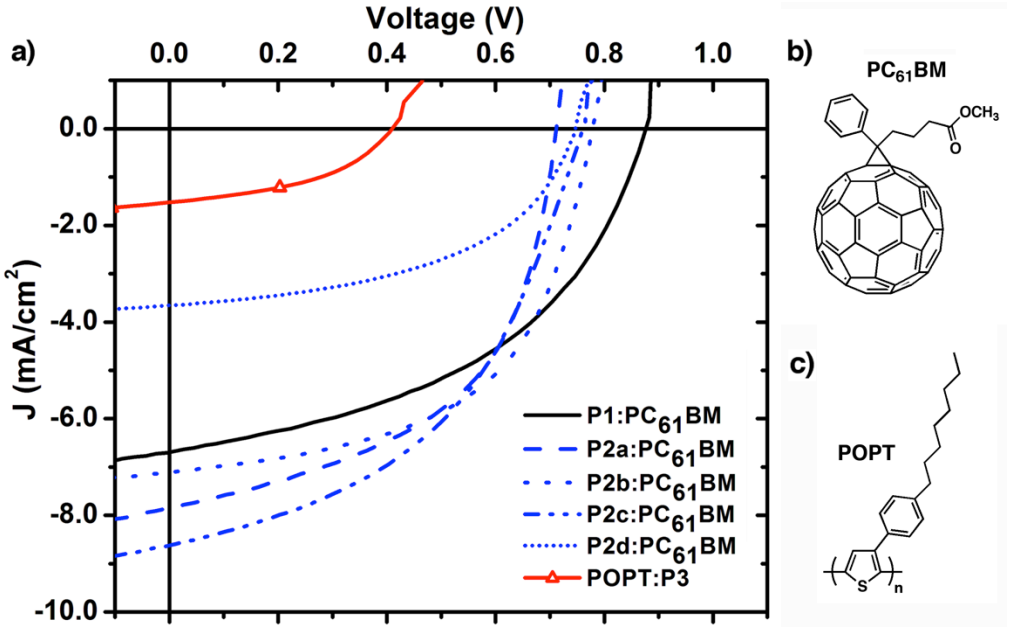

Figure 4.5. a) Optimized *J-V* curves of solar cells based on **P1-P2d** in BHJ blends with $PC_{61}BM$ and a bilayer of **P3** and POPT, under illumination of AM 1.5 G, 100 mW/cm^2. The structure of b) $PC_{61}BM$ and c) poly(3-(4-*n*-octyl)-phenylthiophene) (POPT).

In contrast to **P1** and **P2**, nitrile-substituted **P3** does not perform as a p-type material with $PC_{61}BM$; instead, it functions as an n-type material. To perform as a p-type material, the polymer must have a sufficient excited-state energy level offset with the n-type material; however, in the case of **P3**, the polymer excited state (HOMO + E_g = -4.28 eV) is lower in energy than the LUMO of $PC_{61}BM$ (-4.2 eV),[3] energetically hindering charge separation at the interface. As a result of **P3**'s low energy levels, it was found that **P3** performs as an n-type material when combined with poly(3-(4-*n*-octyl)-phenylthiophene) (POPT) in bilayer devices. Additionally, thermal annealing was found to improve the device performance by one order of magnitude to give solar cells with a maximum PCE of 0.28%.

Table 4.1. Polymer and optoelectronic properties of **P1**-**P3**, and photovoltaic performance of **P1**-**P3** based devices

	Polymer Properties			Optoelectronic Properties			Photovoltaic Performance			
	Functional Group	M_n (kDa)	PDI	HOMO[a] (eV)	LUMO[a] (eV)	E_g[b] (eV)	V_{oc} (V)	J_{sc} (mA/cm^2)	FF	PCE (%)
P1[c]	Ester	24	2.2	-5.59	-3.48	1.60	0.87	6.69	0.46	2.70 (2.74)
P2a[d]	Imide	19	2.2	-5.66	-3.63	1.54	0.71	7.70	0.53	2.88 (2.94)
P2b[e]	Imide	40	4.2	-5.63	-3.63	1.51	0.78	7.05	0.55	3.01 (3.07)
P2c[f]	Imide	43	4.2	-5.69	-3.64	1.57	0.76	8.46	0.47	3.01 (3.04)
P2d[g]	Imide	35	4.6	-5.64	-3.66	1.53	0.75	3.66	0.48	1.32 (1.36)
P3[h]	Nitrile	16	2.3	-5.79	-4.16	1.51	0.39	1.33	0.45	0.24 (0.28)

Average device properties are reported with maximum values in parentheses. [a] CV determined HOMO and LUMO values are reported relative to Fc/Fc^+ at -5.13 eV. [b] Optical band gap in thin films based on onset of absorption. [c] **P1**:$PC_{61}BM$ blend ratio of 1:2.5 in chlorobenzene (CB) with no additives. [d] **P2a**:$PC_{61}BM$ blend ratio of 1:1.5 in CB with 1% vol. 1,8-diiodooctane. [e] **P2b**:$PC_{61}BM$ blend ratio of 1:1.5 in CB with 5% vol. chloronaphthalene. [f] **P2c**:$PC_{61}BM$ blend ratio of 1:1.5 in CB with 1% vol. 1.8-diiodooctane. [g] **P2d**:$PC_{61}BM$ blend ratio of 1:2.5 in CB with no additives. [h] POPT:**P3** bilayer device annealed at 120 °C for 45 min.

Conclusions

We have synthesized a series of new ITN-based donor-acceptor copolymers with strong quinoidal character and various electron-withdrawing substituents that function as active layer materials in OPV devices. The ester, imide and nitrile ITN-derivatives were each obtained through a new and facile synthetic route comprising only four linear steps. We also showed that the electron-withdrawing character of functional groups can strongly influence the polymer electronic behavior, where the ester- and imide-based polymers behave as p-type materials and the nitrile-based polymer performs as an n-type. We were able to fabricate BHJ OPV devices with PCEs up to 3.0% using a **P2b**:$PC_{61}BM$ blend, and all-polymer bilayer devices showing up to 0.28% with **P3** as the n-type material. The three ITN-based acceptor monomers are promising building blocks for a new generation of low band gap polymers with strong quinoidal character. Understanding how to combine quinoidal character with the effect of electron-withdrawing substituents on OPV polymer properties may help to guide the future design of acceptor monomers.

Experimental

Materials.

All commercially available reagents obtained from suppliers were used without further purification. Unless otherwise noted, all reactions were carried out under nitrogen with standard Schlenk techniques, and all glassware used in dry reactions was flame dried under high-vacuum prior to use. Dichloromethane (DCM), tetrahydrofuran (THF), dimethylformamide (DMF), and toluene were purified and dried by passing through two columns of neutral alumina, under nitrogen, prior to use. Flash chromatography was performed using Silicycle SiliaFlash ® P60 (particle size 40-63 μm, 230-400 mesh) silica gel.

P-type material poly(3-(4-*n*-octyl)-phenylthiophene) (POPT) and monomer 2,6-bis(trimethyltin)-4,8-bis(octyloxy)benzo[1,2-*b*:4,5-*b*']dithiophene (BDT-O) were synthesized according to the procedures reported in the literature.[47,48] Monomer 2,6-bis(trimethyltin)-4,8-bis(2-ethylhexyloxy)benzo[1,2-*b*:4,5-*b*']dithiophene (BDT-EH) was synthesized according to the procedure in the previous chapters.

Material Characterization.

All ^{1}H and ^{13}C NMR spectra were obtained with a Bruker AVQ-400, AVB-400 or AV-600 instrument and ^{13}C spectra were measured with a proton-decoupling pulse program. NMR abbreviations: d = doublet, m = multiplet, s = singlet, and t = triplet. Elemental analysis (CHN) was performed by the UC Berkeley microanalysis laboratory. Data from high-resolution mass spectrometry (HRMS) using electron impact (EI) were obtained by the UC Berkeley mass spectrometry facility.

For polymer molecular weight determination, polymer solutions (1 mg/mL) were prepared using HPLC grade THF. Samples were briefly heated and then allowed to return to room temperature prior to filtering through a 0.45 μm PVDF filter. Size exclusion chromatography (SEC) was performed by passing HPLC grade THF (1.0 mL/min) through three PLgel columns (7.5 x 300 mm) with pore sizes of 10^5, 10^3, and 500 Å. The particle size in the columns was 5 μm and the columns were thermostated at 35 °C. The SEC system consisted of a Waters 510 pump, a Waters 717 autosampler, and a Waters 486 tunable absorption detector. The apparent molecular weights and polydispersities (M_w/M_n) were determined with a calibration based on linear polystyrene standards using Empower software from Waters.

Solution and thin-film UV-vis absorption spectra were gathered at room temperature using a Varian Cary 50 Conc spectrophotometer. The absorption spectra in chloroform solutions were measured using a quartz cuvette with a 1 cm path length. Thin-film measurements were collected by spincoating a chloroform solution of the sample onto ITO-coated glass substrates. The thickness of the thin films was measured by profilometry (Veeco Dektat 150) and determined to be 80±10 nm. A blank ITO-coated glass substrate was used as reference.

Cyclic voltammograms (CV) were collected using a Solartron 1285 potentiostat under the control of CorrWare II software. A standard three electrode cell based on a Pt wire working electrode, a silver wire reference electrode (calibrated vs. Fc/Fc^+ at -5.13 eV), and a Pt wire counter electrode was purged with nitrogen and maintained under a nitrogen atmosphere during all measurements. Anhydrous acetonitrile was purchased from Aldrich, and tetrabutylammonium hexafluorophosphate (0.1 M) was used as the supporting electrolyte. Polymer films were drop cast onto a Pt wire working electrode from a 1% (w/w) chloroform solution and dried under nitrogen prior to measurement.

Synthesis.

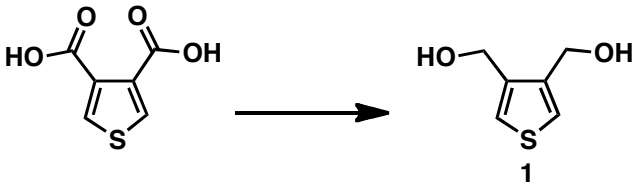

1

*Thiophene-3,4-diyldimethanol (**1**).* Thiophene-3,4-dicarboxylic acid (4.00 g, 23.2 mmol) was combined with dry THF (80 mL) in a 500 mL flask and chilled to 0 °C. Diisobutylaluminium hydride (139 mL, 1.0 M in hexanes, 139 mmol) was then added to the flask, and the reaction contents were stirred for 16 h at room temperature. The reaction mixture was quenched with methanol and water, and then hydrochloric acid (200 mL, 2.0 M) was added to the flask to break-up solid chunks. The reaction mixture was extracted with ethyl acetate (aqueous layer is saturated with sodium chloride), washed with brine, dried over $MgSO_4$, filtered and volatiles were removed under reduced pressure to yield 2.57 g of an orange oil (77 %). The crude product

was used in subsequent reactions without further purification. ^{1}H NMR (400 MHz, DMSO-d_6, δ): 7.26 (s, 2 H), 4.46 (s, 4 H). ^{13}C (100 MHz, DMSO-d_6, δ): 141.7, 122.2, 58.1.

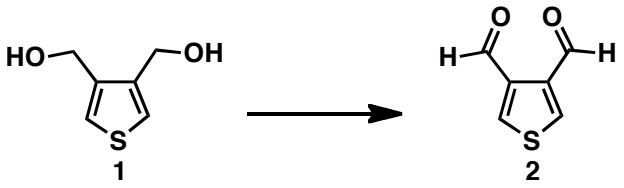

*Thiophene-3,4-dicarbaldehyde (**2**).* Compound **1** (3.80 g, 26.4 mmol) was combined with dry DCM (100 mL) and $MgSO_4$ powder (16 g) in a 250 mL flask. Pyridinium chlorochromate (17.0 g, 79.1 mmol) was added to the flask, and the reaction mixture was stirred for 16 h at room temperature. The reaction mixture was then poured onto a silica pad (DCM), and volatiles from the filtrate were removed under reduced pressure to yield 1.59 g of a white solid (43 %). ^{1}H NMR (400 MHz, $CDCl_3$, δ): 10.25 (s, 2 H), 8.20 (s, 2 H). ^{13}C (100 MHz, $CDCl_3$, δ): 186.0, 140.2, 137.9. EI-MS (*m/z*): $[M]^+$ calculated for $C_6H_4O_2S$, 139.9932; found, 139.9935. Anal. calculated for $C_6H_4O_2S$: C, 51.42; H, 2.88; found: C. 51.43; H, 2.96.

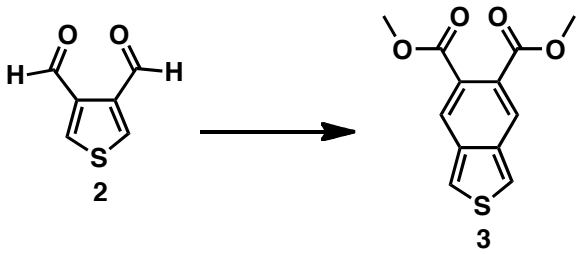

*Dimethyl benzo[c]thiophene-5,6-dicarboxylate (**3**).*[32] Dimethyl maleate (750 mg, 5.21 mmol), Compound **2** (487 mg, 3.47 mmol) and dry DCM (17 mL) were combined in a 100 mL flask and chilled to 0 °C. Triethylphosphine (616 mg, 5.20 mmol) and diazabicycloundecene (53 mg, 0.347 mmol) were combined with dry DCM (5 mL), and then the mixture was added to the reaction flask. After stirring for 1 h at room temperature, volatiles were removed from the reaction under reduced pressure. The crude material was purified by flash chromatography (88:10:2 DCM:hexanes:ethyl acetate) to yield 647 mg of a yellow oil (74 %). The crude product was used without any further purification. ^{1}H NMR (400 MHz, $CDCl_3$, δ): 7.99 (s, 2 H), 7.82 (s, 2 H), 3.85 (s, 6 H). ^{13}C (100 MHz, $CDCl_3$, δ): 168.3, 136.6, 126.4, 125.0, 120.8, 51.8.

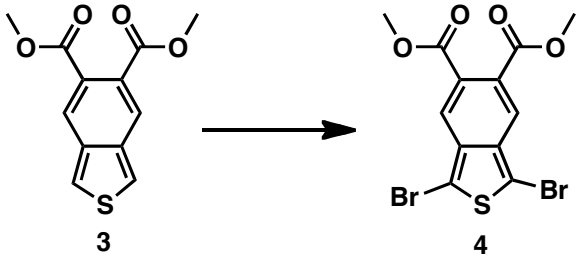

*Dimethyl 1,3-dibromobenzo[c]thiophene-5,6-dicarboxylate (**4** = **ITNME**).* Compound **3** (647 mg, 2.59 mmol) and chloroform (26 mL) were combined in a 100 mL flask and chilled to 0 °C. *N*-Bromosuccinimide (943 mg, 5.30 mmol) was added to the reaction mixture over 20 min, and the reaction mixture was stirred for 30 min while warming to room temperature. Volatiles were removed from the reaction flask under reduced pressure, and the crude product was purified

by flash chromatography (DCM). The product was then recrystallized (acetone) to yield 30 mg of amber colored crystals (3 %). ^{1}H NMR (400 MHz, $CDCl_3$, δ): 7.86 (s, 2 H), 3.92 (s, 6 H). ^{13}C (100 MHz, $CDCl_3$, δ): 167.7, 136.0, 128.2, 123.9, 107.7, 52.9. EI-MS (*m/z*): $[M]^+$ calculated for $C_{12}H_8Br_2O_4S_2$, 407.8490; found, 407.8497. Anal. calculated for $C_{12}H_8Br_2O_4S_2$: C, 35.32; H, 1.98; found: C, 35.59; H, 1.75.

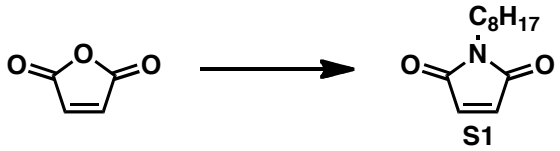

S1

*N-Octylmaleimide (**S1**)*.[49] Octylamine (3.59 g, 27.8 mmol) was dissolved in dry toluene (50 mL) and added to a 500 mL flask containing maleic anhydride (3.00 g, 30.6 mmol) and dry toluene (80 mL). The reaction mixture was heated to 30 °C and stirred for 40 min before adding zinc bromide (6.89 g, 30.6 mmol) and hexamethyl disilazane (6.72 g, 41.6 mmol, in 20 mL dry toluene). After 2 h of heating at 115 °C, the reaction was cooled to room temperature and hydrochloric acid (200 mL, 0.5 M) was added to the flask. The reaction contents were extracted with ethyl acetate, washed with a saturated sodium bicarbonate solution and brine, dried over $MgSO_4$, filtered and volatiles were removed under reduced pressure to yield a brown solid. The crude product was sublimed (100 mTorr, 50 °C) to yield 4.21 g of a white solid (72 %). ^{1}H NMR (600 MHz, $CDCl_3$, δ): 6.67 (s, 2 H), 3.49 (t, *J* = 7.34 Hz, 2 H), 1.56 (m, 2 H), 1.22-1.27 (m, 10 H), 0.86 (t, *J* = 7.01 Hz, 3 H). ^{13}C (150 MHz, $CDCl_3$, δ): 171.0, 134.2, 38.1, 31.9, 29.3, 29.2, 28.7, 26.9, 22.7, 14.2. EI-MS (*m/z*): $[M]^+$ calculated for $C_{12}H_{19}NO_2$, 209.1416; found, 209.1420. Anal. calculated for $C_{12}H_{19}NO_2$: C, 68.87; H, 9.15; N, 6.69; found: C, 69.01; H, 8.90; N, 6.93.

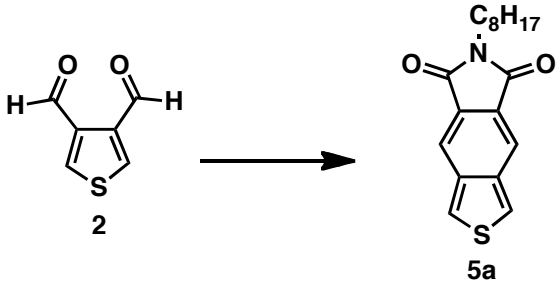

2 **5a**

*Benzo[c]thiophene-N-octyl-5,6-dicarboxyimide (**5a**)*. Compound **2** (600 mg, 4.28 mmol), Compound **S1** (1.34 g, 6.42 mmol) and dry DCM (20 mL) were combined in a 50 mL flask and chilled to 0 °C. Triethylphosphine (759 mg, 6.42 mmol) and diazabicycloundecene (65 mg, 0.428 mmol) were combined with dry DCM (6 mL), and then the mixture was added to the reaction flask. After stirring for 1 h at room temperature, volatiles were removed from the reaction under reduced pressure. The crude material was purified by flash chromatography (DCM) to yield 1.29 g of a white solid (96 %). ^{1}H NMR (600 MHz, $CDCl_3$, δ): 8.11 (s, 2 H), 8.00 (s, 2 H), 3.70 (t, *J* = 7.41 Hz, 2 H), 1.68 (m, 2 H), 1.30-1.34 (m, 4 H), 1.29-1.23 (m, 6 H), 0.85 (t, *J* = 7.04 Hz, 3 H). ^{13}C (150 MHz, $CDCl_3$, δ): 168.0, 138.4, 126.2, 122.9, 119.6, 38.5, 31.9, 29.31, 29.29, 28.6, 27.1, 22.8, 14.2. EI-MS (*m/z*): $[M]^+$ calculated for $C_{18}H_{21}NO_2S$, 315.1293; found, 315.1301. Anal. calculated for $C_{18}H_{21}NO_2S$: C, 68.54; H, 6.71; N, 4.44; found: C, 68.67; H, 6.74; N, 4.71.

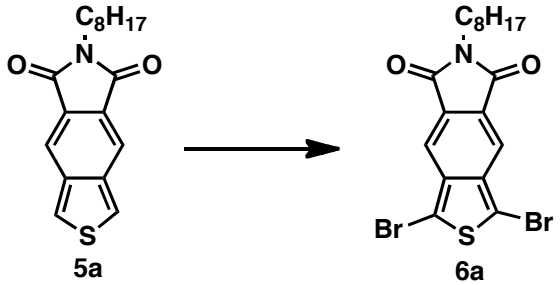

5a 6a

*1,3-Dibromobenzo[c]thiophene-N-octyl-5,6-dicarboxyimide (**6a** = **ITNOI**)*. Compound **5a** (1.29 g, 4.09 mmol) and chloroform (41 mL) were combined in a 100 mL flask and chilled to 0 °C. *N*-Bromosuccinimide (1.49 g, 8.38 mmol) was added to the reaction mixture over 20 min, and the reaction was stirred for 16 h at room temperature. The reaction mixture was quenched with water, extracted with chloroform, washed with a saturated sodium bicarbonate solution and brine, dried over $MgSO_4$, filtered and volatiles were removed under reduced pressure. The crude product was purified by flash chromatography (2:1 DCM:Hexanes) to yield 1.17 g of a yellow solid (61 %). ^{1}H NMR (400 MHz, $CDCl_3$, δ): 7.94 (s, 2 H), 3.72 (t, *J* = 7.38 Hz, 2 H), 1.69 (m, 2 H), 1.33-1.30 (m, 4 H), 1.28-1.25 (m, 6 H), 0.86 (t, *J* = 6.86 Hz, 3 H). ^{13}C (100 MHz, $CDCl_3$, δ): 167.1, 138.0, 127.4, 118.5, 110.1, 38.8, 31.9, 29.3, 28.5, 27.1, 22.8, 14.2. EI-MS (*m/z*): $[M]^+$ calculated for $C_{18}H_{19}Br_2NO_2S$, 472.9483; found, 472.9485. Anal. calculated for $C_{18}H_{19}Br_2NO_2S$: C, 45.69; H, 4.05; N, 2.96; found: C, 45.83; H, 3.88; N, 3.23.

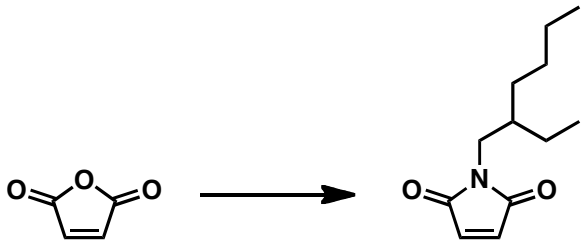

S2

*N-(2-Ethylhexyl)maleimide (**S2**)*. 2-ethylhexylamine (3.59 g, 27.8 mmol) was dissolved in dry toluene (50 mL) and added to a 500 mL flask containing maleic anhydride (3.00 g, 30.6 mmol) and dry toluene (80 mL). The reaction mixture was heated to 30 °C and stirred for 30 min before adding zinc bromide (6.89 g, 30.6 mmol) and hexamethyl disilazane (6.72 g, 41.6 mmol, in 20 mL dry toluene). After 90 min of heating at 110 °C, the reaction mixture was cooled to room temperature and hydrochloric acid (100 mL, 1.0 M) was added to the flask. The reaction contents were extracted with ethyl acetate, washed with a saturated sodium bicarbonate solution and brine, dried over $MgSO_4$, filtered and volatiles were removed under reduced pressure to yield 4.58 g of a clear, light yellow oil (79 %). ^{1}H NMR (600 MHz, $CDCl_3$, δ): 6.66 (s, 2 H), 3.37 (d, *J* = 7.41 Hz, 2 H), 1.68 (m, 1H), 1.27-1.15 (m, 8 H), 0.84 (t, *J* = 7.47 Hz, 3 H), 0.84 (t, *J* = 6.95 Hz, 3 H). ^{13}C (150 MHz, $CDCl_3$, δ): 171.2, 134.0, 41.8, 38.3, 30.5, 28.5, 23.8, 23.0, 14.1, 10.4. EI-MS (*m/z*): $[M]^+$ calculated for $C_{12}H_{19}NO_2$, 209.1416; found, 209.1421. Anal. calculated for $C_{12}H_{19}NO_2$: C, 68.87; H, 9.15; N, 6.69; found: C, 68.64; H, 9.20; N, 6.67.

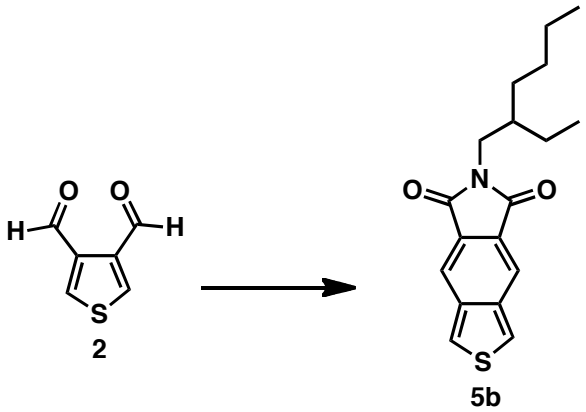

*Benzo[c]thiophene-N-2'-ethylhexyl-5,6-dicarboxyimide (**5b**)*. Compound **2** (590 mg, 4.21 mmol), Compound **S2** (1.32 g, 6.31 mmol) and dry DCM (20 mL) were combined in a 100 mL flask and chilled to 0 °C. Triethylphosphine (746 mg, 6.31 mmol) and diazabicycloundecene (64 mg, 0.421 mmol) were combined with dry DCM (6 mL), and then the mixture was added to the reaction flask. After stirring for 1 h at room temperature, volatiles were removed from the reaction mixture under reduced pressure. The crude material was purified by flash chromatography (DCM) to yield 704 mg of a white solid (53 %). ^{1}H NMR (600 MHz, $CDCl_3$, δ): 8.12 (s, 2 H), 8.01 (s, 2 H), 3.62 (d, *J* = 7.25 Hz, 2 H), 1.88 (m, 1 H), 1.39-1.28 (m, 8 H), 0.92 (t, *J* = 7.46 Hz, 3 H), 0.88 (t, *J* = 7.04 Hz, 3 H). ^{13}C (150 MHz, $CDCl_3$, δ): 168.3, 138.5, 126.2, 122.9, 119.6, 42.4, 38.4, 30.8, 28.7, 24.1, 23.1, 14.2, 10.6. EI-MS (*m/z*): $[M]^+$ calculated for $C_{18}H_{21}NO_2S$, 315.1293; found, 315.1293. Anal. calculated for $C_{18}H_{21}NO_2S$: C, 68.54; H, 6.71; N, 4.44; found: C, 68.69; H, 6.75; N, 4.44.

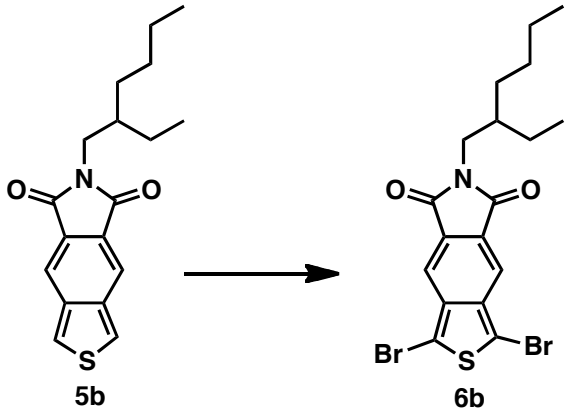

*1,3-Dibromobenzo[c]thiophene-N-2'-ethylhexyl-5,6-dicarboxyimide (**6b** = **ITNEHI**)*. Compound **5b** (677 mg, 2.15 mmol) and chloroform (25 mL) were combined in a 100 mL flask and chilled to 0 °C. *N*-Bromosuccinimide (783 mg, 4.40 mmol) was added to the reaction mixture over 20 min, and the reaction was stirred for 16 h at room temperature. The reaction mixture was quenched with water, extracted with chloroform, washed with a saturated sodium bicarbonate solution and brine, dried over $MgSO_4$, filtered and volatiles were removed under reduced pressure. The crude product was purified by flash chromatography (2:1 DCM:Hexanes) to yield 590 mg of a yellow solid (58 %). ^{1}H NMR (600 MHz, $CDCl_3$, δ): 7.99 (s, 2 H), 3.63 (d, *J* = 7.45 Hz, 2 H), 1.88 (m, 1 H), 1.35-1.27 (m, 8 H), 0.92 (t, *J* = 7.46 Hz, 3 H), 0.88 (t, *J* = 7.05 Hz, 3 H). ^{13}C (150 MHz, $CDCl_3$, δ): 167.5, 138.1, 127.4, 118.6, 110.0, 42.7, 38.3, 30.7, 28.6, 24.1, 23.1, 14.2, 10.6. EI-MS (*m/z*): $[M]^+$ calculated for $C_{18}H_{19}Br_2NO_2S$, 472.9483; found,

472.9478. Anal. calculated for $C_{18}H_{19}Br_2NO_2S$: C, 45.69; H, 4.05; N, 2.96; found: C, 45.73; H, 4.15; N, 2.93.

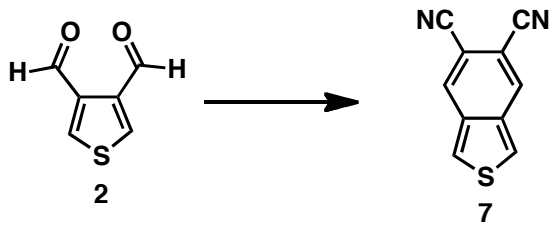

*Benzo[c]thiophene-5,6-dicarbonitrile (**7**)*.[32] Fumaronitrile (1.15 g, 14.7 mmol), Compound **2** (1.59 g, 11.3 mmol) and dry DCM (40 mL) were combined in a 100 mL flask and chilled to 0 °C. Triethylphosphine (1.74 g, 14.7 mmol) and diazabicycloundecene (172 mg, 1.13 mmol) were combined with dry DCM (7 mL), and then the mixture was added to the reaction flask. After stirring for 2 h at room temperature, volatiles were removed from the reaction mixture under reduced pressure. The crude material was purified by flash chromatography (DCM) to yield 1.71 g of a yellow solid (82 %). The crude product was used without any further purification. ^{1}H NMR (600 MHz, DMSO-d_6, δ): 8.63 (s, 2 H), 8.55 (s, 2 H). ^{13}C (150 MHz, DMSO-d_6, δ): 134.8, 132.5, 125.8, 116.9, 105.0.

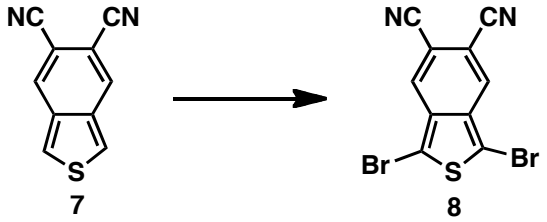

*1,3-Dibromobenzo[c]thiophene-5,6-dicarbonitrile (**8** = **ITNCN**)*. Compound **7** (1.71g, 9.28 mmol) and dry DMF (93 mL) were combined in a 250 mL flask and chilled to 0 °C. *N*-Bromosuccinimide (3.63 g, 20.4 mmol) was added to the reaction mixture over 20 min, and the reaction was stirred for 2 h while warming to room temperature. Volatiles were removed from the reaction flask under reduced pressure, and the crude product was recrystallized (acetone) to yield 1.54 g of fine, olive green needles (48 %). ^{1}H NMR (600 MHz, DCM-d_2, δ): 8.06 (s, 2 H). ^{13}C (150 MHz, DCM-d_2, δ): 135.5, 131.0, 116.3, 111.3, 109.2. EI-MS (*m/z*): $[M]^+$ calculated for $C_{10}H_2Br_2N_2S$, 341.8285; found, 341.8282. Anal. calculated for $C_{10}H_2Br_2N_2S$: C, 35.12; H, 0.59; N, 8.19; found: C, 35.41; H, 0.45; N, 8.06.

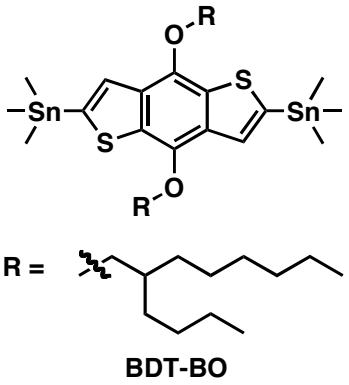

BDT-BO

*2,6-Bis(trimethyltin)-4,8-di(2-butyloctyloxy)benzo[1,2-b:4,5-b']dithiophene (**BDT-BO**)*. **BDT-BO** was synthesized according to the literature procedure[50] except that the crude product was recrystallized (mixed solvent system of ethanol, acetone and methanol) to yield fine, light peach needles (56%). ^{1}H NMR (600 MHz, $CDCl_3$, δ): 7.52 (s, 2 H), 4.19 (d, J = 5.24 Hz, 4 H), 1.86 (m, 2 H), 1.67 (m, 4 H), 1.52-1.33 (m, 28 H), 0.96 (t, J = 6.77 Hz, 6 H), 0.91 (t, J = 6.60 Hz, 6 H), 0.45 (t, J = 27.2 Hz, 18 H). ^{13}C (150 MHz, $CDCl_3$, δ): 143.4, 140.5, 134.0, 133.1, 128.1, 76.0, 39.4, 32.1, 31.6, 31.3, 30.0, 29.4, 27.2, 23.3, 22.9, 14.4, 14.3, -8.2. EI-MS (*m/z*): $[M]^+$ calculated for $C_{40}H_{70}O_2S_2Sn_2$, 884.2855; found, 884.2836. Anal. calculated for $C_{40}H_{70}O_2S_2Sn_2$: C, 54.31; H, 7.98; found: C, 54.57; H, 8.22.

Polymer Synthesis.

Copolymer P1. ITNME (30.0 mg, 73.5 μmol), BDT-BO (65.0 mg, 73.5 μmol) and chlorobenzene (3 mL) were combined in a 50 mL Schlenk flask and degassed with nitrogen for 20 min. Tris(dibenzylideneacetone)dipalladium(0) (2.02 mg, 2.21 μmol), and tri-*o*-tolylphosphine (2.69 mg, 8.82 μmol) were added to the flask and the reaction mixture was stirred for 36 h at 110 °C. A strong complexing ligand (N,N-diethyl-2-phenyldiazenecarbothioamide) was added to the reaction mixture to remove residual catalyst before precipitating the reaction contents into methanol (100 mL). The precipitate was filtered through a Soxhlet thimble and purified via Soxhlet extraction for 2 h with methanol, 4 h with hexanes, and was finally collected in chloroform. The chloroform solution was then concentrated under reduced pressure, precipitated into methanol (100 mL) and filtered to yield 51.5 mg of a dark solid (87 %). SEC analysis: M_n = 24 kDa, M_w = 53 kDa, PDI = 2.2.

Copolymer P2a. Synthesized with the same procedure that was used for **P1** except ITNOI (140 mg, 296 μmol) and BDT-EH (229 mg, 296 μmol) were copolymerized to yield 220 mg of a dark solid (98 %). SEC analysis: M_n = 19 kDa, M_w = 42 kDa, PDI = 2.2.

Copolymer P2b. Synthesized with the same procedure that was used for **P1** except ITNEHI (115 mg, 243 μmol) and BDT-O (188 mg, 243 μmol) were copolymerized to yield 131 mg of a dark solid (71 %). SEC analysis: M_n = 40 kDa, M_w = 168 kDa, PDI = 4.2.

Copolymer P2c. Synthesized with the same procedure that was used for **P1** except ITNEHI (140 mg, 296 μmol) and BDT-EH (229 mg, 296 μmol) were copolymerized to yield 119 mg of a dark solid (53 %). SEC analysis: M_n = 43 kDa, M_w = 181 kDa, PDI = 4.2.

Copolymer P2d. Synthesized with the same procedure that was used for **P1** except ITNOI (100 mg, 211 μmol) and BDT-O (163 mg, 211 μmol) were copolymerized to yield 30.0 mg of a dark solid (19 %). SEC analysis: M_n = 35 kDa, M_w = 161 kDa, PDI = 4.6.

Copolymer P3. Synthesized with the same procedure that was used for **P1** except ITNCN (50.0 mg, 146 μmol) and BDT-BO (129 mg, 146 μmol) were copolymerized to yield 102 mg of a dark solid (94 %). SEC analysis: M_n = 16 kDa, M_w = 37 kDa, PDI = 2.3.

Device Fabrication.

All devices were fabricated on indium tin oxide (ITO) coated glass substrates (pre-patterned, R = 20 Ω /sq, Thin Film Devices, Inc.). Prior to use, the ITO substrates were cleaned by sonication with a surfactant solution (Hellmanex III, 2% in deionized water), deionized water, acetone, and isopropyl alcohol for 20 minutes each. The substrates were rinsed with isopropyl alcohol, dried under a nitrogen stream, and then exposed to UV/O_3 for 5 minutes (UVOCS, Inc. ultraviolet-ozone cleaning system, model T10X10). A thin layer of filtered PEDOT:PSS (Clevios PH, 40 nm) was deposited by spincoating (4000 RPM for 40 s), and then dried on a hotplate for 15 minutes at 140 °C in air. All substrates were then moved to a nitrogen-filled glove box to perform the following fabrication steps.

Bulk heterojunction devices. Solutions of **P1** and **P2a-d** polymers (15 mg/mL) and $PC_{61}BM$ (40 mg/mL) in chlorobenzene (CB) were prepared separately and stirred overnight at 110 °C. The solutions were passed through a 0.45 μm polytetrafluoroethylene (PTFE) filter prior to the preparation of the blend solutions. 1,8-Diodooctane (DIO - purchased from Sigma Aldrich, used as received) with 1% vol. ratio for **P2a** and **P2c** and 1-chloronaphthalene (CN - purchased from Sigma Aldrich, used as received) with 5% vol. ratio for **P2b** were then added to the respective blend solutions and stirred overnight before spin-coating.

Bilayer devices. Solutions of **P3** polymer (4 mg/mL in THF) and POPT (4 mg/mL in CB) were prepared separately and stirred overnight at 50 °C and 110 °C, respectively. The solutions were passed through a 0.45 μm PTFE filter prior to spin-coating.

The active layer solutions were spin-coated at 1200 RPM for 40 sec followed by 1 sec at 2000 RPM, producing films with a thickness of 80-90 nm. Cathodes (20 nm Ca followed by 100 nm Al) were thermally evaporated under vacuum (~10^{-7} torr) through a shadow mask, resulting in eight distinct devices per substrate, each with an active area of ~0.03 cm^2. The **P3**-based bilayer device was thermally annealed at 120°C for 45 minutes by placing the complete device on a temperature-controlled hot plate with the active layer facing up. During device optimization, different solution concentrations and polymer:$PC_{61}BM$ ratios were tested in order to obtain the optimized process conditions, and the experiments were repeated multiple times to ensure data reproducibility. Details of the optimized processing conditions for BHJ devices based on **P1** and **P2a-d** are shown in Table 4.2.

Table 4.2. Optimized processing conditions for BHJ devices based on **P1** and **P2a-d**

	Blend Concentration (mg/mL)	Polymer:$PC_{61}BM$ Blend Ratio	Additive
P1	20	1:2.5	--
P2a	20	1:1.5	1% DIO
P2b	18	1:1.5	5% CN
P2c	20	1:1.5	1% DIO
P2d	18	1:2.5	--

Device Characterization.

Solar cell devices were tested under AM 1.5 G solar illumination at 100 mW/cm^2 (1 sun) using a Thermal-Oriel 150W solar simulator. Current-voltage (*J-V*) curves were measured using a Keithley 2400 source-measure unit.

The thickness of the thin-film active layers was measured by profilometry (Veeco Dektat 150).

References

(1) Günes, S.; Neugebauer, H.; Sariciftci, N. S. *Chem. Rev.* **2007**, *107*, 1324–1338.
(2) Scharber, M. C.; Mühlbacher, D.; Koppe, M.; Denk, P.; Waldauf, C.; Heeger, A. J.; Brabec, C. J. *Adv. Mater.* **2006**, *18*, 789–794.
(3) Thompson, B. C.; Fréchet, J. M. J. *Angew. Chem. Int. Ed.* **2008**, *47*, 58–77.
(4) Zhu, Z.; Waller, D.; Gaudiana, R.; Morana, M.; Mühlbacher, D.; Scharber, M.; Brabec, C. *Macromolecules* **2007**, *40*, 1981–1986.
(5) Havinga, E. E.; Ten Hoeve, W.; Wynberg, H. *Polym. Bull.* **1992**, *126*, 119–126.
(6) Havinga, E. E.; Ten Hoeve, W.; Wynberg, H. *Synt. Met.* **1993**, *57*, 299–306.
(7) Dennler, G.; Scharber, M. C.; Brabec, C. J. *Adv. Mater.* **2009**, *21*, 1323–1338.
(8) Chen, H.-Y.; Hou, J.; Zhang, S.; Liang, Y.; Yang, G.; Yang, Y.; Yu, L.; Wu, Y.; Li, G. *Nat. Photon.* **2009**, *3*, 649–653.
(9) Zhou, H.; Yang, L.; Stuart, A. C.; Price, S. C.; Liu, S.; You, W. *Angew. Chem. Int. Ed.* **2011**, *50*, 2995–2998.
(10) Price, S. C.; Stuart, A. C.; Yang, L.; Zhou, H.; You, W. *J. Am. Chem. Soc.* **2011**, *133*, 4625–4631.
(11) Chu, T.-Y.; Lu, J.; Beaupré, S.; Zhang, Y.; Pouliot, J.-R.; Wakim, S.; Zhou, J.; Leclerc, M.; Li, Z.; Ding, J.; Tao, Y. *J. Am. Chem. Soc.* **2011**, *133*, 4250–4253.
(12) Amb, C. M.; Chen, S.; Graham, K. R.; Subbiah, J.; Small, C. E.; So, F.; Reynolds, J. R. *J. Am. Chem. Soc.* **2011**, *133*, 10062–10065.
(13) Van Mullekom, H. A. M.; Vekemans, J. A. J. M.; Havinga, E. E.; Meijer, E. W. *Mater. Sci. Eng., R* **2001**, *32*, 1–40.
(14) Cheng, Y.-J.; Yang, S.-H.; Hsu, C.-S. *Chem. Rev.* **2009**, *109*, 5868–5923.
(15) Wudl, F.; Kobayashi, M.; Heeger, A. J. *J. Org. Chem.* **1984**, *49*, 3382–3384.
(16) Nayak, K.; Marynick, D. S. *Macromolecules* **1990**, *23*, 2237–2245.
(17) Peart, P. A.; Repka, L. M.; Tovar, J. D. *Eur. J. Org. Chem.* **2008**, 2193–2206.
(18) Kobayashi, M.; Colaneri, N.; Boysel, M.; Wudl, F.; Heeger, A. J. *J. Chem. Phys.* **1985**, *93106*, 5717–5723.
(19) Colaneri, N.; Kobayashi, M.; Heeger, A. J.; Wudl, F. *Synt. Met.* **1986**, *14*, 45–52.
(20) Brédas, J. L.; Heeger, A. J.; Wudl, F. *J. Chem. Phys.* **1986**, *85*, 4673–4678.
(21) Brooke, G. M.; Mawson, S. D. *J. Chem. Soc., Perkin Trans. 1* **1990**, 1919–1923.
(22) Pomerantz, M.; Chaloner-Gill, B.; Harding, L. O.; Tseng, J. J.; Pomerantz, W. J. *Synt. Met.* **1993**, *55*, 960–965.
(23) King, G.; Higgins, S. J. *J. Chem. Soc., Chem. Commun.* **1994**, 825–826.
(24) Burbridge, S. J.; Page, H.; Drury, A.; Davey, A. P.; Callaghan, J.; Blau, W. *J. Mod. Opt.* **1994**, *41*, 1217–1225.
(25) King, G.; Higgins, S. J. *J. Mater. Chem.* **1995**, *5*, 447–455.
(26) Meng, H.; Wudl, F. *Macromolecules* **2001**, *34*, 1810–1816.
(27) Shaheen, S. E.; Vangeneugden, D.; Kiebooms, R.; Vanderzande, D.; Fromherz, T.; F, P.; Brabec, C. J.; Sariciftci, N. S. *Synt. Met.* **2001**, *121*, 1583–1584.
(28) Vangeneugden, D. L.; Vanderzande, D. J. M.; Duisburg, G.; Duisburg, D.- *J. Phys. Chem. B* **2001**, *105*, 11106–11113.
(29) Qin, Y.; Kim, J. Y.; Frisbie, C. D.; Hillmyer, M. a. *Macromolecules* **2008**, *41*, 5563–5570.
(30) Meng, H.; Tucker, D.; Chaffins, S.; Chen, Y.; Helgeson, R.; Dunn, B.; Wudl, F. *Adv. Mater.* **2003**, *15*, 146–149.
(31) Cava, M. P.; Pollack, N. M.; Mamer, O. A.; Mitchell, M. J. *J. Org. Chem.* **1971**, *36*, 3932–3937.
(32) Hsu, D.-T.; Lin, C.-H. *J. Org. Chem.* **2009**, *74*, 9180–9187.
(33) Hou, J.; Park, M.-H.; Zhang, S.; Yao, Y.; Chen, L.-M.; Li, J.-H.; Yang, Y. *Macromolecules* **2008**, *41*, 6012–6018.
(34) Pan, H.; Li, Y.; Wu, Y.; Liu, P.; Ong, B. S.; Zhu, S.; Xu, G. *J. Am. Chem. Soc.* **2007**, *129*, 4112–4113.
(35) Piliego, C.; Holcombe, T. W.; Douglas, J. D.; Woo, C. H.; Beaujuge, P. M.; Fréchet, J. M. J. *J. Am. Chem. Soc.* **2010**, *132*, 7595–7597.
(36) Zhou, H.; Yang, L.; Price, S. C.; Knight, K. J.; You, W. *Angew. Chem. Int. Ed.* **2010**, *49*, 7992–7995.

(37) Szarko, J. M.; Guo, J.; Liang, Y.; Lee, B.; Rolczynski, B. S.; Strzalka, J.; Xu, T.; Loser, S.; Marks, T. J.; Yu, L.; Chen, L. X. *Adv. Mater.* **2010**, *22*, 5468–5472.
(38) Chen, M.-H.; Hou, J.; Hong, Z.; Yang, G.; Sista, S.; Chen, L.-M.; Yang, Y. *Adv. Mater.* **2009**, *21*, 4238–4242.
(39) Roncali, J. *Chem. Rev.* **1997**, *97*, 173–205.
(40) Son, H. J.; He, F.; Carsten, B.; Yu, L. *J. Mater. Chem.* **2011**, *21*, 18934–18945.
(41) Zou, Y.; Najari, A.; Berrouard, P.; Beaupré, S.; Aïch, B. R.; Tao, Y.; Leclerc, M. *J. Am. Chem. Soc.* **2010**, *132*, 5330–5311.
(42) Zhang, Y.; Hau, S. K.; Yip, H.; Sun, Y.; Acton, O.; Jen, A. K. *Chem. Mater.* **2010**, *22*, 2696–2698.
(43) Brédas, J. L. *J. Chem. Phys.* **1985**, *82*, 3808–3811.
(44) Brédas, J. L. *Synt. Met.* **1987**, *17*, 115–121.
(45) Peet, J.; Kim, J. Y.; Coates, N. E.; Ma, W. L.; Moses, D.; Heeger, A. J.; Bazan, G. C. *Nat. Mater.* **2007**, *6*, 497–500.
(46) Mühlbacher, D.; Scharber, M.; Morana, M.; Zhu, Z.; Waller, D.; Gaudiana, R.; Brabec, C. *Adv. Mater.* **2006**, *18*, 2884–2889.
(47) Holcombe, T. W.; Woo, C. H.; Kavulak, D. F. J.; Thompson, B. C.; Fréchet, J. M. J. *J. Am. Chem. Soc.* **2009**, *131*, 14160–14161.
(48) Huo, L.; Hou, J.; Chen, H.-Y.; Zhang, S.; Jiang, Y.; Chen, T. L.; Yang, Y. *Macromolecules* **2009**, *42*, 6564–6571.
(49) Wang, Z.; Kim, C.; Facchetti, A.; Marks, T. J. *J. Am. Chem. Soc.* **2007**, *129*, 13362–13363.
(50) Subramaniyan, S.; Xin, H.; Kim, F. S.; Jenekhe, S. A. *Macromolecules* **2011**, *44*, 6245–6248.

Chapter 5. Non-fullerene Materials for Small-Molecule, Solution-Processed Organic Photovoltaics that Generate Charge Carriers through Hole Transfer[§]

Abstract

Solution-processed organic photovoltaic devices containing p-type and non-fullerene n-type small molecules obtain power conversion efficiencies as high as 2.4%. The optoelectronic properties of n-type material BT(TTI-*n*12)$_2$ allows our devices to display high open-circuit voltages (>0.85 V) and generate charge carriers through hole transfer in addition to the electron transfer pathway, which is common in fullerene-based devices.

Introduction

Organic photovoltaics (OPVs) continue to attract considerable attention for their potential to be flexible, lightweight, and inexpensive devices for power generation.[1–3] Recent synthetic work has primarily focused on the development of p-type polymers for bulk heterojunction (BHJ) devices with fullerene-based phenyl-C_{61}-butyric acid methyl ester ($PC_{61}BM$) and $PC_{71}BM$ as n-type materials. Although polymer:PCBM solar cells have achieved power conversion efficiencies (PCEs) beyond 8%,[4–7] the reproducibility of these OPVs is limited by batch-to-batch variations in the device components.[8,9] Semiconducting polymers are polydisperse, and fullerene derivatives are costly to synthesize and difficult to purify.[10,11] An attractive alternative to polymer:PCBM systems is one comprised entirely of small molecules, none of which are fullerene-based.

Despite their high cost of production, fullerene derivatives have become the canonical n-type material in OPVs due to their unmatched chemical properties that promote efficient exciton dissociation[12,13] and electron transport.[14] The high electron affinities of fullerene derivatives, however, are difficult to tune and often lead to devices with low open-circuit voltages (V_{oc}).[11,15] In addition, fullerene derivatives such as $PC_{61}BM$ are plagued with low extinction coefficients in the visible spectrum[10,16] and a tendency to form large crystallites upon annealing in BHJ blends.[17,18] These characteristics suppress charge generation from the fullerene material because poor light absorption limits exciton generation, and large n-type domains restrict exciton diffusion to an interface and subsequent hole transfer.[19] New n-type materials have the potential to enhance device V_{oc} and photocurrent generation because they can be engineered to exhibit higher LUMO energy levels, stronger absorptions in the visible spectrum, and smaller solid-state domains than fullerene derivatives.

Solution-processable, non-fullerene n-type materials have been investigated as both small molecules and polymers.[20–29] The highest-performing fullerene alternative, reported by Blocking *et al.*, is a small molecule which has obtained an average PCE of 2.3% in blends with poly(3-hexylthiophene) (P3HT).[26] This OPV device has a V_{oc} roughly 0.4 V higher than standard P3HT:$PC_{61}BM$ devices because the new n-type material has a lower electron affinity than PCBM. Non-fullerene materials with higher LUMO energies that can maintain efficient electron transfer are advantageous because they provide favorable energy level alignment between the p- and n-type materials, resulting in devices with maximized voltages.

[§] Reproduced in part with permission from Douglas, J. D.; Niskala, J. R.; Lee, O. P.; Yiu, A. T.; Young, E. P.; Chen, M. S.; Fréchet, J. M. J. *Submitted*, **2013**.

In order to further enhance material purity and the reproducibility of OPV active layers, p-type small molecules have been developed as an alternative to polymers. Small molecules are attractive polymer substitutes because they are intrinsically monodisperse, due to their well-defined chemical structure, and can be definitively purified and characterized.[30–32] Recently, PCEs over 5% have been obtained with solution-processed small molecule:PCBM BHJ devices.[33–39] Much like their polymer counterparts, these high-performing small molecules have been rationally designed to have favorable π-π interactions that enhance molecular interconnectivity. In particular, our group previously developed a diketopyrrolopyrrole-based small molecule (DPP-Py) that self-assembles through planar pyrene end-groups to form highly ordered domains that favor efficient charge transport (Figure 5.1).[40]

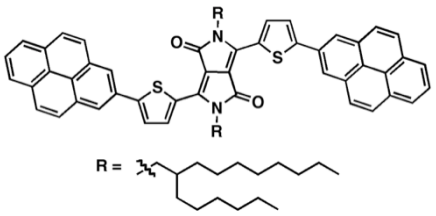

Figure 5.1. Structure of p-type small molecule DPP-Py.

We propose that batch-to-batch variations with polymer synthesis and PCBM purification can be avoided by fabricating small-molecule, non-fullerene devices. By developing both p- and n-type materials with synthetically tunable electronic properties, we can create active layers of monodisperse materials with high purity, complementary absorptions, and optimally aligned energy levels. These features are beneficial for devices since 1) pure materials improve OPV fabrication reproducibility, 2) extended absorption profiles improve exciton generation, and 3) proper energy level alignment enhances device V_{oc} while maintaining efficient exciton dissociation. Active layer materials that have been engineered with the aforementioned properties would provide reproducible solar cells that have two photoactive and charge generating components.

Herein, we demonstrate that solution-processed BHJ solar cells, with efficiencies as high as 2.4%, can be obtained in small-molecule, non-fullerene blends. Compared to PCBM, our n-type materials exhibit improved extinction coefficients and decreased electron affinities, thereby promoting photon absorption and achieving open-circuit voltages above 0.85 V in devices. External quantum efficiency (EQE) analysis shows that photoexcitation of our n-type materials, followed by hole transfer, significantly contributes to charge generation. With an open circuit voltage above 1 V and a fill factor of 0.60, our best DPP-Py:non-fullerene solution-processed OPV represents the highest performing non-fullerene, small-molecule device in the literature.[28]

Results and Discussion

The n-type small molecules presented in this report contain a symmetric donor (D) - acceptor (A) motif of A-D-A-D-A, with solubilizing chains extending from the terminal acceptors (Scheme 5.1). To ensure that the new molecules have a high electron affinity, electron-deficient π-conjugated subunits, benzothiadiazole (BT) and isothianaphthene-nitrile (ITNCN), were chosen for the structural cores. BT is a well-known acceptor monomer that has been incorporated into a variety of high performing p- and n-type materials,[26,41–47] and ITNCN is a promising core that we recently used to synthesize a n-type polymer.[48] As a flanking donor unit, thiophene (T) was appended to the core subunits to extend conjugation and increase the absorption breadth of the small molecules. Phthalimide (PI) and thienoimide (TI) were chosen as the terminal acceptor units for their electron-withdrawing imide functionality and solubilizing aliphatic side chains. In particular, TI was an attractive moiety because of its isomeric relationship to the thienopyrroledione (TPD) building block, which is used in several high-performing OPV polymers.[5,49–51] Since the extent of side-chain branching has been shown to

affect OPV device performance,[49,52–54] linear *n*-dodecyl (*n*12) and 2-ethylhexyl (EH) alkyl groups were appended to the small molecules to provide a range of material processability.

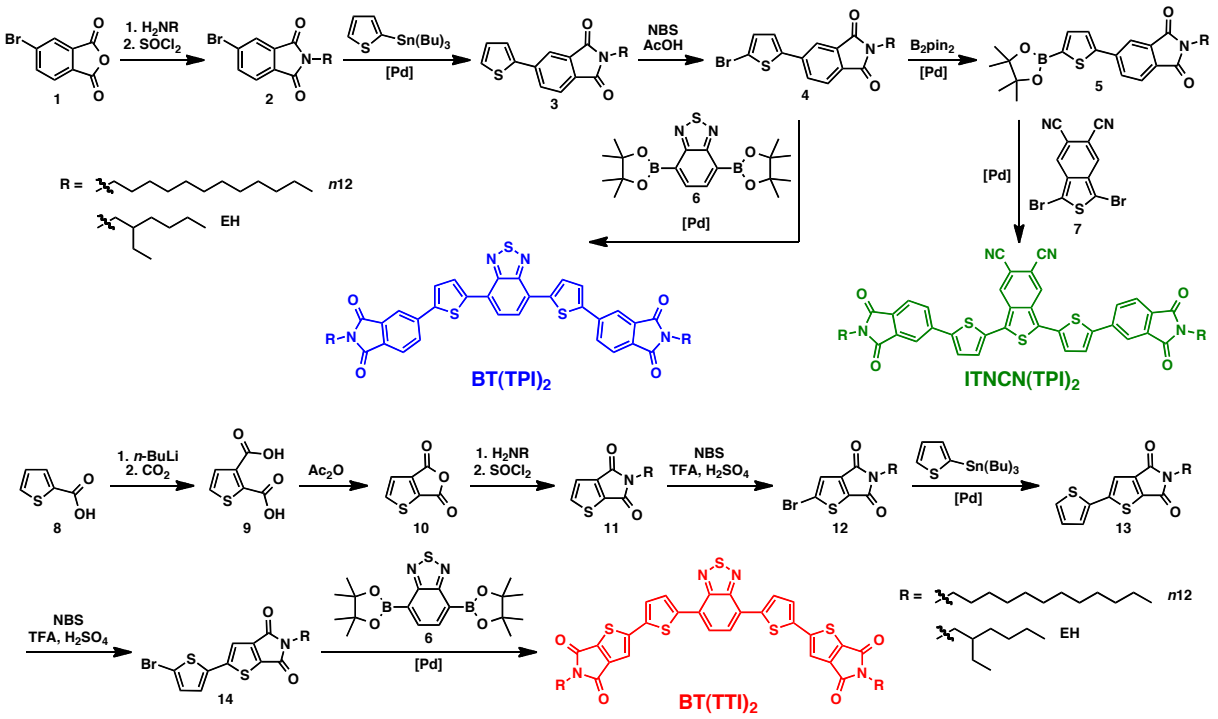

Scheme 5.1. Synthetic routes toward top) phthalimide-functionalized small-molecules $BT(TPI)_2$ and $ITNCN(TPI)_2$, and bottom) thienoimide-functionalized small-molecule $BT(TTI)_2$.

Small-molecules $BT(TPI)_2$, $ITNCN(TPI)_2$, and $BT(TTI)_2$ were synthesized through a convergent route that culminated in a Suzuki cross-coupling between the core (BT or ITNCN) and the end-group coupling partners (TPI or TTI) (Scheme 5.1). Since the PI and TI moieties have side chains that impart solubility to their intermediates, we determined that appending the thiophene linker to the end-group units, rather than the cores, would ease the overall synthesis. The PI-containing coupling partner was synthesized with a bromide (**4**) and a boronate ester (**5**) to allow for cross-coupling with BT (**6**) and ITNCN (**7**), thereby providing $BT(TPI)_2$ and $ITNCN(TPI)_2$, respectively. The TI-based coupling partner was synthesized with a bromide (**14**) and coupled with BT (**6**) to furnish $BT(TTI)_2$.

In order to analyze the conformation of our molecules, we performed density functional theory (DFT) calculations with a hybrid B3LYP correlation functional and a 6-31G(d) basis set. Our calculations show that the BT core is nearly coplanar with its flanking thiophene units, while the ITNCN core is twisted 30.3° (Figures 5.2). The six-membered phthalimide ring was also found to lie out of plane with adjacent thiophene linkers, which leads to $BT(TPI)_2$ and $ITNCN(TPI)_2$ veering from coplanarity by 22.2° and 24.0°, respectively. Although small-molecule $BT(TTI)_2$ was postulated to be the most planar molecule in the series, it also experienced a dihedral twist of 12.0° between its thienoimide end group and thiophene linker units.

The solution (Figure 5.3a) and thin-film (Figure 5.3b) absorption spectra of the six n-type materials show that quinoidal character and backbone coplanarity affect the optical properties of the n-type molecules. With an alternating phenyl-thiophenyl backbone structure, the $BT(TPI)_2$

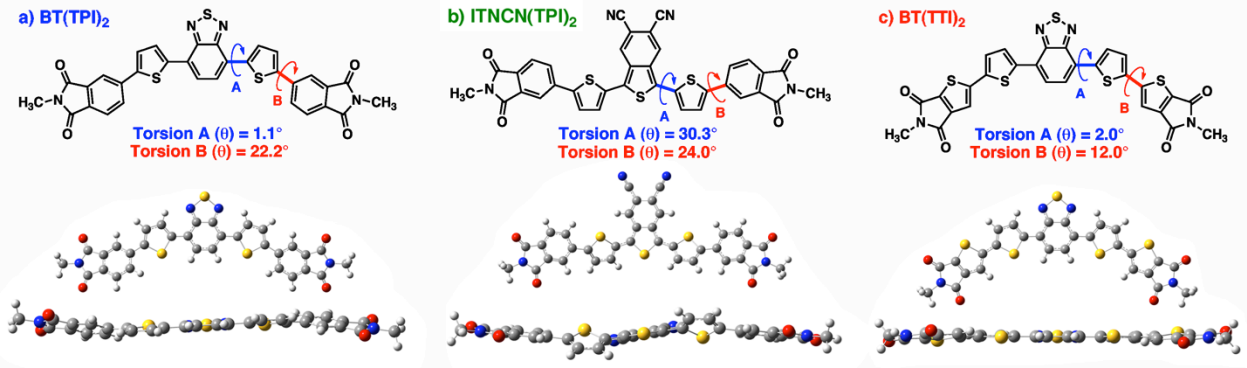

Figure 5.2. DFT calculated torsion angles, and the front and side molecular conformations of n-type molecules a) $BT(TPI)_2$, b) $ITNCN(TPI)_2$, and c) $BT(TTI)_2$.

molecules have the most blue-shifted onsets of absorption (*n*12 at 615 nm and EH at 620 nm) and the largest band gaps (2.02 eV for *n*12 and 2.00 eV for EH) in the series. Replacement of PI for TI yields $BT(TTI)_2$ molecules with an increased degree of coplanarity and slightly lower optical band gaps (1.89 eV for *n*12 and 1.92 eV for EH). Since the $BT(TPI)_2$ and $BT(TTI)_2$ molecules have the same electronic core, this shift in absorption is likely the result of increased intermolecular interaction between the relatively planar $BT(TTI)_2$ molecules. The $ITNCN(TPI)_2$ small molecules have the most red-shifted onsets of absorption (710 nm for *n*12 and EH) in the series because the isothianaphthene portion of the molecules imparts a significant degree of quinoidal character to the compounds, thereby decreasing the band gaps (1.75 eV for *n*12 and EH).[55] Toward broadening the active layer absorption profile, the $BT(TPI)_2$ and $BT(TTI)_2$ small molecules have complementary absorption spectra with p-type material DPP-Py (onset at 710 nm, 1.75 eV band gap). The narrow band gap of DPP-Py gives our small-molecule devices an increased absorption breadth relative to P3HT:non-fullerene devices. In addition, these non-fullerene devices are anticipated to absorb more light than PCBM-based solar cells because all six of the new small molecules exhibit higher extinction coefficients than $PC_{71}BM$ (measured $\alpha = 3.26 \times 10^4$ cm^{-1} at λ_{max}, Table 5.1).

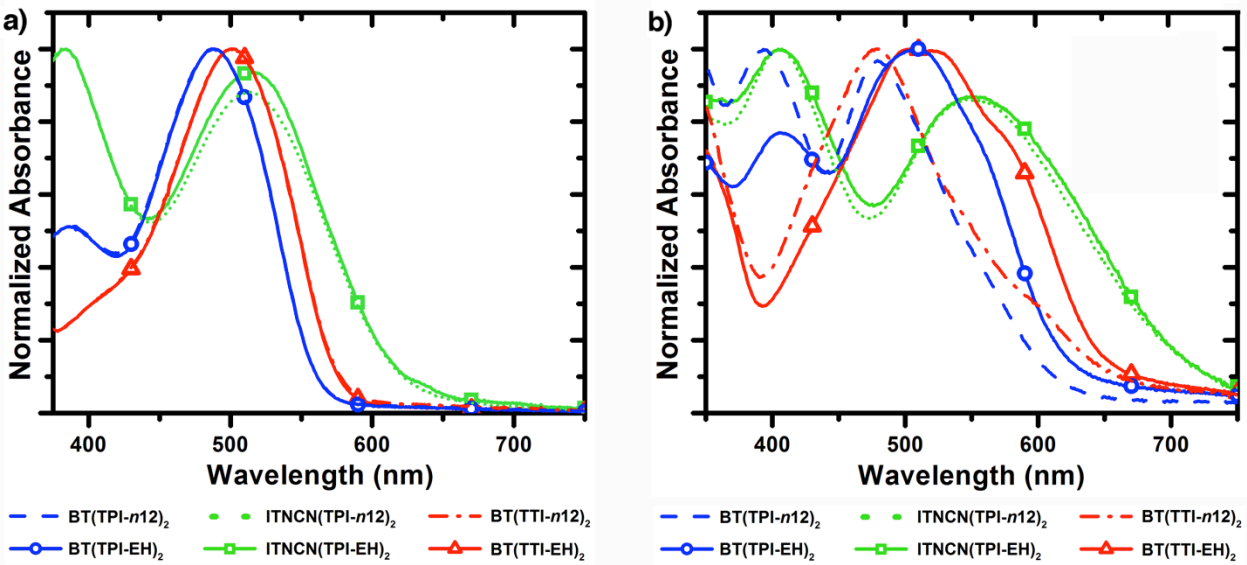

Figure 5.3. UV-vis absorption spectra of n-type molecules $BT(TPI)_2$, $ITNCN(TPI)_2$, and $BT(TTI)_2$ in a) chloroform solutions and b) thin films.

The electrochemical properties of the six small molecules were measured by cyclic voltammetry (CV). The relative HOMO and LUMO energy levels of the materials were strongly influenced by the central acceptor subunits, where ITNCN-containing materials had narrower band gaps than their BT-based counterparts. The competing aromatic and quinoidal resonance forms of isothianaphthene cause ITN-based materials to have a destabilized HOMO and a stabilized LUMO relative to molecules with less quinoidal character.[56,57] For the same molecular backbone, changing the side-chain branching does not significantly affect the material energy levels. In addition, when comparing BT(TPI)$_2$ and BT(TTI)$_2$, the end-groups have minimal influence on the HOMO and LUMO energy levels (variations within 0.1 eV).

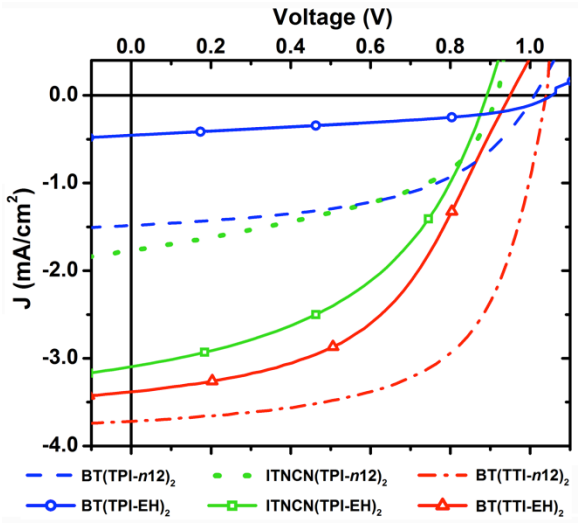

Figure 5.4. Optimized *J-V* curves for DPP-Py:acceptor BHJ devices.

The OPV performance of the non-fullerene materials was evaluated in all-small-molecule BHJ devices with the following architecture: ITO/PEDOT:PSS/DPP-Py:non-fullerene n-type/Ca/Al (Figure 5.4). It was found that annealing at 130 °C improved the performance of all the devices, while solvent additives were not necessary to achieve optimal performance. Under AM 1.5 G illumination at 100 mW/cm^2, devices fabricated with BT(TPI-*n*12)$_2$ and BT(TPI-EH)$_2$ obtained V_{oc} values above 1 V but were plagued with low short-circuit current densities (J_{sc}) and subsequently low PCEs (0.8% and 0.2%, respectively). The relatively low extinction coefficients and narrow absorption ranges of the BT(TPI)$_2$ molecules likely restricted the J_{sc} of these devices. In contrast, the ITNCN(TPI)$_2$ molecules had higher extinction coefficients and broader absorption profiles, which gave ITNCN(TPI)$_2$ devices greater J_{sc} and PCE values. With the highest extinction coefficients and device currents, BT(TTI-*n*12)$_2$ and BT(TTI-EH)$_2$-based solar cells obtained

Table 5.1. Small molecule optoelectronic properties and photovoltaic performance in BHJ devices

Non-fullerene Small Molecule	Optoelectronic Properties				Photovoltaic Performance			
	HOMO[a] (eV)	LUMO[a] (eV)	E_g[b] (eV)	α[c] (x10^4 cm^{-1})	V_{oc} (V)	J_{sc} (mA/cm^2)	FF	PCE (%)
BT(TPI-*n*12)$_2$[d]	5.93	3.47	2.02	5.81	1.01	-1.44	0.54	0.78 (0.85)
BT(TPI-EH)$_2$[e]	5.86	3.55	2.00	8.68	1.07	-0.46	0.41	0.20 (0.23)
ITNCN(TPI-*n*12)$_2$[f]	5.81	3.96	1.75	8.45	0.92	-1.77	0.47	0.77 (0.82)
ITNCN(TPI-EH)$_2$[g]	5.85	3.89	1.75	10.1	0.89	-3.13	0.46	1.29 (1.44)
BT(TTI-*n*12)$_2$[h]	5.99	3.53	1.89	18.5	1.05	-3.72	0.60	2.34 (2.40)
BT(TTI-EH)$_2$[i]	5.96	3.61	1.92	11.0	0.95	-3.37	0.49	1.57 (1.71)

Average device properties are reported with maximum values in parentheses. [a] CV-determined HOMO and LUMO values are reported relative to Fc/Fc$^+$ at -5.13 eV. [b] Optical band gaps in thin films are calculated based on the onset of absorption. [c] Thin-film extinction coefficients were measured at λ_{max}. $PC_{71}BM$ was measured to have and extinction coefficient of 3.26 x 10^4 cm^{-1}. [d] DPP-Py:BT(TPI-*n*12)$_2$ blend ratio of 1:2 in chloroform and annealed at 130 °C for 10 min. [e] DPP-Py:BT(TPI-EH)$_2$ blend ratio of 1:2 in chloroform and annealed at 130 °C for 10 min. [f] DPP-Py:ITNCN(TPI-*n*12)$_2$ blend ratio of 1:1 in chloroform and annealed at 130 °C for 5 min. [g] DPP-Py:ITNCN(TPI-EH)$_2$ blend ratio of 1:1 in chloroform and annealed at 130 °C for 5 min. [h] DPP-Py:BT(TTI-*n*12)$_2$ blend ratio of 1:2 in chloroform and annealed at 130 °C for 15 min. [i] DPP-Py:BT(TTI-EH)$_2$ blend ratio of 1:2 in chloroform and annealed at 130 °C for 15 min.

average efficiencies of 2.3% and 1.6%, respectively. To the best of our knowledge, with a maximum PCE of 2.4%, the solution-processed OPVs based on BT(TTI-*n*12)$_2$ are the highest performing small molecule, non-fullerene devices.

Grazing-incidence X-ray diffraction (GIXD) and atomic force microscopy (AFM) were used to study the device active layer nanostructure and morphology, which could be correlated to overall OPV performance. The nearly planar small molecule BT(TTI-*n*12)$_2$ is the most crystalline material in neat and blended GIXD films (Figures 5.5 and 5.6), contributing to the high J_{sc} of DPP-Py:BT(TTI-*n*12)$_2$ devices (3.72 mA/cm^2). The GIXD data also show that side chains affect intermolecular packing, where EH-substituted materials appear to have less order than their *n*12-substituted counterparts. AFM height images of the active layer surfaces show that the high-performing BT(TTI)$_2$ molecules have the finest intermixing and the lowest RMS roughness (Figure 5.7). Both BT(TTI-*n*12)$_2$ and BT(TTI-EH)$_2$ blends display favorable film morphologies that likely contribute to the molecules' demonstration of high fill factors, short-circuit current density and overall performance in OPV devices. While a nanoscale film morphology is critical for harvesting excitons, other parameters such as energy-level alignment between the p- and n-type materials can strongly influence how charge carriers are separated at the interface.

Energy conversion by an OPV device begins with photon absorption by an active layer component, and subsequent exciton formation via excitation of an electron from the material's HOMO to its LUMO. As an exciton diffuses to a p-n interface, charge carriers can be generated through two mechanisms. In most OPV solar cells, the p-type material is the major light absorber, and excitons formed on the p-type material dissociate into free charges via electron transfer from the LUMO$_{p\text{-type}}$ to the LUMO$_{n\text{-type}}$.[58] In contrast, when a n-type material absorbs light, free charges are formed upon hole transfer from the photogenerated vacancy on the HOMO$_{n\text{-type}}$ to the HOMO$_{p\text{-type}}$.[59,60]

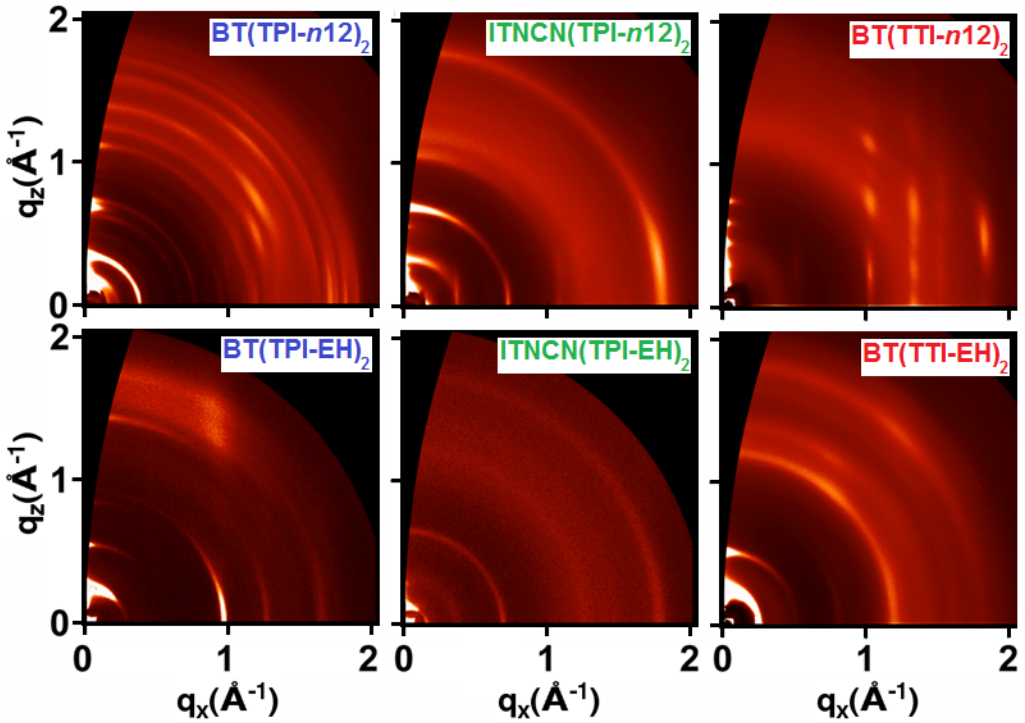

Figure 5.5. Grazing incidence X-ray diffraction (GIXD) spectra of neat films of each n-type material.

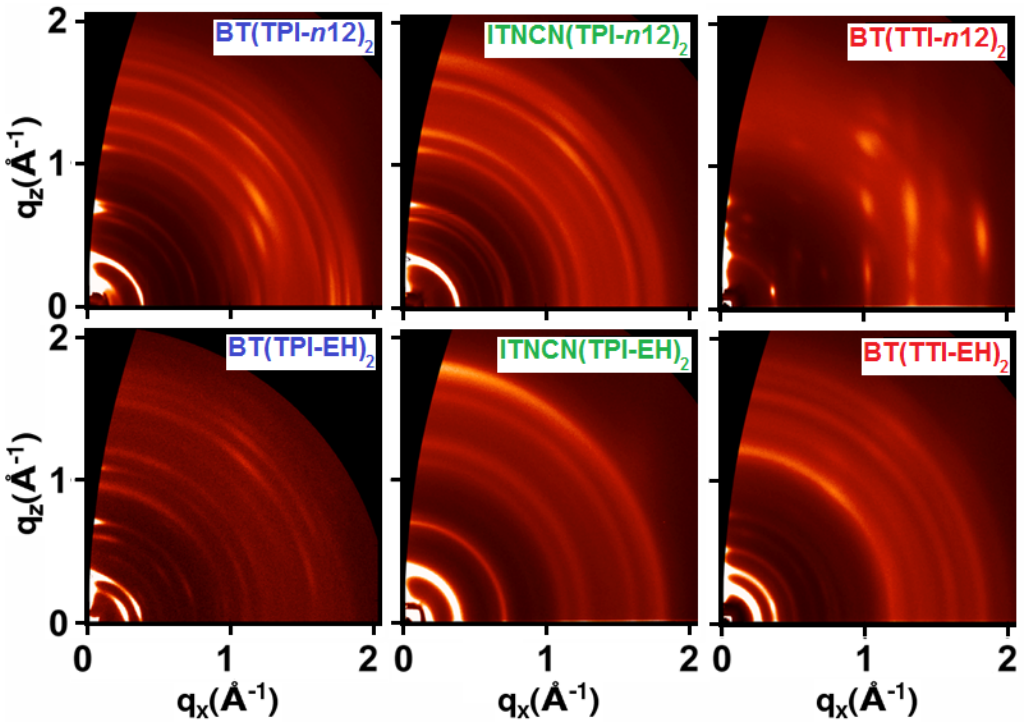

Figure 5.6. Grazing incidence X-ray diffraction (GIXD) spectra of DPP-Py:n-type molecule blends.

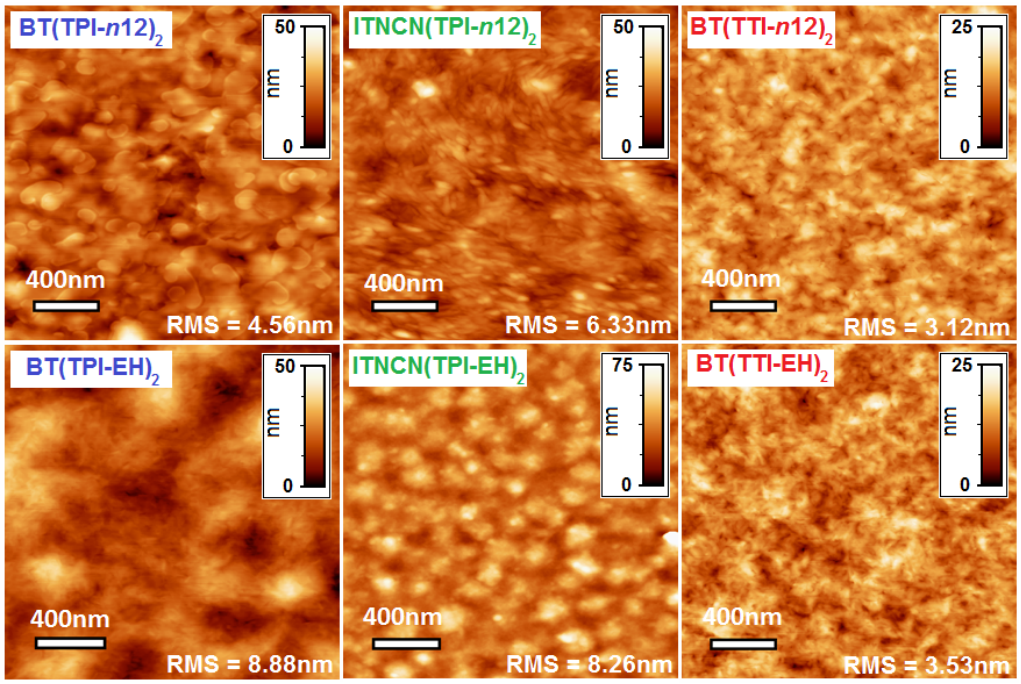

Figure 5.7. Tapping mode atomic force microscopy (AFM) height images of DPP-Py:n-type molecule blends.

In a device where p- and n-type materials exhibit complementary absorptions, such as with n-type BT-containing molecules and p-type DPP-Py, external quantum efficiency (EQE) analysis can help identify which active layer component most efficiently generates excitons. In

the case of $BT(TPI)_2$ devices, poor device currents correspond with low EQE spectra, which are difficult to analyze because quantum efficiencies below 15% are observed (Figure 5.8a). With higher device J_{sc} values, the $BT(TTI)_2$ blends have EQEs of 15-25% in the 400-600 nm spectral region, which matches the absorption of the $BT(TTI)_2$ acceptors (Figure 5.8b). This overlap between EQE and absorption spectra indicates that there is a strong contribution from the n-type materials to the overall device photocurrent in DPP-Py:$BT(TTI)_2$ blends, and that charge generation is more efficient from excitation of the n-type, rather than the p-type material.

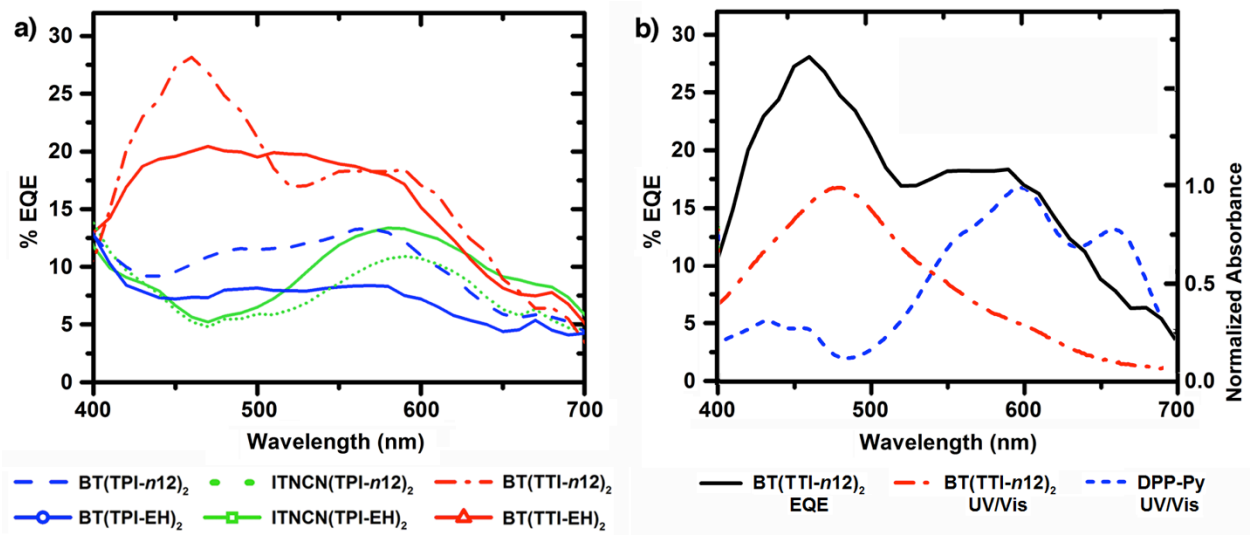

Figure 5.8. a) External quantum efficiency (EQE) spectra of n-type molecules $BT(TPI)_2$, $ITNCN(TPI)_2$, and $BT(TTI)_2$ in thin films. b) The external quantum efficiency spectrum of a DPP-Py:$BT(TTI\text{-}n12)_2$ blend overlaid with the absorption spectra of the individual device components in thin films shows that current generation from excitation of $BT(TTI\text{-}n12)_2$ is more efficient than from DPP-Py.

With both charge generation mechanisms, a greater $LUMO_{p\text{-}type}$-$LUMO_{n\text{-}type}$ or $HOMO_{p\text{-}type}$-$HOMO_{n\text{-}type}$ energy offset provides a stronger driving force for exciton dissociation.[61] Blends of DPP-Py and $BT(TTI\text{-}n12)_2$ have a small LUMO-LUMO offset (singlet excited state of -3.59 eV and LUMO of -3.53 eV, respectively) while the difference in HOMO levels is much larger (-5.34 eV and -5.99 eV, respectively). In this system, there is a lack of energetic driving force for electron transfer upon excitation of the p-type material (Figure 5.9a), while there is sufficient potential for hole transfer after n-type photoexcitation (Figure 5.9b). The process of generating free charges in DPP-Py:$BT(TTI)_2$-based devices appears to rely on the driving force for hole transfer from $HOMO_{n\text{-}type}$ to $HOMO_{p\text{-}type}$. In addition, the higher extinction coefficient of $BT(TTI\text{-}n12)_2$ versus DPP-Py (α =1.9 x 10^5 cm^{-1} vs. 6.3 x 10^4 cm^{-1}) further enhances charge generation via formation of excitons within the n-type material. Lastly, the fine blend morphology in $BT(TTI)_2$ devices facilitates effective exciton diffusion to a p-n interface and

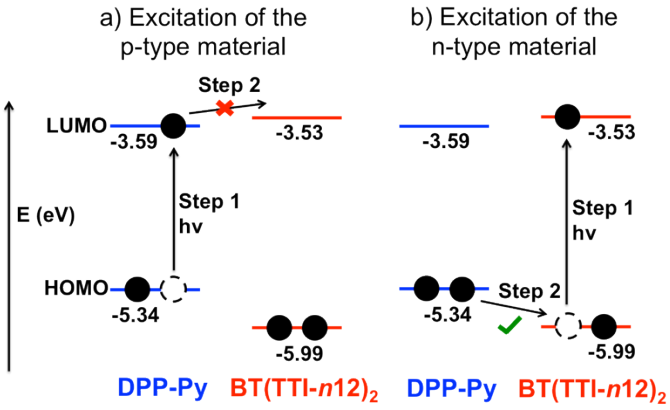

Figure 5.9. Charge generation in DPP-Py:$BT(TTI\text{-}n12)_2$ blends is a) not efficient from excitation of p-type DPP-Py, but is b) effective from excitation of n-type $BT(TTI\text{-}n12)_2$.

subsequent hole transfer. Although photoexcitation of the n-type material is rarely invoked as a mechanism for generating free charges,[62,63] our devices demonstrate that it can be a significant pathway for charge current generation in non-fullerene OPV devices.

Conclusions

In conclusion, we report the synthesis and OPV performance of six non-fullerene n-type materials in small-molecule devices. We correlate the molecular planarity and quinoidal character of our molecules with data from DFT calculations, UV-vis spectroscopy, CV, GIXD, AFM and observed OPV device parameters. As the most planar and crystalline n-type molecule in the series, BT(TTI-*n*12)$_2$ exhibits a V_{oc} above 1 V, a FF of 0.60, and a device efficiency as high as 2.4% in BHJ blends with DPP-Py. We demonstrate that devices fabricated with this molecule generate charge carriers through excitation of the n-type material and subsequent hole transfer to the p-type material. Charge generation upon light absorption by the n-type material is promoted in these OPVs because the active layer components have a large HOMO-HOMO energy level offset and a nanoscale morphology. This record-performance for non-fullerene devices shows that light absorbing fullerene-substitutes are viable components for OPVs.

Experimental

Materials.

All commercially available reagents obtained from suppliers were used without further purification. Unless otherwise noted, all reactions were carried out under nitrogen with standard Schlenk techniques, and all glassware used in dry reactions was flame dried under high-vacuum prior to use. Tetrahydrofuran (THF), dimethylformamide (DMF), and toluene were purified and dried by passing through two columns of neutral alumina, under nitrogen, prior to use. Water was degassed by free-pump-thaw, and degassed, dry dioxane was used from a Sure-seal bottle. Flash chromatography was performed using Silicycle SiliaFlash ® P60 (particle size 40-63 μm, 230-400 mesh) silica gel.

P-type material 2,5-bis(2-hexyldecyl)-3,6-bis(5-(pyren-2-yl)thiophen-2-yl)pyrrolo[3,4-c]pyrrole-1,4(2H,5H)-dione (DPP-Py) was synthesized according to the procedure reported in the literature,[40] and building block ITNCN (**7**) was synthesized according to the procedure in the previous chapter.

Material Characterization.

All ^{1}H and ^{13}C NMR spectra were obtained with a Bruker AVQ-400, AVB-400, AV-500 or AV-600 instrument, and ^{13}C spectra were collected with a proton-decoupling pulse program. NMR abbreviations: at = apparent triplet, bs = broad singlet, d = doublet, m = multiplet, s = singlet, and t = triplet. Elemental analysis (CHN) was performed by the UC Berkeley microanalysis laboratory. Data from high-resolution mass spectrometry (HRMS) using electron impact (EI) were obtained by the UC Berkeley mass spectrometry facility.

Matrix-assisted laser desorption/ionization-time of flight mass spectrometry (MALDI-TOF MS) was performed on a PerSeptive Biosystems Voyager-DE using 2,2':5',2''-terthiophene as the matrix. Samples were prepared by diluting the molecule of interent in chloroform, with the matrix.

Gas chromatography-mass spectrometry (GC-MS) data was collected on an Agilent 7890A GC system fitted with an Agilent HP-5 chromatography column. Helium carrier gas at a flow rate of 2.2 mL/min was used as the mobile phase. The sample inlet was 250 °C and a

pressure of 8.8 PSI was used to load the vaporized compounds onto the column at a split ratio of 50:1. The oven temperature was equilibrated at 50 °C for 30 seconds, and then a 19 minute temperature program was run as follows: 50 °C for 1 minute, ramp to 310 °C at 20 °C/min for 13 minutes, hold at 310 °C for 5 minutes. An auxiliary heater was kept at 150 °C between the GC column and the Agilent 5975C VL MSD system (electron impact (EI)) in order to prevent precipitation of the separated compounds from the He carrier gas at the MSD system inlet. MS information was collected by the 5975C system and analyzed with Agilent Chemstation software.

Density functional theory (DFT) calculations for each n-type molecule was carried out with Gaussian 09 using a hybrid B3LYP correlation functional and the 6-31G(d) basis set.

Solution and thin-film UV-vis absorption spectra were gathered at room temperature using a Varian Cary 50 Conc spectrophotometer. The absorption spectra in chloroform solutions were measured using a quartz cuvette with a 1 cm path length. Thin films were spin-coated from $CHCl_3$ onto untreated quartz slides.

Cyclic voltammograms (CV) were collected using a Solartron 1285 potentiostat under the control of CorrWare II software. A standard three electrode cell based on a Pt wire working electrode, a silver wire reference electrode (calibrated vs. Fc/Fc^+ at -5.13 eV), and a Pt wire counter electrode was purged with nitrogen and maintained under a nitrogen atmosphere during all measurements. Anhydrous acetonitrile was purchased from Aldrich, and tetrabutylammonium hexafluorophosphate (0.1 M) was used as the supporting electrolyte. Polymer films were drop cast onto a Pt wire working electrode from a 1% (w/w) chloroform solution and dried under nitrogen prior to measurement.

Synthesis.

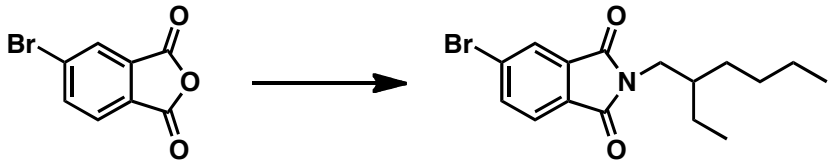

1 **EH-2**

*5-Bromo-2-(2-ethylhexyl)isoindoline-1,3-dione (**EH-2**).* 4-Bromophthalic anhydride (**1**) (4.00 g, 17.6 mmol) and 2-ethylhexylamine (2.32 g, 18.0 mmol) were combined with THF (40 mL) in a 100 mL flask and heated to 60 °C for 2 h. After cooling the reaction mixture to room temperature, thionyl chloride (9 mL) was added, and the reaction contents were stirred at 60 °C for another 2 h. The reaction mixture was quenched with water, and THF was removed under reduced pressure. The resulting residue was extracted with diethyl ether, washed with brine, dried over $MgSO_4$, and filtered. Volatiles were removed under reduced pressure. The crude product was dissolved into $CHCl_3$, poured onto a silica pad and eluted with $CHCl_3$. The volatiles from the filtrate were removed under reduced pressure to yield 4.31 g of white solid (72 %). ^1H NMR (400 MHz, $CDCl_3$, δ): 7.94 (s, 1 H), 7.82 (d, J = 7.90 Hz, 1 H), 7.68 (d, J = 7.90 Hz, 1 H), 3.55 (d, J = 7.30 Hz, 2 H), 1.84-1.75 (m, 1 H), 1.35-1.19 (m, 8 H), 0.88 (t, J = 7.42 Hz, 3 H), 0.86 (t, J = 6.39 Hz, 3 H). ^{13}C (100 MHz, $CDCl_3$, δ): 168.0, 167.4, 136.9, 133.8, 130.7, 128.8, 126.7, 124.6, 42.2, 38.3, 30.6, 28.6, 23.9, 23.1, 14.2, 10.5. GC-MS (*m/z*): $[M]^+$ calculated for $C_{16}H_{20}BrNO_2$, 337.1; found, 337.1.

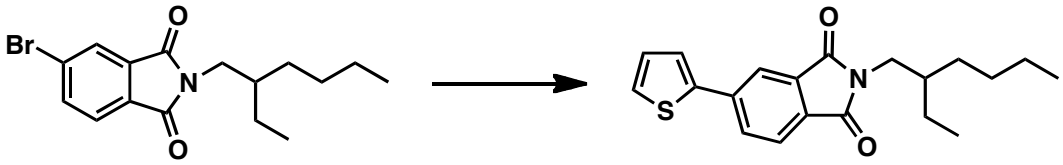

EH-2 **EH-3**

*2-(2-Ethylhexyl)-5-(thiophen-2-yl)isoindoline-1,3-dione (**EH-3**).* Compound **EH-2** (4.00 g, 11.8 mmol) and 2-(tributylstannyl)thiophene (6.18 g, 16.6 mmol) were combined with tris(dibenzylideneacetone)dipalladium(0) (Pd_2dba_3) (217 mg, 237 μmol) and tri(*o*-tolyl)phosphine (P(*o*-tol)$_3$) (288 mg, 946 μmol) in a 100 mL flask. The reaction vessel was purged with three vacuum/nitrogen cycles before toluene (39.2 mL) and DMF (7.8 mL) were added to the reaction flask. After stirring at 90 °C for 16 h, the reaction mixture was quenched with water, and the reaction contents were extracted with diethyl ether, washed with brine, dried over $MgSO_4$, and filtered. Volatiles were removed under reduced pressure. The crude material was purified by flash chromatography (1:1 $CHCl_3$:hexanes) to yield 4.20 g of a yellow oil (100%). ^{1}H NMR (400 MHz, $CDCl_3$, δ): 8.01 (s, 1 H), 7.87 (d, *J* = 7.82 Hz, 1 H), 7.78 (d, *J* = 7.81 Hz, 1 H), 7.45 (d, *J* = 3.55 Hz, 1 H), 7.39 (d, *J* = 5.03 Hz, 1 H), 7.11 (at, *J* = 4.32 Hz, 1 H), 3.56 (d, *J* = 7.25 Hz, 2 H), 1.87-1.76 (m, 1 H), 1.40-1.19 (m, 8 H), 0.91 (t, *J* = 7.32 Hz, 3 H), 0.87 (t, *J* = 6.45 Hz, 3 H). ^{13}C (100 MHz, $CDCl_3$, δ): 168.5, 168.4, 142.1, 140.2, 133.2, 130.6, 130.2, 128.7, 127.3, 125.4, 123.9, 120.1, 42.0, 38.3, 30.6, 28.6, 23.9, 23.1, 14.2, 10.5. GC-MS (*m/z*): $[M]^+$ calculated for $C_{20}H_{23}NO_2S$, 341.1; found, 341.1.

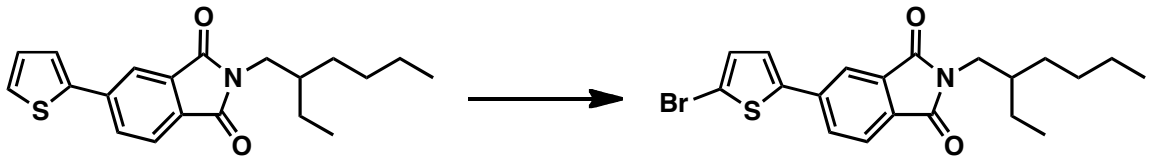

EH-3 **EH-4**

*5-(5-Bromothiophen-2-yl)-2-(2-ethylhexyl)isoindoline-1,3-dione (**EH-4**).* Compound **EH-3** (4.20 g, 11.8 mmol) was dissolved in $CHCl_3$ (40 mL) and acetic acid (20 mL) in a 250 mL flask and chilled to 0 °C. *N*-Bromosuccinimide (NBS) (2.21 g, 12.4 mmol) was added to the reaction mixture in one portion, and the reaction mixture was stirred for 16 h at room temperature. The reaction contents were quenched with water, extracted with $CHCl_3$, washed with brine, dried over $MgSO_4$, and filtered. Volatiles were removed under reduced pressure to yield 4.59 g of light yellow solid (92 %). The crude product was used without any further purification. ^{1}H NMR (400 MHz, $CDCl_3$, δ): 7.95 (s, 1 H), 7.84-7.76 (m, 2 H), 7.22 (d, *J* = 3.82 Hz, 1 H), 7.10 (d, *J* = 3.83 Hz, 1 H), 3.58 (d, *J* = 7.27 Hz, 2 H), 1.89-1.79 (m, 1 H), 1.40-1.21 (m, 8 H), 0.91 (t, *J* = 7.16 Hz, 3 H), 0.88 (t, *J* = 6.12 Hz, 3 H). ^{13}C (100 MHz, $CDCl_3$, δ): 168.41, 168.35, 143.5, 139.4, 133.4, 131.6, 130.6, 130.4, 125.7, 124.1, 119.8, 114.4, 42.2, 38.4, 30.6, 28.6, 23.9, 23.1, 14.2, 10.5. GC-MS (*m/z*): $[M]^+$ calculated for $C_{20}H_{22}BrNO_2S$, 419.1; found, 419.1.

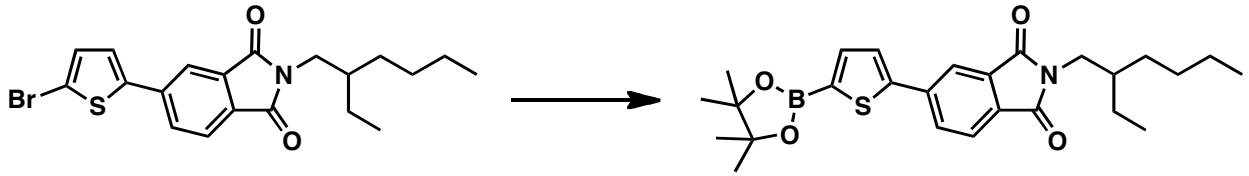

EH-4 **EH-5**

*2-(2-Ethylhexyl)-5-(5-(4,4,5,5-tetramethyl-1,3,2-dioxaborolan-2-yl)thiophen-2-yl)isoindoline-1,3-dione (**EH-5**)*. Compound **EH-4** (700 mg, 1.67 mmol) and bis(pinacolato)diboron (B_2pin_2) (846 mg, 3.33 mmol) were combined with [1,1'-bis(diphenylphosphino)ferrocene] dichloropalladium(II), dichloromethane adduct ($Pd(dppf)Cl_2$-DCM) (40.8 mg, 50.0 μmol) and potassium acetate (KOAc) (490 mg, 5.00 mmol) in a 100 mL flame-dried flask. The reaction vessel was purged with three vacuum/nitrogen cycles before dioxane (34 mL) was added to the reaction flask. After stirring at 80 °C for 24 h, the reaction mixture was quenched with water, and the reaction contents were extracted with $CHCl_3$, washed with brine, dried over $MgSO_4$, and filtered. Volatiles were removed under reduced pressure. The crude material was purified by flash chromatography (gradient of 1:1 DCM:hexanes to pure DCM) to yield 578 mg of green solid (74%). ^{1}H NMR (500 MHz, $CDCl_3$, δ): 8.05 (s, 1 H), 7.91 (d, J = 7.82 Hz, 1 H), 7.80 (d, J = 7.80 Hz, 1 H), 7.60 (d, J = 3.63 Hz, 1 H), 7.50 (d, J = 3.63 Hz, 1 H), 3.55 (d, J = 7.29 Hz, 2 H), 1.86-1.76 (m, 1 H), 1.34 (s, 12 H), 1.32-1.18 (m, 8 H), 0.89 (t, J = 7.52 Hz, 3 H), 0.85 (t, J = 6.97 Hz, 3 H). ^{13}C (150 MHz, $CDCl_3$, δ): 168.4, 168.3, 148.6, 140.1, 138.4, 133.3, 131.0, 130.6, 126.5, 123.9, 120.4, 84.5, 83.6, 42.1, 38.4, 30.6, 28.6, 25.1, 24.9, 23.9, 23.1, 14.1, 10.5. MALDI-TOF MS (*m/z*): $[M]^-$ calculated for $C_{26}H_{34}BNO_4S$, 467.2; found, 467.2.

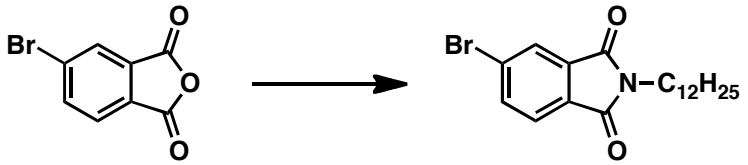

1 ***n*12-2**

*5-Bromo-2-dodecylisoindoline-1,3-dione (**n12-2**)*. 4-Bromophthalic anhydride (**1**) (4.00 g, 17.6 mmol) and dodecylamine (3.59 g, 19.4 mmol) were combined with THF (40 mL) in a 100 mL flask and heated to 50 °C for 16 h. After cooling the reaction mixture to room temperature, thionyl chloride (5 mL) was added, and the reaction contents were stirred at 60 °C for another 2 h. The reaction mixture was quenched with water, and THF was removed under reduced pressure. The resulting residue was extracted with $CHCl_3$, washed with brine, dried over $MgSO_4$, and filtered. Volatiles were removed under reduced pressure. The crude material was purified by flash chromatography (2:1 $CHCl_3$:hexanes) to yield 4.36 g of white solid (63 %). ^{1}H NMR (600 MHz, $CDCl_3$, δ): 7.96 (s, 1 H), 7.84 (d, J = 7.89 Hz, 1 H), 7.70 (d, J = 7.89 Hz, 1 H), 3.66 (t, J = 7.35 Hz, 2 H), 1.68-1.60 (m, 2 H), 1.35-1.18 (m, 18 H), 0.87 (t, J = 7.02 Hz, 3 H). ^{13}C (150 MHz, $CDCl_3$, δ): 167.8, 167.2, 137.0, 134.0, 130.9, 128.9, 126.7, 124.7, 38.5, 32.1, 29.8, 29.7, 29.6, 29.5, 29.3, 28.7, 27.0, 22.8, 14.3. GC-MS (*m/z*): $[M]^+$ calculated for $C_{20}H_{28}BrNO_2$, 393.1; found, 393.1.

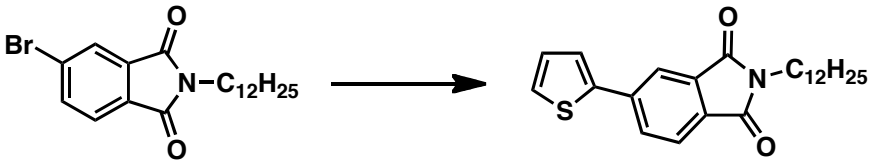

***n*12-2** ***n*12-3**

*2-Dodecyl-5-(thiophen-2-yl)isoindoline-1,3-dione (**n12-3**)*. Compound ***n*12-2** (4.00 g, 10.1 mmol) and 2-(tributylstannyl)thiophene (5.68 g, 15.2 mmol) were combined with Pd_2dba_3 (186 mg, 203 μmol) and P(*o*-tol)$_3$ (247 mg, 811 μmol) in a 100 mL flask. The reaction vessel was purged with three vacuum/nitrogen cycles before toluene (33.6 mL) and DMF (6.7 mL) were added to the reaction flask. After stirring at 90 °C for 16 h, the reaction mixture was quenched with water, and the reaction contents were extracted with diethyl ether, washed with brine, dried over $MgSO_4$, and filtered. Volatiles were removed under reduced pressure. The crude material was purified by flash chromatography (3:1 $CHCl_3$:hexanes) to yield 4.57 g of white solid (98%). ^{1}H NMR (400 MHz, $CDCl_3$, δ): 8.05 (s, 1 H), 7.90 (d, *J* = 7.81 Hz, 1 H), 7.81 (d, *J* = 7.81 Hz, 1 H), 7.48 (d, *J* = 3.39 Hz, 1 H), 7.41 (d, *J* = 4.97 Hz, 1 H), 7.14 (at, *J* = 4.32 Hz, 1 H), 3.68 (t, *J* = 7.30 Hz, 2 H), 1.73-1.63 (m, 2 H), 1.38-1.18 (m, 18 H), 0.87 (t, *J* = 6.69 Hz, 3 H). ^{13}C (100 MHz, $CDCl_3$, δ):168.4, 168.3, 142.2, 140.3, 133.4, 130.6, 130.3, 128.7, 127.3, 125.5, 124.0, 120.2, 38.3, 32.0, 29.8, 29.7, 29.6, 29.5, 29.3, 28.8, 27.0, 22.8, 14.3. MALDI-TOF MS (*m/z*): $[M]^-$ calculated for $C_{24}H_{31}NO_2S$, 397.6; found, 397.2.

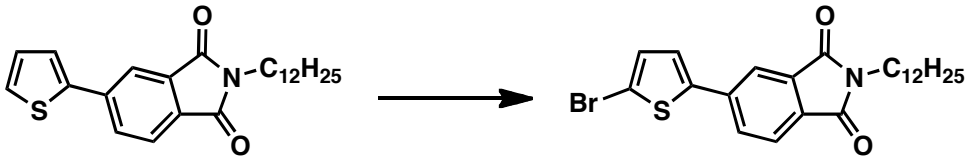

***n*12-3** ***n*12-4**

*5-(5-Bromothiophen-2-yl)-2-dodecylisoindoline-1,3-dione (**n12-4**)*. Compound ***n*12-3** (4.40 g, 11.1 mmol) was dissolved in $CHCl_3$ (40 mL) and acetic acid (20 mL) in a 100 mL flask and chilled to 0 °C. NBS (2.17 g, 12.2 mmol) was added to the reaction mixture in one portion, and the reaction mixture was stirred for 16 h at room temperature. The reaction contents were quenched with water, extracted with $CHCl_3$, washed with brine, dried over $MgSO_4$, and filtered. Volatiles were removed under reduced pressure to yield 5.21 g of light beige solid (99 %). The crude product was used without any further purification. ^{1}H NMR (600 MHz, $CDCl_3$, δ): 7.95 (s, 1 H), 7.83-7.77 (m, 2 H), 7.22 (d, *J* = 3.65 Hz, 1 H), 7.10 (d, *J* = 3.65 Hz, 1 H), 3.67 (t, *J* = 7.29 Hz, 2 H), 1.70-1.63 (m, 2 H), 1.36-1.18 (m, 18 H), 0.87 (t, *J* = 6.91 Hz, 3 H). ^{13}C (150 MHz, $CDCl_3$, δ): 168.13, 168.05, 143.5, 139.4, 133.5, 131.6, 130.7, 130.3, 125.7, 124.1, 119.8, 114.5, 38.4, 32.1, 29.8, 29.7, 29.6, 29.5, 29.3, 28.7, 27.0, 22.8, 14.3. MALDI-TOF MS (*m/z*): $[M]^-$ calculated for $C_{24}H_{30}BrNO_2S$, 475.1; found, 474.8.

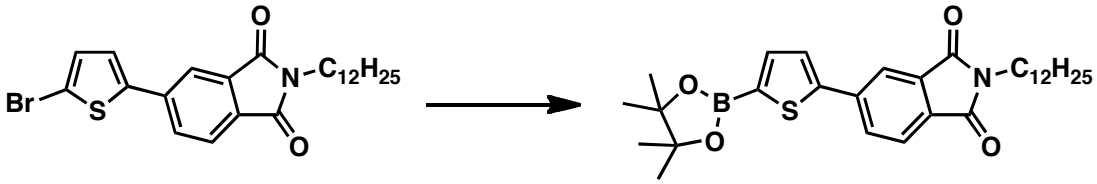

n*12-4** **n*12-5

*2-Dodecyl-5-(5-(4,4,5,5-tetramethyl-1,3,2-dioxaborolan-2-yl)thiophen-2-yl)isoindoline-1,3-dione (**n12-5**)*. Compound ***n*12-4** (600 mg, 1.26 mmol) and B_2pin_2 (640 mg, 2.52 mmol) were combined with Pd(dppf)Cl_2-DCM (30.9 mg, 37.8 μmol) and KOAc (371 mg, 3.78 mmol) in a 100 mL flame-dried flask. The reaction vessel was purged with three vacuum/nitrogen cycles before dioxane (25 mL) was added to the reaction flask. After stirring at 80 °C for 24 h, the reaction mixture was quenched with water, and the reaction contents were extracted with $CHCl_3$, washed with brine, dried over $MgSO_4$, and filtered. Volatiles were removed under reduced pressure. The crude material was purified by flash chromatography (gradient of 1:1 DCM:hexanes to pure DCM) to yield 494 mg of green solid (75%).^{1}H NMR (500 MHz, $CDCl_3$, δ): 8.08 (s, 1 H), 7.93 (d, *J* = 7.80 Hz, 1 H), 7.82 (d, *J* = 7.81 Hz, 1 H), 7.63 (d, *J* = 3.64 Hz, 1 H), 7.53 (d, *J* = 3.65 Hz, 1 H), 3.67 (t, *J* = 7.34 Hz, 2 H), 1.70-1.63 (m, 2H), 1.36 (s, 12 H), 1.34-1.19 (m, 18 H), 0.86 (t, *J* = 6.94 Hz, 3 H). ^{13}C (150 MHz, $CDCl_3$, δ): 167.94, 167.88, 148.4, 139.9, 138.3, 133.2, 130.8, 130.5, 126.4, 123.8, 120.3, 84.3, 83.4, 38.1, 31.9, 29.6, 29.5, 29.4, 29.3, 29.1, 28.5, 26.8, 25.0, 24.7, 22.6, 14.1. MALDI-TOF MS (*m/z*): $[M]^-$ calculated for $C_{30}H_{42}BNO_4S$, 523.3; found, 522.8.

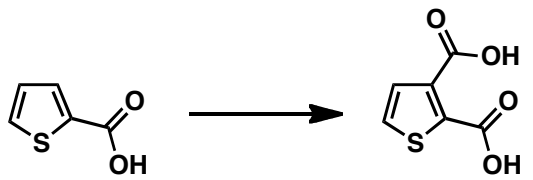

8 **9**

*Thiophene-2,3-dicarboxylic acid (**9**)*.[64] Thiophene-2-carboxylic acid (**8**) (6.00 g, 46.8 mmol) was added to a flame-dried 500 mL flask. The reaction vessel was purged with three vacuum/nitrogen cycles before THF (150 mL) was added, and the reaction contents were chilled to -78 °C. *N*-Butyllithium (39.3 mL of a 2.5 M solution in hexanes, 6.31 mmol) was added to the reaction mixture over 30 min. After stirring for 1 h on the melting bath, 1 cup of crushed dry ice was added to the reaction mixture. The reaction contents were stirred for another 2 h at room temperature before water (50 mL) was added to the reaction mixture. After stirring at room temperature for 16 h, volatiles were removed from the reaction mixture under reduced pressure. Concentrated hydrochloric acid (18 mL) was added the reaction contents, and the resulting precipitates were filtered to yield 7.11 g of beige solid (88 %). The crude product was used without any further purification. ^{1}H NMR (400 MHz, DMSO-d_6, δ): 10.60-8.70 (bs, 2 H), 7.82 (d, *J* = 5.11 Hz, 1 H), 7.39 (d, *J* = 5.12 Hz, 1 H). ^{13}C (100 MHz, DMSO-d_6, δ): 165.5, 162.7, 137.4, 136.5, 131.2, 130.0.

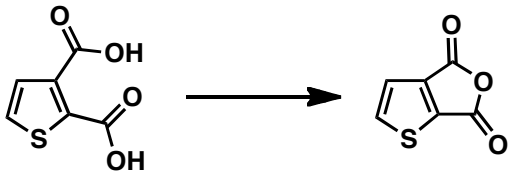

9 10

*Thieno[2,3-c]furan-4,6-dione (**10**)*.[65] Compound **9** (7.09 g, 41.2 mmol) was combined with acetic anhydride (40 mL) in a 100 mL flask and heated at 110 °C for 2 h. The reaction contents were cooled to room temperature, and volatiles were removed under reduced pressure to yield 6.46 g of beige crystals (100 %). The crude product was used without any further purification. ^{1}H NMR (600 MHz, Acetone-d_6, δ): 8.42 (d, J = 4.84 Hz, 1 H), 7.57 (d, J = 4.83 Hz, 1 H). ^{13}C (150 MHz, $CDCl_3$, δ): 158.8, 158.1, 146.7, 144.7, 142.6, 122.6. GC-MS (*m/z*): $[M]^+$ calculated for $C_6H_2O_3S$, 154.0; found, 154.0.

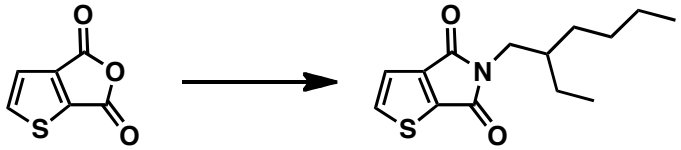

10 EH-11

*5-(2-Ethylhexyl)-4H-thieno[2,3-c]pyrrole-4,6(5H)-dione (**EH-11**)*. Compound **10** (3.44 g, 22.3 mmol) and 2-ethylhexylamine (3.17 g, 24.5 mmol) were combined with THF (45 mL) in a 100 mL flask and heated to 50 °C for 16 h. After cooling the reaction mixture to room temperature, thionyl chloride (8 mL) was added, and the reaction contents were stirred at 50 °C for another 2 h. The reaction mixture was quenched with water, and THF was removed under reduced pressure. The resulting residue was extracted with diethyl ether, washed with brine, dried over $MgSO_4$, and filtered. Volatiles were removed under reduced pressure. The crude material was purified by flash chromatography (3:1 $CHCl_3$:hexanes) to yield 5.05 g of a yellow oil (85 %). ^{1}H NMR (600 MHz, $CHCl_3$, δ): 7.74 (d, J = 4.69 Hz, 1 H), 7.29 (d, J = 4.68 Hz, 1 H), 3.48 (d, J = 7.26 Hz, 2 H), 1.81-1.74 (m, 1 H), 1.37-1.21 (m, 8 H), 0.89 (t, J = 7.39 Hz, 3 H), 0.87 (t, J = 6.65 Hz, 3 H). ^{13}C (150 MHz, $CHCl_3$, δ): 164.4, 163.1, 144.7, 140.9, 137.3, 121.2, 42.4, 38.5, 30.5, 28.6, 23.8, 23.1, 14.2, 10.5. GC-MS (*m/z*): $[M]^+$ calculated for $C_{14}H_{19}NO_2S$, 265.1 found, 265.1.

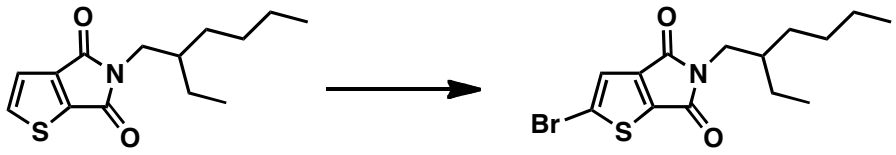

EH-11 EH-12

*2-Bromo-5-(2-ethylhexyl)-4H-thieno[2,3-c]pyrrole-4,6(5H)-dione (**EH-12**)*. Compound **EH-11** (2.50 g, 9.42 mmol) was dissolved in trifluoroacetic acid (TFA) (38 mL) in a 100 mL flask and chilled to 0 °C. Sulfuric acid (4.5 mL) and NBS (1.76 g, 9.89 mmol) were added to the reaction mixture, and the reaction contents were stirred for 1 h at room temperature. The reaction mixture was quenched with water, extracted with DCM, washed with brine, dried over $MgSO_4$, and filtered. Volatiles were removed under reduced pressure. The crude material was purified by flash chromatography (1:1 $CHCl_3$:hexanes) to yield 2.68 g of light beige solid (83 %). ^{1}H NMR

(600 MHz, $CHCl_3$, δ): 7.25 (s, 1 H), 3.42 (d, *J* = 7.25 Hz, 2 H), 1.74-1.66 (m, 1 H), 1.31-1.15 (m, 8 H), 0.84 (t, *J* = 7.44 Hz, 3 H), 0.82 (t, *J* = 6.96 Hz, 3 H). ^{13}C (150 MHz, $CHCl_3$ δ): 163.1, 162.1, 143.8, 140.4, 125.3, 123.8, 42.4, 38.3, 30.4, 28.4, 23.7, 23.0, 14.1, 10.4. GC-MS (*m/z*): $[M]^+$ calculated for $C_{14}H_{18}BrNO_2S$, 343.0; found, 343.0.

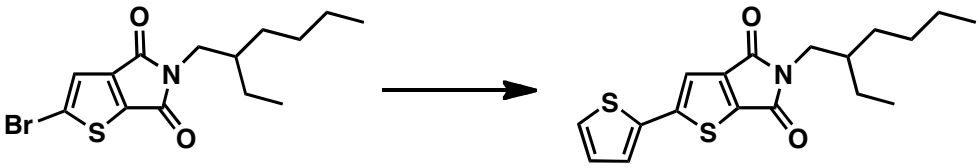

EH-12 **EH-13**

*5-(2-Ethylhexyl)-2-(thiophen-2-yl)-4H-thieno[2,3-c]pyrrole-4,6(5H)-dione (**EH-13**)*. Compound **EH-12** (1.60 g, 4.65 mmol) and 2-(tributylstannyl)thiophene (2.60 g, 6.97 mmol) were combined with Pd_2dba_3 (85.1 mg, 93.0 μmol) and P(*o*-tol)$_3$ (113 mg, 372 μmol) in a 50 mL flask. The reaction vessel was purged with three vacuum/nitrogen cycles before toluene (15.5 mL) and DMF (3.1 mL) were added to the reaction flask. After stirring at 90 °C for 16 h, the reaction mixture was quenched with water, and the reaction contents were extracted with DCM, washed with brine, dried over $MgSO_4$, and filtered. Volatiles were removed under reduced pressure. The crude material was purified by flash chromatography (1:1 $CHCl_3$:hexanes) to yield 1.29 g of yellow solid (80%). ^1H NMR (400 MHz, $CDCl_3$, δ): 7.38 (d, *J* = 5.00 Hz, 1 H), 7.33 (d, *J* = 5.16 Hz, 1 H), 7.32 (s, 1 H), 7.09 (at, *J* = 4.33 Hz, 1 H), 3.50 (d, *J* = 7.28 Hz, 2 H), 1.84-1.74 (m, 1 H), 1.40-1.20 (m, 8 H), 0.91 (t, *J* = 7.67 Hz, 3 H), 0.89 (t, *J* = 7.34 Hz, 3 H). ^{13}C (150 MHz, $CDCl_3$, δ): 164.4, 163.3, 150.3, 145.3, 137.6, 135.4, 128.5, 127.4, 126.2, 116.8, 42.6, 38.6, 30.6, 28.7, 24.0, 23.2, 14.2, 10.6. GC-MS (*m/z*): $[M]^+$ calculated for $C_{18}H_{21}NO_2S_2$, 347.1; found, 347.1.

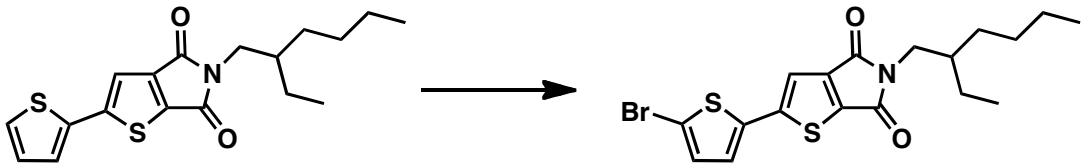

EH-13 **EH-14**

*2-(5-Bromothiophen-2-yl)-5-(2-ethylhexyl)-4H-thieno[2,3-c]pyrrole-4,6(5H)-dione (**EH-14**)*. Compound **EH-13** (800 mg, 2.30 mmol) was dissolved in $CHCl_3$ (4.5 mL) and TFA (4.5 mL) in a 25 mL flask and chilled to 0 °C. Sulfuric acid (0.9 mL) and NBS (430 mg, 2.42 mmol) were added to the reaction mixture, and the reaction contents were stirred for 16 h at room temperature. The reaction contents were quenched with water, extracted with DCM, washed with brine, dried over $MgSO_4$, and filtered. Volatiles were removed under reduced pressure. The crude material was purified by flash chromatography (1:2 $CHCl_3$:hexanes) to yield 750 mg of yellow solid (76%). ^1H NMR (400 MHz, $CDCl_3$, δ): 7.25 (s, 1 H), 7.07 (d, *J* = 3.86 Hz, 1 H), 7.04 (d, *J* = 3.88 Hz, 1 H), 3.49 (d, *J* = 7.26 Hz, 2 H), 1.84-1.74 (m, 1 H), 1.39-1.21 (m, 8 H), 0.90 (t, *J* = 7.56 Hz, 3 H), 0.89 (t, *J* = 7.23 Hz, 3 H). ^{13}C (100 MHz, $CDCl_3$, δ): 164.2, 163.1, 148.9, 145.2, 137.9, 136.7, 131.3, 126.3, 117.0, 114.5, 42.6, 38.6, 30.6, 28.6, 23.9, 23.2, 14.2, 10.6. GC-MS (*m/z*): $[M]^+$ calculated for $C_{18}H_{20}BrNO_2S_2$, 425.0; found, 425.0.

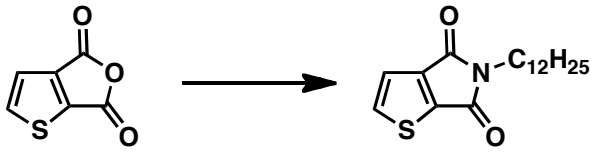

10 ***n*12-11**

*5-Dodecyl-4H-thieno[2,3-c]pyrrole-4,6(5H)-dione (**n12-11**)*. Compound **10** (1.50 g, 9.73 mmol) and dodecylamine (1.89 g, 10.2 mmol) were combined with THF (20 mL) in a 100 mL flask and heated to 60 °C for 16 h. After cooling the reaction mixture to room temperature, thionyl chloride (6 mL) was added, and the reaction contents were stirred at 50 °C for another 16 h. The reaction mixture was quenched with water, and THF was removed under reduced pressure. The resulting residue was extracted with diethyl ether, washed with brine, dried over $MgSO_4$, and filtered. Volatiles were removed under reduced pressure. The crude material was purified by flash chromatography (1:2 $CHCl_3$:hexanes) to yield 2.62 g of beige solid (84 %). ^{1}H NMR (400 MHz, $CDCl_3$, δ): 7.74 (d, *J* = 4.74 Hz, 1 H), 7.30 (d, *J* = 4.74 Hz, 1 H), 3.59 (t, *J* = 7.25 Hz, 2 H), 1.67-1.59 (m, 2 H), 1.36-1.20 (m, 18 H), 0.87 (t, *J* = 6.80 Hz, 3 H). ^{13}C (150 MHz, $CDCl_3$, δ): 164.0, 162.8, 144.8, 141.0, 137.3, 1321.1, 38.6, 32.0, 29.70, 29.68, 29.64, 29.58, 29.4, 28.9, 26.9, 22.8, 14.2. GC-MS (*m/z*): $[M]^+$ calculated for $C_{18}H_{27}NO_2S$, 321.2; found, 321.2.

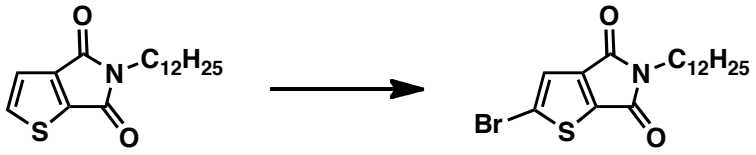

***n*12-11** ***n*12-12**

*2-Bromo-5-dodecyl-4H-thieno[2,3-c]pyrrole-4,6(5H)-dione (**n12-12**)*. Compound ***n*12-11** (2.40 g, 7.47 mmol) was dissolved in TFA (30 mL) in a 100 mL flask and chilled to 0 °C. Sulfuric acid (4 mL) and NBS (1.40 g, 7.84 mmol) were added to the reaction mixture, and the reaction contents were stirred for 1 h at room temperature. The reaction mixture was quenched with water, and the reaction contents were extracted with $CHCl_3$, washed with brine, dried over $MgSO_4$, and filtered. Volatiles were removed under reduced pressure. The crude material was purified by flash chromatography (1:2 $CHCl_3$:hexanes) to yield 2.58 g of white solid (86 %). ^{1}H NMR (400 MHz, $CDCl_3$, δ): 7.30 (s, 1 H), 3.57 (t, *J* = 7.30 Hz, 2 H), 1.66-1.56 (m, 2 H), 1.34-1.20 (m, 18 H), 0.87 (t, *J* = 6.58 Hz, 3 H). ^{13}C (100 MHz, $CDCl_3$, δ): 163.1, 162.1, 144.0, 140.6, 125.5, 123.9, 38.8, 32.1, 29.8, 29.7, 29.6, 29.5, 29.3, 28.9, 26.9, 22.8, 14.3. GC-MS (*m/z*): $[M]^+$ calculated for $C_{18}H_{26}BrNO_2S$, 399.1; found, 399.1.

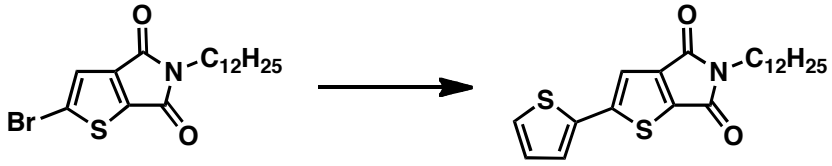

***n*12-12** ***n*12-13**

*5-Dodecyl-2-(thiophen-2-yl)-4H-thieno[2,3-c]pyrrole-4,6(5H)-dione (**n12-13**)*. Compound ***n*12-12** (1.20 g, 3.00 mmol) and 2-(tributylstannyl)thiophene (1.34 g, 3.60 mmol) were combined with Pd_2dba_3 (55.0 mg, 60.0 μmol) and P(*o*-tol)$_3$ (73.0 mg, 240 μmol) in a 25 mL flask. The

reaction vessel was purged with three vacuum/nitrogen cycles before toluene (10 mL) and DMF (2 mL) were added to the reaction flask. After stirring at 90 °C for 16 h, the reaction mixture was quenched with water, and the reaction contents were extracted with $CHCl_3$, washed with brine, dried over $MgSO_4$, and filtered. Volatiles were removed under reduced pressure. The crude material was purified by flash chromatography (1:1 $CHCl_3$:hexanes) to yield 1.16 g of yellow solid (96%). ^{1}H NMR (600 MHz, $CDCl_3$, δ): 7.38 (d, J = 5.03 Hz, 1 H), 7.32 (d, J = 3.59 Hz, 1 H), 7.31 (s, 1 H), 7.08 (at, J = 4.36 Hz, 1 H), 3.59 (d, J = 7.31 Hz, 2 H), 1.66-1.60 (m, 2 H), 1.33-1.21 (m, 18 H), 0.87 (t, J = 6.97 Hz, 3 H). ^{13}C (150 MHz, $CDCl_3$, δ): 164.1, 163.0, 150.3, 145.3, 137.6, 135.3, 128.5, 127.4, 126.2, 116.7, 38.7, 32.0, 29.8, 29.73, 29.69, 29.6, 29.5, 29.3, 26.9, 22.8, 14.2. MALDI-TOF MS (*m/z*): $[M]^-$ calculated for $C_{22}H_{29}NO_2S_2$, 403.2; found, 403.0.

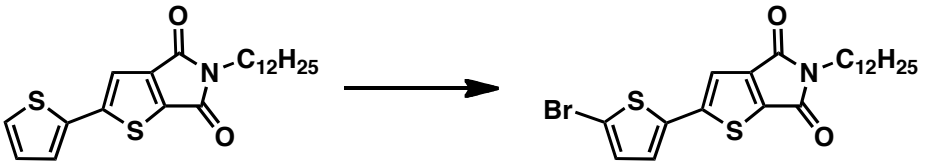

***n*12-13** ***n*12-14**

2-(5-Bromothiophen-2-yl)-5-dodecyl-4H-thieno[2,3-c]pyrrole-4,6(5H)-dione ***(n12-14)***. Compound ***n*12-13** (1.00 g, 2.48 mmol) was dissolved in $CHCl_3$ (5 mL) and TFA (5 mL) in a 25 mL flask and chilled to 0 °C. Sulfuric acid (1 mL) and NBS (463 mg, 2.60 mmol) were added to the reaction mixture, and the reaction contents were stirred for 16 h at room temperature. The reaction contents were quenched with water, extracted with $CHCl_3$, washed with brine, dried over $MgSO_4$, and filtered. Volatiles were removed under reduced pressure. The crude material was purified by flash chromatography (1:2 $CHCl_3$:hexanes) to yield 460 mg of yellow solid (34%). ^{1}H NMR (600 MHz, $CDCl_3$, δ): 7.24 (s, 1 H), 7.07 (d, J = 3.66 Hz, 1 H), 7.04 (d, J = 3.62 Hz, 1 H), 3.58 (d, J = 7.24 Hz, 2 H), 1.66-1.59 (m, 2 H), 1.34-1.20 (m, 18 H), 0.87 (t, J = 6.86 Hz, 3 H). ^{13}C (150 MHz, $CDCl_3$, δ): 164.0, 162.8, 148.9, 145.3, 137.9, 136.7, 131.3, 126.3, 116.9, 114.5, 38.8, 32.1, 29.8, 29.7, 29.6, 29.5, 29.3, 28.9, 26.9, 22.8, 14.3. MALDI-TOF MS (*m/z*): $[M]^-$ calculated for $C_{22}H_{28}BrNO_2S_2$, 481.1; found, 480.8.

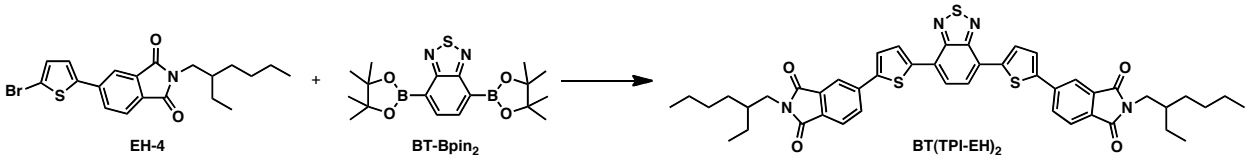

EH-4 **BT-Bpin$_2$** **BT(TPI-EH)$_2$**

5,5'-(5,5'-(Benzo[c][1,2,5]thiadiazole-4,7-diyl)bis(thiophene-5,2-diyl))bis(2-(2-ethylhexyl)isoindoline-1,3-dione) ***(BT(TPI-EH)$_2$)***. Compound **EH-4** (596 mg, 1.42 mmol) and 4,7-bis(4,4,5,5-tetramethyl-1,3,2-dioxaborolan-2-yl)benzo[c][1,2,5]thiadiazole (**BT-Bpin$_2$**) (250 mg, 644 mmol) were combined with Pd_2dba_3 (17.7 mg, 19.3 μmol), P(o-tol)$_3$ (23.5 mg, 77.3 μmol), potassium carbonate (K_2CO_3) (712 mg, 5.15 mmol) and Aliquat 336 (1 drop) in a 50 mL Schlenk tube. The reaction vessel was purged with three vacuum/nitrogen cycles before toluene (12.9 mL) and water (2.6 mL) were added to the reaction flask. After stirring at 90 °C for 16 h, the reaction contents were cooled to room temperature, diluted with $CHCl_3$ (10 mL) and then precipitated into methanol (175 mL). The crude solid was purified by flash chromatography ($CHCl_3$) followed by precipitation into hexanes (100 mL) to yield 205 mg of reddish black solid (39%). ^{1}H NMR (500 MHz, $CDCl_3$, δ): 8.17 (d, J = 4.21 Hz, 2 H), 8.16 (s, 2 H), 8.02 (d, J = 7.82 Hz, 2 H), 7.98 (s, 2 H), 7.87 (d, J = 7.77 Hz, 2 H), 7.61 (d, J = 3.95 Hz, 2 H), 3.61 (d,

J = 7.28 Hz, 4 H), 1.89-1.83 (m, 2 H), 1.41-1.25 (m, 16 H), 0.93 (t, J = 7.44 Hz, 6 H), 0.90 (t, J = 6.94 Hz, 6 H). EI-MS (*m/z*): $[M]^+$ calculated for $C_{46}H_{46}N_4O_4S_3$, 814.2681; found, 814.2687. Anal. calculated for $C_{46}H_{46}N_4O_4S_3$: C, 67.78; H, 5.69; N, 6.87; found: C, 67.72; H, 5.89; N, 6.63.

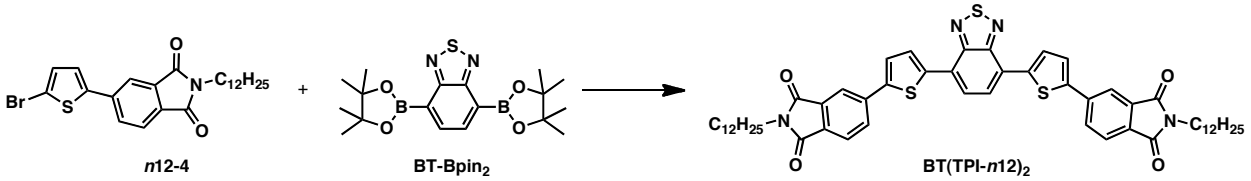

*5,5'-(5,5'-(Benzo[c][1,2,5]thiadiazole-4,7-diyl)bis(thiophene-5,2-diyl))bis(2-dodecylisoindoline-1,3-dione) (**BT(TPI-n12)$_2$**)*. Compound ***n*12-4** (675 mg, 1.42 mmol) and **BT-Bpin$_2$** (250 mg, 644 mmol) were combined with Pd_2dba_3 (17.7 mg, 19.3 μmol), P(*o*-tol)$_3$ (23.5 mg, 77.3 μmol), K_2CO_3 (712 mg, 5.15 mmol) and Aliquat 336 (1 drop) in a 50 mL Schlenk tube. The reaction vessel was purged with three vacuum/nitrogen cycles before toluene (12.9 mL) and water (2.6 mL) were added to the reaction flask. After stirring at 90 °C for 16 h, the reaction contents were cooled to room temperature, diluted with $CHCl_3$ (10 mL) and then precipitated into methanol (200 mL). The crude solid was purified by flash chromatography ($CHCl_3$) followed by precipitation into hexanes (150 mL) to yield 195 mg of black solid (33%). ^{1}H NMR (500 MHz, $CDCl_3$, δ): 8.17 (d, J = 4.00 Hz, 2 H), 8.16 (s, 2 H), 8.02 (d, J = 7.80 Hz, 2 H), 7.98 (s, 2 H), 7.87 (d, J = 7.84 Hz, 2 H), 7.61 (d, J = 3.96 Hz, 2 H), 3.70 (7, J = 7.36 Hz, 4 H), 1.73-1.65 (m, 4 H), 1.39-1.21 (m, 36 H), 0.88 (t, J = 6.95 Hz, 6 H). EI-MS (*m/z*): $[M]^+$ calculated for $C_{54}H_{62}N_4O_4S_3$, 926.3933; found, 926.3914. Anal. calculated for $C_{54}H_{62}N_4O_4S_3$: C, 69.94; H, 6.74; N, 6.04; found: C, 69.80; H, 6.80; N, 6.00.

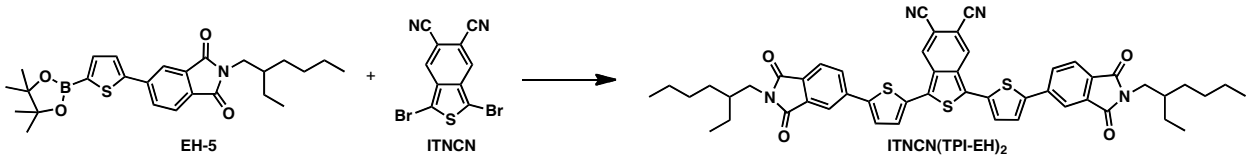

*1,3-Bis(5-(2-(2-ethylhexyl)-1,3-dioxoisoindolin-5-yl)thiophen-2-yl)benzo[c]thiophene-5,6-dicarbonitrile (**ITNCN(TPI-EH)$_2$**)*. Compound **EH-5** (222 mg, 475 μmol) and 1,3-dibromobenzo[*c*]thiophene-5,6-dicarbonitrile (**ITNCN**) (73.8 mg, 216 mmol) were combined with Pd_2dba_3 (5.93 mg, 6 μmol), P(*o*-tol)$_3$ (7.88 mg, 26 μmol), K_2CO_3 (239 mg, 1.73 mmol) and Aliquat 336 (1 drop) in a 50 mL Schlenk tube. The reaction vessel was purged with three vacuum/nitrogen cycles before toluene (4.3 mL) and water (0.8 mL) were added to the reaction flask. After stirring at 90 °C for 16 h, the reaction contents were cooled to room temperature diluted with $CHCl_3$ (10 mL) and then precipitated into methanol (200 mL). The crude solid was purified by flash chromatography ($CHCl_3$) followed by precipitation into methanol (150 mL) to yield 90 mg of black solid (48%). ^{1}H NMR (600 MHz, $CDCl_3$, δ): 8.49 (s, 2 H), 8.11 (s, 2 H), 7.98 (d, J = 7.92 Hz, 2 H), 7.90 (d, J = 7.92 Hz, 2 H), 7.60 (d, J = 3.93 Hz, 2 H), 7.47 (d, J = 3.96 Hz, 2 H), 3.61 (d, J = 7.27 Hz, 4 H), 1.90-1.82 (m, 2 H), 1.41-1.22 (m, 16 H), 0.93 (t, J = 7.43 Hz, 6 H), 0.89 (t, J = 6.93 Hz, 6 H). EI-MS (*m/z*): $[M]^+$ calculated for $C_{50}H_{46}N_4O_4S_3$, 862.2681; found, 862.2664. Anal. calculated for $C_{50}H_{46}N_4O_4S_3$: C, 69.58; H, 5.37; N, 6.49; found: C, 69.27; H, 5.44; N, 6.49.

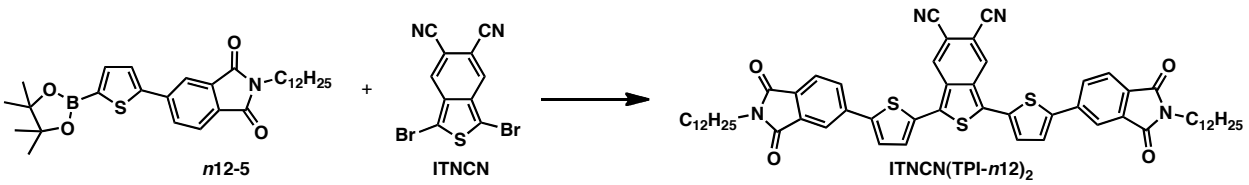

*1,3-Bis(5-(2-dodecyl-1,3-dioxoisoindolin-5-yl)thiophen-2-yl)benzo[c]thiophene-5,6-dicarbonitrile (**ITNCN(TPI-n12)$_2$**)*. Compound ***n*12-5** (523 mg, 999 μmol) and **ITNCN** (155 mg, 454 mmol) were combined with Pd_2dba_3 (12.5 mg, 13.6 μmol), P(*o*-tol)$_3$ (16.6 mg, 54.5 μmol), K_2CO_3 (415 mg, 3.00 mmol) and Aliquat 336 (1 drop) in a 50 mL Schlenk tube. The reaction vessel was purged with three vacuum/nitrogen cycles before toluene (14.1 mL) and water (1.5 mL) were added to the reaction flask. After stirring at 90 °C for 16 h, the reaction contents were cooled to room temperature, diluted with $CHCl_3$ (10 mL) and then precipitated into methanol (175 mL). The crude solid was purified by flash chromatography ($CHCl_3$) followed by recrystallization via solvent diffusion in $CHCl_3$ (100 mL) and hexanes (100 mL) to yield 45 mg of black solid (10%). ^{1}H NMR (500 MHz, $CDCl_3$, δ): 8.51 (s, 2 H), 8.13 (s, 2 H), 7.99 (d, *J* = 7.81 Hz, 2 H), 7.91 (d, *J* = 7.78 Hz, 2 H), 7.61 (d, *J* = 3.86 Hz, 2 H), 7.47 (d, *J* = 3.81 Hz, 2 H), 3.71 (t, *J* = 7.28 Hz, 4 H), 1.71-1.65 (m, 4 H), 1.67 (m, 4 H), 1.39-1.20 (m, 36 H), 0.87 (t, *J* = 6.89 Hz, 6 H). EI-MS (*m/z*): $[M]^+$ calculated for $C_{58}H_{62}N_4O_4S_3$, 974.3933; found, 974.3906. Anal. calculated for $C_{58}H_{62}N_4O_4S_3$: C, 71.42; H, 6.41; N, 5.74; found: C, 71.04; H, 6.33; N, 5.84.

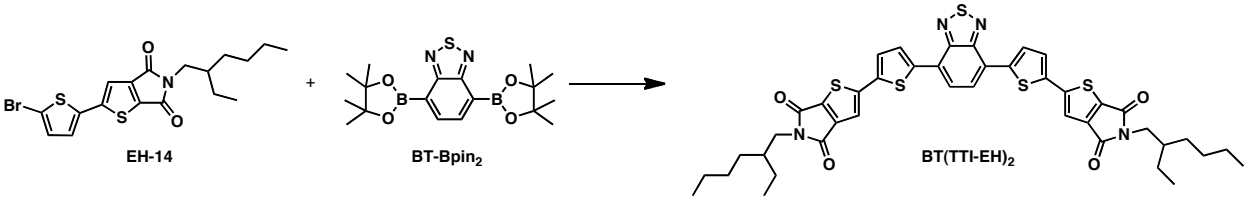

*2,2'-(5,5'-(Benzo[c][1,2,5]thiadiazole-4,7-diyl)bis(thiophene-5,2-diyl))bis(5-(2-ethylhexyl)-4H-thieno[2,3-c]pyrrole-4,6(5H)-dione) (**BT(TTI-EH)$_2$**)*. Compound **EH-14** (363 mg, 850 μmol) and **BT-Bpin$_2$** (150 mg, 386 mmol) were combined with tetrakis(triphenylphosphine)palladium(0) ($Pd(PPh_3)_4$) (22.3 mg, 19.3 μmol) and cesium fluoride (CsF) (126 mg, 850 μmol) in a 50 mL Schlenk tube. The reaction vessel was purged with three vacuum/nitrogen cycles before dioxane (7.5 mL) was added to the reaction flask. After stirring at 90 °C for 16 h, the reaction contents were cooled to room temperature, diluted with $CHCl_3$ (10 mL) and then precipitated into methanol (150 mL). The crude solid was purified by flash chromatography (gradient from 3:1 $CHCl_3$:hexanes to $CHCl_3$) followed by recrystallization via solvent diffusion in $CHCl_3$ (25 mL) and hexanes (100 mL) to yield 150 mg of black solid (47%). ^{1}H NMR (600 MHz, $CDCl_3$, δ): 8.09 (d, *J* = 3.93 Hz, 2 H), 7.94 (s, 2 H), 7.44 (s, 2 H), 7.44 (d, *J* = 4.65 Hz, 2 H), 3.52 (d, *J* = 7.25 Hz, 4 H), 1.84-1.77 (m, 2 H), 1.40-1.24 (m, 16 H), 0.92 (t, *J* = 7.59 Hz, 6 H), 0.90 (t, *J* = 7.04 Hz, 6 H). EI-MS (*m/z*): $[M]^+$ calculated for $C_{42}H_{42}N_4O_4S_5$, 826.1810; found, 826.1804. Anal. calculated for $C_{42}H_{42}N_4O_4S_5$: C, 60.99; H, 5.12; N, 6.77; found: C, 61.06; H, 5.26; N, 6.54.

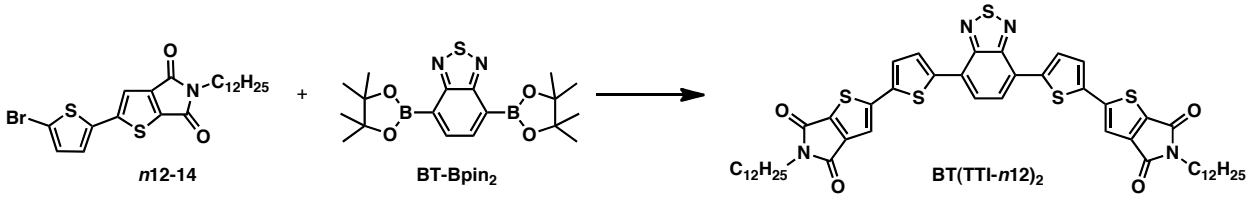

*n*12-14 BT-Bpin$_2$ BT(TTI-*n*12)$_2$

*2,2'-(5,5'-(Benzo[c][1,2,5]thiadiazole-4,7-diyl)bis(thiophene-5,2-diyl))bis(5-dodecyl-4H-thieno[2,3-c]pyrrole-4,6(5H)-dione) (**BT(TTI-n12)$_2$**)*. Compound ***n*12-14** (374 mg, 776 μmol) and **BT-Bpin$_2$** (140 mg, 361 mmol) were combined with $Pd(PPh_3)_4$ (20.8 mg, 18.0 μmol) and CsF (121 mg, 794 μmol) in a 50 mL Schlenk tube. The reaction vessel was purged with three vacuum/nitrogen cycles before dioxane (12.2 mL) was added to the reaction flask. After stirring at 90 °C for 16 h, the reaction contents were cooled to room temperature, diluted with $CHCl_3$ (10 mL) and then precipitated into methanol (150 mL). The crude solid was purified by flash chromatography (gradient from 3:1 $CHCl_3$:hexanes to $CHCl_3$) followed by recrystallization via solvent diffusion in $CHCl_3$ (125 mL) and methanol (125 mL) to yield 191 mg of black solid (56%). ^{1}H NMR (400 MHz, $CDCl_3$, δ): 8.08 (d, J = 3.92 Hz, 2 H), 7.93 (s, 2 H), 7.43 (s, 2 H), 7.43 (d, J = 4.91 Hz, 2 H), 3.61 (t, J = 7.22 Hz, 4 H), 1.70-1.61 (m, 4 H), 1.38-1.21 (m, 36 H), 0.88 (t, J = 6.71 Hz, 6 H). EI-MS (*m/z*): $[M]^+$ calculated for $C_{50}H_{58}N_4O_4S_5$, 938.3062; found, 938.3038. Anal. calculated for $C_{50}H_{58}N_4O_4S_5$: C, 63.93; H, 6.22; N, 5.96; found: C, 63.69; H, 6.27; N, 5.94.

Device Fabrication.

Thin-film BHJ solar cells were fabricated using DPP-Py as the p-type material and $BT(TPI)_2$, $ITNCN(TPI)_2$, or $BT(TTI)_2$ (*n*12 or EH) as the n-type material. All devices were fabricated on indium tin oxide (ITO) coated glass substrates (pre-patterned, R = 20 Ω/sq, Thin Film Devices, Inc.). Prior to use, the ITO substrates were cleaned by sonication with a surfactant solution (Hellmanex III, 2% in deionized water), deionized water, acetone, and isopropyl alcohol for 20 minutes each. The substrates were rinsed with isopropyl alcohol, dried under a nitrogen stream, and then exposed to UV/O_3 for 5 minutes (UVOCS, Inc. ultraviolet-ozone cleaning system, model T10X10). A thin layer of PEDOT:PSS (Clevios PVP AI, 30–40 nm) was deposited by spincoating (4000 RPM for 40 s), and then dried on a hotplate for 10 minutes at 140 °C in air. The samples were transferred to a N_2 filled glovebox where the active layers were spin-coated (2000 RPM for 40 s then 4000 RPM for 4 s). Cathodes (20 nm Ca followed by 100 nm Al) were thermally evaporated under vacuum (~10^{-7} torr) through a shadow mask, resulting in eight distinct devices per substrate, each with an active area of ~0.03 cm^2. Some of the samples were then thermally annealed by placing them substrate-side down (active layer facing up) on a hot plate. During device optimization, different solution concentrations and p-type:n-type ratios were tested in order to obtain the optimized process conditions, and the experiments were repeated multiple times to ensure data reproducibility. Details of the optimized processing conditions for each device are shown in Table 5.2.

Table 5.2. Optimized processing conditions for DPP-Py:non-fullerene devices

Non-fullerene N-type Small Molecule	P-type Concentration (mg/mL)	N-type Concentration (mg/mL)	P-type:N-type Blend Ratio	Annealing Time at 130°C (min)	Average Film Thickness (nm)
BT(TPI-*n*12)$_2$	15	15	1:2	10	132
BT(TPI-EH)$_2$	15	15	1:2	10	124
ITNCN(TPI-*n*12)$_2$	15	10	1:1	5	105
ITNCN(TPI-EH)$_2$	20	10	1:1	5	93
BT(TTI-*n*12)$_2$	15	20	1:2	15	104
BT(TTI-EH)$_2$	15	20	1:2	15	116

Device Characterization.

Solar cell devices were tested under AM 1.5 G solar illumination at 100 mW/cm^2 (1 sun) using a Thermal-Oriel 150W solar simulator. Current-voltage (*J-V*) curves were measured using a Keithley 2400 source-measure unit.

The thickness of the thin-film active layers was measured by profilometry (Veeco Dektat 150).

Height profiles of the device active layers were imaged using a Veeco Multimode V Atomic Force Microscope (AFM). The AFM was operated in tapping mode, under ambient conditions, using an aluminum coated silicon cantilever (Veeco; TAP150A, f_o = 122-169 kHz, k = 5N/m).

Grazing-incidence x-ray diffraction (GIXD) experiments were conducted at the Stanford Synchrotron Radiation Lightsource on beam-line 11-3. Substituting Si for ITO on glass, thin-film samples were prepared following the aforementioned procedure for solar cell devices. Both neat films and p-type:n-type material blends using the optimal solar cell conditions were tested. Samples were irradiated at a fixed incident angle of approximately 0.1°, and the GIXD patterns were recorded with a 2-D image detector (MAR345 image plate detector) at an X-ray energy of 12.71 keV (λ = 0.975 Å). To maximize the intensity from the sample, the incident angle (~0.08° – 0.12°) was carefully chosen such that the X-ray beam penetrated the sample completely but did not interact significantly with the silicon substrate. Typical exposure times were 30-900 s.

For external quantum efficiency (EQE) measurements, a 150 W xenon light source (Newport 6255), housed within an arc lamp housing unit (Newport 66902), was directed through a Princeton Instruments Spectra Pro 2300i monochromator. The light source was chopped at 30 Hz with a Scitec optical chopper and referenced with a calibrated silicon photodiode (ThorLabs S120VC). Signal from the substrate was moderated with a Stanford Research Systems low-noise current preamplifier followed by a Scitec 420 dual-phase lock-in amplifier (referenced to the optical shopper). EQE curves were measured using a Keithly 2612A source-measure unit.

References

(1) Scharber, M. C.; Mühlbacher, D.; Koppe, M.; Denk, P.; Waldauf, C.; Heeger, A. J.; Brabec, C. J. *Adv. Mater.* **2006**, *18*, 789–794.

(2) Günes, S.; Neugebauer, H.; Sariciftci, N. S. *Chem. Rev.* **2007**, *107*, 1324–1338.

(3) Thompson, B. C.; Fréchet, J. M. J. *Angew. Chem. Int. Ed.* **2008**, *47*, 58–77.

(4) He, Z.; Zhong, C.; Huang, X.; Wong, W.-Y.; Wu, H.; Chen, L.; Su, S.; Cao, Y. *Adv. Mater.* **2011**, *23*, 4636–4643.

(5) Small, C. E.; Chen, S.; Subbiah, J.; Amb, C. M.; Tsang, S.-W.; Lai, T.-H.; Reynolds, J. R.; So, F. *Nat. Photon.* **2012**, *6*, 115–120.

(6) He, Z.; Zhong, C.; Su, S.; Xu, M.; Wu, H.; Cao, Y. *Nat. Photon.* **2012**, *6*, 591–595.

(7) Lu, L.; Luo, Z.; Xu, T.; Yu, L. *Nano Lett.* **2013**, *13*, 59–64.

(8) Dang, M. T.; Hirsch, L.; Wantz, G. *Adv. Mater.* **2011**, *23*, 3597–3602.
(9) Paek, S.; Cho, N.; Cho, S.; Lee, J. K.; Ko, J. *Org. Lett.* **2012**, *14*, 6326–6329.
(10) Hesse, H. C.; Weickert, J.; Hundschell, C.; Feng, X.; Müllen, K.; Nickel, B.; Mozer, A. J.; Schmidt-Mende, L. *Adv. Energy Mater.* **2011**, *1*, 861–869.
(11) He, Y.; Chen, H.-Y.; Hou, J.; Li, Y. *J. Am. Chem. Soc.* **2010**, *132*, 1377–1382.
(12) Brabec, C. J.; Zerza, G.; Cerullo, G.; Silvestri, S. De; Luzzati, S.; Hummelen, J. C.; Sariciftci, S. *Chem. Phys. Lett.* **2001**, *340*, 232–236.
(13) Schilinsky, P.; Waldauf, C.; Brabec, C. J. *Appl. Phys. Lett.* **2002**, *81*, 3885–3887.
(14) Mihailetchi, V. D.; Van Duren, J. K. J.; Blom, P. W. M.; Hummelen, J. C.; Janssen, R. A. J.; Kroon, J. M.; Rispens, M. T.; Verhees, W. J. H.; Wienk, M. M. *Adv. Funct. Mater.* **2003**, *13*, 43–46.
(15) Brabec, C. J.; Cravino, A.; Meissner, D.; Sariciftci, N. S.; Fromherz, T.; Rispens, M. T.; Sanchez, L.; Hummelen, J. C. *Adv. Funct. Mater.* **2001**, *11*, 374–380.
(16) Wienk, M. M.; Kroon, J. M.; Verhees, W. J. H.; Knol, J.; Hummelen, J. C.; Van Hal, P. A.; Janssen, R. A. J. *Angew. Chem. Int. Ed.* **2003**, *42*, 3371–3375.
(17) Savenije, T. J.; Kroeze, J. E.; Yang, X.; Loos, J. *Adv. Funct. Mater.* **2005**, *15*, 1260–1266.
(18) Bartelt, J. A.; Beiley, Z. M.; Hoke, E. T.; Mateker, W. R.; Douglas, J. D.; Collins, B. A.; Tumbleston, J. R.; Graham, K. R.; Amassian, A.; Ade, H.; Fréchet, J. M. J.; Toney, M. F.; McGehee, M. D. *Adv. Energy Mater.* **2013**, *3*, 364–374.
(19) Burkhard, G. F.; Hoke, E. T.; Scully, S. R.; McGehee, M. D. *Nano Lett.* **2009**, *9*, 4037–4041.
(20) Brunetti, F. G.; Gong, X.; Tong, M.; Heeger, A. J.; Wudl, F. *Angew. Chem. Int. Ed.* **2010**, *49*, 532–536.
(21) Shu, Y.; Lim, Y.-F.; Li, Z.; Purushothaman, B.; Hallani, R.; Kim, J. E.; Parkin, S. R.; Malliaras, G. G.; Anthony, J. E. *Chem. Sci.* **2011**, *2*, 363–368.
(22) Schwenn, P. E.; Gui, K.; Nardes, A. M.; Krueger, K. B.; Lee, K. H.; Mutkins, K.; Rubinstein-Dunlop, H.; Shaw, P. E.; Kopidakis, N.; Burn, P. L.; Meredith, P. *Adv. Energy Mater.* **2011**, *1*, 73–81.
(23) Zhou, E.; Cong, J.; Wei, Q.; Tajima, K.; Yang, C.; Hashimoto, K. *Angew. Chem. Int. Ed.* **2011**, *50*, 2799–2803.
(24) Zhou, T.; Jia, T.; Kang, B.; Li, F.; Fahlman, M.; Wang, Y. *Adv. Energy Mater.* **2011**, *1*, 431–439.
(25) Ren, G.; Ahmed, E.; Jenekhe, S. A. *Adv. Energy Mater.* **2011**, *1*, 946–953.
(26) Bloking, J. T.; Han, X.; Higgs, A. T.; Kastrop, J. P.; Pandey, L.; Norton, J. E.; Risko, C.; Chen, C. E.; Brédas, J.-L.; McGehee, M. D.; Sellinger, A. *Chem. Mater.* **2011**, *23*, 5484–5490.
(27) Zhou, Y.; Ding, L.; Shi, K.; Dai, Y.-Z.; Ai, N.; Wang, J.; Pei, J. *Adv. Mater.* **2012**, *24*, 957–961.
(28) Walker, B.; Han, X.; Kim, C.; Sellinger, A.; Nguyen, T.-Q. *ACS Appl. Mater. Interfaces* **2012**, *4*, 244–250.
(29) Fang, Y.; Pandey, A. K.; Nardes, A. M.; Kopidakis, N.; Burn, P. L.; Meredith, P. *Adv. Energy Mater.* **2012**, *3*, 54–59.
(30) Lloyd, M. T.; Anthony, J. E.; Malliaras, G. G. *Mater. Today* **2007**, *10*, 34–41.
(31) Roncali, J. *Acc. Chem. Res.* **2009**, *42*, 1719–1730.
(32) Walker, B.; Kim, C.; Nguyen, T.-Q. *Chem. Mater.* **2011**, *23*, 470–482.
(33) Liu, Y.; Wan, X.; Wang, F.; Zhou, J.; Long, G.; Tian, J.; You, J.; Yang, Y.; Chen, Y. *Adv. Energy Mater.* **2011**, *1*, 771–775.
(34) Liu, Y.; Wan, X.; Wang, F.; Zhou, J.; Long, G.; Tian, J.; Chen, Y. *Adv. Mater.* **2011**, *23*, 5387–5391.
(35) Wei, G.; Wang, S.; Sun, K.; Thompson, M. E.; Forrest, S. R. *Adv. Energy Mater.* **2011**, *1*, 184–187.
(36) Zhou, J.; Wan, X.; Liu, Y.; Long, G.; Wang, F.; Li, Z.; Zuo, Y.; Li, C.; Chen, Y. *Chem. Mater.* **2011**, *23*, 4666–4668.
(37) Li, Z.; He, G.; Wan, X.; Liu, Y.; Zhou, J.; Long, G.; Zuo, Y.; Zhang, M.; Chen, Y. *Adv. Energy Mater.* **2012**, *2*, 74–77.
(38) Sun, Y.; Welch, G. C.; Leong, W. L.; Takacs, C. J.; Bazan, G. C.; Heeger, A. J. *Nat. Mater.* **2012**, *11*, 44–48.
(39) Van der Poll, T. S.; Love, J. A.; Nguyen, T.-Q.; Bazan, G. C. *Adv. Mater.* **2012**, *24*, 3646–3649.
(40) Lee, O. P.; Yiu, A. T.; Beaujuge, P. M.; Woo, C. H.; Holcombe, T. W.; Millstone, J. E.; Douglas, J. D.; Chen, M. S.; Fréchet, J. M. J. *Adv. Mater.* **2011**, *23*, 5359–5363.
(41) Mühlbacher, D.; Scharber, M.; Morana, M.; Zhu, Z.; Waller, D.; Gaudiana, R.; Brabec, C. *Adv. Mater.* **2006**, *18*, 2884–2889.
(42) Peet, J.; Kim, J. Y.; Coates, N. E.; Ma, W. L.; Moses, D.; Heeger, A. J.; Bazan, G. C. *Nat. Mater.* **2007**, *6*, 497–500.
(43) Blouin, N.; Michaud, A.; Leclerc, M. *Adv. Mater.* **2007**, *19*, 2295–2300.

(44) Park, S. H.; Roy, A.; Beaupré, S.; Cho, S.; Coates, N.; Moon, J. S.; Moses, D.; Leclerc, M.; Lee, K.; Heeger, A. J. *Nat. Photon.* **2009**, *3*, 297–303.
(45) Zhou, H.; Yang, L.; Stuart, A. C.; Price, S. C.; Liu, S.; You, W. *Angew. Chem. Int. Ed.* **2011**, *50*, 2995–2998.
(46) Stuart, A. C.; Tumbleston, J. R.; Zhou, H.; Li, W.; Liu, S.; Ade, H.; You, W. *J. Am. Chem. Soc.* **2013**.
(47) Woo, C. H.; Holcombe, T. W.; Unruh, D. A.; Sellinger, A.; Fréchet, J. M. J. *Chem. Mater.* **2010**, *22*, 1673–1679.
(48) Douglas, J. D.; Griffini, G.; Holcombe, T. W.; Young, E. P.; Lee, O. P.; Chen, M. S.; Fréchet, J. M. J. *Macromolecules* **2012**, *45*, 4069–4074.
(49) Piliego, C.; Holcombe, T. W.; Douglas, J. D.; Woo, C. H.; Beaujuge, P. M.; Fréchet, J. M. J. *J. Am. Chem. Soc.* **2010**, *132*, 7595–7597.
(50) Chu, T.-Y.; Lu, J.; Beaupré, S.; Zhang, Y.; Pouliot, J.-R.; Wakim, S.; Zhou, J.; Leclerc, M.; Li, Z.; Ding, J.; Tao, Y. *J. Am. Chem. Soc.* **2011**, *133*, 4250–4253.
(51) Amb, C. M.; Chen, S.; Graham, K. R.; Subbiah, J.; Small, C. E.; So, F.; Reynolds, J. R. *J. Am. Chem. Soc.* **2011**, *133*, 10062–10065.
(52) Inganäs, O.; Svensson, M.; Zhang, F.; Gadisa, A.; Persson, N. K.; Wang, X.; Andersson, M. R. *Appl. Phys. A* **2004**, *79*, 31–35.
(53) Chen, M.-H.; Hou, J.; Hong, Z.; Yang, G.; Sista, S.; Chen, L.-M.; Yang, Y. *Adv. Mater.* **2009**, *21*, 4238–4242.
(54) Szarko, J. M.; Guo, J.; Liang, Y.; Lee, B.; Rolczynski, B. S.; Strzalka, J.; Xu, T.; Loser, S.; Marks, T. J.; Yu, L.; Chen, L. X. *Adv. Mater.* **2010**, *22*, 5468–5472.
(55) Brédas, J. L. *J. Chem. Phys.* **1985**, *82*, 3808–3811.
(56) Brédas, J. L.; Heeger, A. J.; Wudl, F. *J. Chem. Phys.* **1986**, *85*, 4673–4678.
(57) Brédas, J. L. *Synt. Met.* **1987**, *17*, 115–121.
(58) Koster, L. J. A.; Shaheen, S. E.; Hummelen, J. C. *Adv. Energy Mater.* **2012**, *2*, 1246–1253.
(59) Cook, S.; Katoh, R.; Furube, A. *J. Phys. Chem. C* **2009**, *113*, 2547–2552.
(60) Bakulin, A. A.; Hummelen, J. C.; Pshenichnikov, M. S.; Van Loosdrecht, P. H. M. *Adv. Funct. Mater.* **2010**, *20*, 1653–1660.
(61) Bakulin, A. A.; Dimitrov, S. D.; Rao, A.; Chow, P. C. Y.; Nielsen, C. B.; Schroeder, B. C.; McCulloch, I.; Bakker, H. J.; Durrant, J. R.; Friend, R. H. *J. Phys. Chem. Lett.* **2013**, *4*, 209–215.
(62) Nicolaidis, N. C.; Routley, B. S.; Holdsworth, J. L.; Belcher, W. J.; Zhou, X.; Dastoor, P. C. *J. Phys. Chem. C* **2011**, *115*, 7801–7805.
(63) Dimitrov, S. D.; Nielsen, C. B.; Shoaee, S.; Tuladhar, P. S.; Du, J.; McCulloch, I.; Durrant, J. R. *J. Phys. Chem. Lett.* **2012**, *3*, 140–144.
(64) Chadwick, D. J.; Plant, A. *Tetrahedron Lett.* **1987**, *28*, 6085–6088.
(65) Reinecke, M. G.; Newsom, J. G.; Chen, L.-J. *J. Am. Chem. Soc.* **1981**, *103*, 2760–2769.

Appendix 1. Thieno[3,4-*b*]furan-Based Polymers with Quinoidal Character and Oxygen Heteroatoms

Abstract

An ester-functionalized thieno[3,4-*b*]furan (TF) monomer was developed and synthesized in six linear steps. The optoelectronic properties of TF-based donor-acceptor polymers were evaluated, and in comparison to thieno[3,4-*b*]thiophene-based (TT) polymer, TF-containing materials have larger band gaps and less quinoidal stabilization.

Introduction

High performing organic photovoltaic (OPV) devices contain semiconducting materials that have optoelectronic and physical properties optimized for photo energy conversion. Toward enhancing light absorption, the incorporation of quinoidal structure into a polymer backbone is a popular design strategy for tightening the band gap of a material.[1,2] In Chapter 4, we showed that the band gap of an imide-based polymer was lower when it contained isothianphthene (ITN) monomers than when it contained simple thiophene units.[3] The phenyl ring on ITN stabilizes the quinoidal resonance form of ITN-based polymers, and decreases the material band gap and bond length alternation along the backbone.[4,5] Similarly, the fused structure of thieno[3,4-*b*]thiophene (TT) promotes quinoidal character in TT-based polymers[6,7] and provides poly(thieno[3,4-*b*]thiophene) a narrow band gap of 0.85 eV.[8] Recently, an ester-functionalized TT monomer has been incorporated in donor-acceptor p-type copolymers and OPV efficiencies above 7% have been reported.[9–12]

Control of the physical arrangement of conjugated materials in an OPV bulk heterojunction (BHJ) is also important for high device performance. In particular, the structure of a polymer can be designed to improve solid-state packing parameters, which affect charge transport. In Chapter 2, the length and bulk of alkyl side chains on a conjugated polymer were shown to affect the π- and lamellar-packing distances of the p-type material.[13] The polymers with shorter and more linear solubilizing groups provided tighter backbone spacing and higher charge carrier mobility.[13,14] Unfortunately, drastically shortening or removing the polymer side chains to further improve the solid-state polymer packing distances compromises solvent solubility and solution processability. The incorporation of furan-based monomers into OPV materials, however, has recently been shown to increase polymer solubility,[15–17] decreasing the need for bulky polymer side groups.[18]

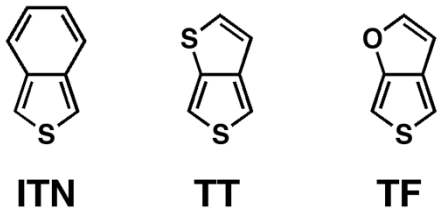

Figure A.1. The chemical structures of isothianaphthene (ITN), thieno[3,4-*b*]thiophene (TT), and thieno[3,4-*b*]furan (TF).

Herein, we report the synthesis of a thieno[3,4-*b*]furan (TF) monomer with a modular route that allows for side chain variation in the final step. The TF building block is an attractive acceptor monomer for p-type polymers because it contains a quinoid-stabilizing fused ring core and incorporates the furan heterocycle that has been shown to improve polymer solubility. In comparison to an analogous TT-based polymer, a donor-acceptor copolymer containing the TF monomer is found to have a 0.2 eV larger band gap. This band gap difference is due to the lower aromaticity of furan,[19,20] which provides less quinoidal stabilization to TF-polymers relative to TT-based materials.

Results and Discussion

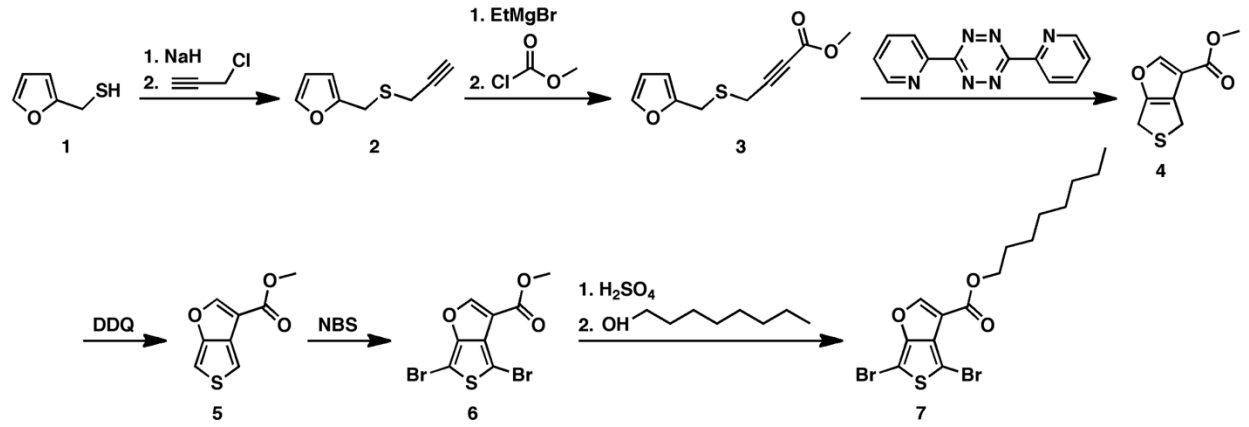

Scheme A.1. Synthetic route toward the thieno[3,4-*b*]furan (TF) monomer.

The ester-functionalized TF monomer was synthesized in six linear steps from furfuryl mercaptan (**1**) (Scheme A.1). Deprotonation of thiol **1**, followed by an S_N2 attack on propargyl chloride, afforded alkyne **2**, which was then easily deprotonated and quenched with methyl chloroformate to provide thioether **3**. The fused dihydothienofuran core (**4**) was then formed via an intramolecular Diels-Alder rection with compound **3**, followed by an intermolecular Diels-Alder reaction with 3,6-di(pyridin-2-yl)-1,2,4,5-tetrazine, and two retro-Diels-Alder reactions which evolved nitrogen gas. Oxidation of compound **4** with 2,3-dichloro-5,6-dicyano-1,4-benzoquinone (DDQ) gave thienofuran **5**, which was then readily dibrominated with *N*-bromosuccinimide (NBS) to produce compound **6**. Acid catalyzed transesterification of **6** finally yielded monomer **7** with a linear octyl side chain. This final transesterification provides a modular synthetic route for synthesizing ester-based TF polymers with different solubilizing side chains. Stille cross-coupling with furan (F), bithiophene (2T), and benzodithiophene (BDT) donor monomers yielded polymers **PTFF**, **PTF2T**, **PTFBDT-Me**, **PTFBDT-EH**, and **PTFBDT-EHT** (Figure A.2).

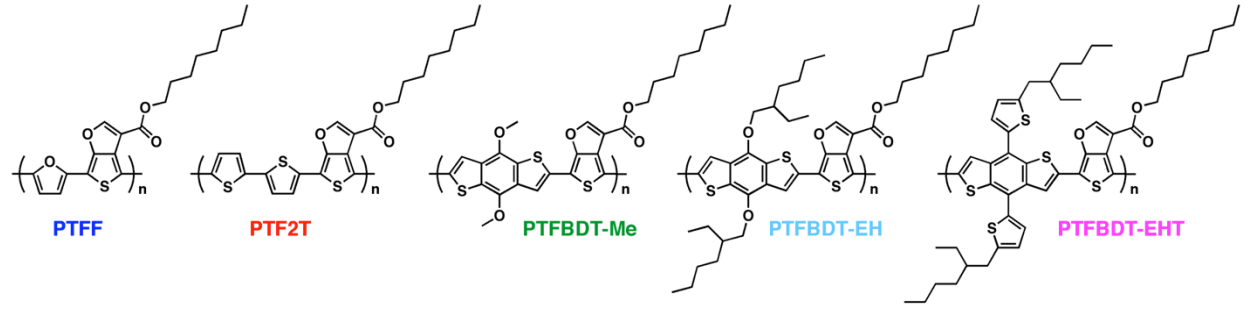

Figure A.2. Thieno[3,4-*b*]furan-based polymers **PTFF**, **PTF2T**, **PTFBDT-Me**, **PTFBDT-EH**, and **PTFBDT-EHT**.

The five TF-based polymers have relatively similar solution (Figure A.3a) and thin-film (Figure A.3b) absorption spectra that overlap with the visible region of the solar spectrum. **PTFF** has a slightly larger band gap than the four thiophene backbone-based polymers, which follows the blue-shifted trend in the literature for polyfuran materials (Table A.1).[20] To evaluate the

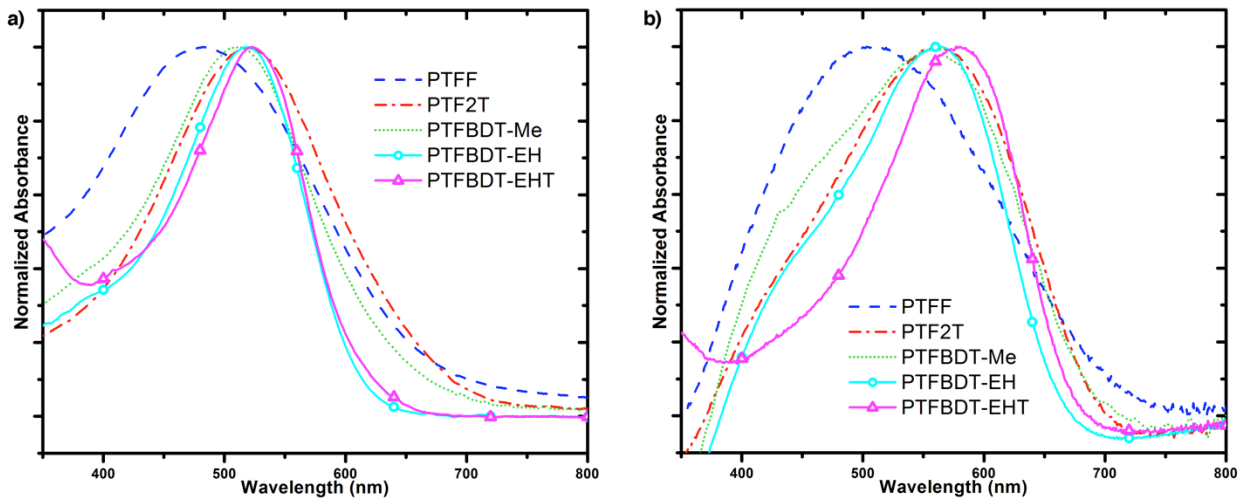

Figure A.3. UV-vis absorption spectra of thienofuran-based polymers in a) chloroform solutions and b) thin films.

quinoidal effect of thienofuran on polymer energy levels, **PTFBDT-EH** can be compared to an analogous thienothiophene polymer, **PTB5** (Figure A.4).[21] Both polymers have a BDT donor monomer with 2-ethylhexyl side chains and an ester-functionalized side group on the quinoidal acceptor monomer. In the literature, **PTB5** is reported to have an onset of absorption of 764 nm and a band gap of 1.62 eV,[21] while here we find that **PTFBDT-EH** has an onset of absorption of 665 nm and a band gap of 1.86 eV. This discrepancy in the polymer band gaps likely stems from the different aromatic stabilization energies of thiophene (29 kcal/mol) and furan (16 kcal/mol).[19] In thieno[3,4-*b*]thiophene, both the aromatic and quinoidal resonance forms of the polymer contain an aromatic thiophene subunit (either the backbone thiophene or the fused thiophene is aromatized, respectively). This competing aromaticity between the two thiophene subunits means that a TT-based polymer equally favors its quinoidal and aromatic resonance structures. In contrast, a thienofuran-based polymer prefers its aromatic conformation because the stabilization gained from having the thiophene subunit aromatized is greater than the stability provided by the aromatized furan subunit in the quinoidal form of the polymer. This preference for TF to exist in its aromatic resonance structure means that TF-based polymers have less quinoidal character than TT-based polymers and resultantly larger band gaps.[22] The electrochemical properties of the five new polymers was determined with cyclic voltammetry and revealed that the HOMO energy level of the BDT-containing polymers was 0.2-0.3 eV lower than the HOMO of **PTFF** or **PTF2T**. This stabilization in the BDT-based polymers could be the result of the aromaticity provided by the phenyl ring in the center of the fused BDT structure.

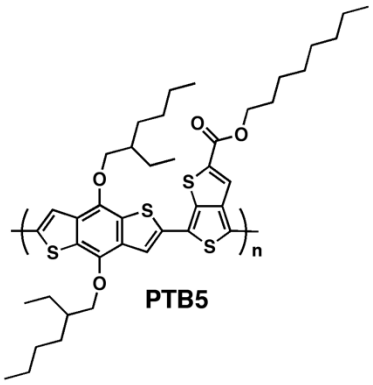

Figure A.4. Structure of TT-based polymer **PTB5**.

Table A.1. Polymer and optoelectronic properties of thienofuran-based polymers

	Polymer Properties		Optoelectronic Properties		
	M_n (kDa)	PDI	HOMO[a] (eV)	LUMO[a] (eV)	E_g[b] (eV)
PTFF	1.6	1.9	5.17	3.29	1.77
PTF2T	2.6	1.4	5.18	3.95	1.78
PTFBDT-Me[c]	--	--	5.49	3.61	1.78
PTFBDT-EH	17	2.0	5.47	3.35	1.86
PTFBDT-EHT	19	1.9	5.36	3.85	1.85

[a] CV determined HOMO values are reported relative to Fc/Fc^+ at -5.13 eV. [b] Optical band gap in thin films based on onset of absorption. [c] **PTFBDT-Me** is too insoluble for SEC analysis in chloroform.

Conclusions

In conclusion, five new thienofuran donor-acceptor copolymers were synthesized and their optoelectronic properties were evaluated. The TF monomer was determined to have less quinoidal character than the TT monomer and in a comparison of analogous polymers, the TF-based material had a larger band gap than the TT-based polymer. Further development of the TF polymer side chain functionalities and solubilizing groups will likely change the molecular weight, solubility, and optoelectronic properties of the material. Incorporation of the TF-based polymers in BHJ OPV devices will reveal if the materials are effective at converting solar energy into an electrical current, and solid-state grazing incidence diffraction will show how the polymers pack in thin films.

Experimental

Materials.

All commercially available reagents obtained from suppliers were used without further purification. Unless otherwise noted, all reactions were carried out under nitrogen with standard Schlenk techniques, and all glassware used in dry reactions was flame dried under high-vacuum prior to use. Tetrahydrofuran (THF), dichloromethane (DCM), and toluene were purified and dried by passing through two columns of neutral alumina, under nitrogen, prior to use. Flash chromatography was performed using Silicycle SiliaFlash ® P60 (particle size 40-63 μm, 230-400 mesh) silica gel.

Building block benzo[1,2-*b*:4,5-*b*']dithiophene-4,8-dione and monomer (4,8-bis((2-ethylhexyl)oxy)benzo[1,2-*b*:4,5-*b*']dithiophene-2,6-diyl)bis(trimethylstannane) (BDT-EH) were synthesized according to the procedure in a previous chapter. Monomer 2,5-bis(trimethylstannyl)furan (F) and 5,5'-bis(trimethylstannyl)-2,2'-bithiophene (2T) were synthesized according to the procedures reported in the literature.[15,23] Monomer (4,8-bis(5-(2-ethylhexyl)thiophen-2-yl)benzo[1,2-*b*:4,5-*b*']dithiophene-2,6-diyl)bis(trimethylstannane) (BDT-EHT) was purchased from SunaTech Inc.

Material Characterization.

All ^1H and ^{13}C NMR spectra were obtained with a Bruker AVQ-400, DRX-500 or AV-600 instrument, and ^{13}C spectra were collected with a proton-decoupling pulse program. NMR abbreviations: d = doublet, m = multiplet, s = singlet, and t = triplet. Elemental analysis (CHN) was performed by the UC Berkeley microanalysis laboratory. Data from high-resolution mass spectrometry (HRMS) using electron impact (EI) were obtained by the UC Berkeley mass spectrometry facility.

Gas chromatography-mass spectrometry (GC-MS) data was collected on an Agilent 7890A GC system fitted with an Agilent HP-5 chromatography column. Helium carrier gas at a flow rate of 2.2 mL/min was used as the mobile phase. The sample inlet was 250 °C and a pressure of 8.8 PSI was used to load the vaporized compounds onto the column at a split ratio of 50:1. The oven temperature was equilibrated at 50 °C for 30 seconds, and then a 19 minute temperature program was run as follows: 50 °C for 1 minute, ramp to 310 °C at 20 °C/min for 13 minutes, hold at 310 °C for 5 minutes. An auxiliary heater was kept at 150 °C between the GC column and the Agilent 5975C VL MSD system (electron impact (EI)) in order to prevent precipitation of the separated compounds from the He carrier gas at the MSD system inlet. MS information was collected by the 5975C system and analyzed with Agilent Chemstation software.

Solution and thin-film UV-vis absorption spectra were gathered at room temperature using a Varian Cary 50 Conc spectrophotometer. The absorption spectra in chloroform solutions were measured using a quartz cuvette with a 1 cm path length. Thin films were spuncoat from chlorobenzene onto untreated quartz slides.

Cyclic voltammograms (CV) were collected using a Solartron 1285 potentiostat under the control of CorrWare II software. A standard three electrode cell based on a Pt wire working electrode, a silver wire reference electrode (calibrated vs. Fc/Fc^+ at -5.13 eV), and a Pt wire counter electrode was purged with nitrogen and maintained under a nitrogen atmosphere during all measurements. Anhydrous acetonitrile was purchased from Aldrich, and tetrabutylammonium hexafluorophosphate (0.1 M) was used as the supporting electrolyte. Polymer films were drop cast onto a Pt wire working electrode from a 1% (w/w) chloroform solution and dried under nitrogen prior to measurement.

Synthesis.

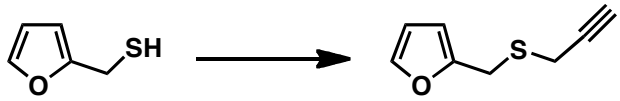

1 **2**

*2-((Prop-2-yn-1-ylthio)methyl)furan (**2**).*[24] Sodium hydride (2.42 g, 101 mmol) was added to a flame-dried 500 mL flask and the reaction vessel was purged with three vacuum/nitrogen cycles before being chilled to 0 °C for 1 h with THF (225 mL). Furan-2-ylmethanethiol (**1**) (10.0 g, 87.6 mmol) was added to the reaction mixture dropwise, and the reaction contents were stirred at 0 °C for 1 h. Propargyl chloride (7.83 g, 105 mmol) was added to the reaction mixture and the reaction contents stirred at room temperature for 16 hr before being quenched with water (100 mL). Volatiles were removed from the reaction mixture under reduced pressure, and the reaction contents were extracted with diethyl ether, washed with a 10 % solution of potassium hydroxide and water, dried over $MgSO_4$, and filtered. Volatiles were removed under reduced pressure to yield 11.3 g of a light yellow oil (85 %). The crude product was used without any further purification. ^{1}H NMR (400 MHz, $CHCl_3$, δ): 7.37 (d, J = 1.12 Hz, 1 H), 6.31 (dd, J = 2.97, 1.99 Hz, 1 H), 6.23 (d, J = 3.10 Hz, 1 H), 3.89 (s, 2 H), 3.19 (d, J = 2.59 Hz, 2 H), 2.28 (t, J = 2.58 Hz, 1 H). ^{13}C (100 MHz, $CDCl_3$, δ): 150.5, 142.5, 110.5, 108.2, 79.6, 71.4, 27.4, 18.9. GC-MS (*m/z*): $[M]^+$ calculated for C_8H_8OS, 152.0; found, 152.0.

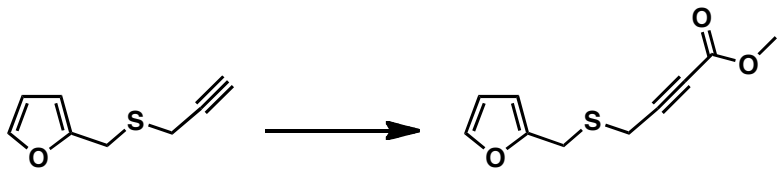

2 3

*Methyl 4-((furan-2-ylmethyl)thio)but-2-ynoate (**3**).*[24] Compound **2** (11.2 g, 73.6 mmol) was added to a flame-dried 1 L flask and the reaction vessel was purged with three vacuum/nitrogen cycles before being chilled to 0 °C for 1 h with THF (250 mL). Ethylmagnesium bromide (88.3 mL of a 1.0 M solution in THF, 88.3 mmol) was added to the reaction mixture over 15 min. After stirring for 2 h on the melting ice bath, 30 min at room temperature and 30 min at 0 °C, methyl chloroformate (9.04 g, 95.7 mmol) was added dropwise to the reaction mixture. The reaction contents were stirred for another 16 h at room temperature before being quenched with water (100 mL). Volatiles were removed from the reaction mixture under reduced pressure, and the reaction contents were extracted with diethyl ether, washed with a solution of saturated ammonium chloride and water, dried over $MgSO_4$, and filtered. Volatiles were removed under reduced pressure to yield 14.7 g of a brown oil (95 %). The crude product was used without any further purification. ^{1}H NMR (400 MHz, $CHCl_3$, δ): 7.37 (d, J = 1.68 Hz, 1 H), 6.31 (dd, J = 3.08, 1.93 Hz, 1 H), 6.24 (d, J = 3.15 Hz, 1 H), 3.88 (s, 2 H), 3.78 (s, 3 H), 3.28 (s, 2 H). ^{13}C (100 MHz, $CDCl_3$, δ):153.9, 150.0, 142.7, 110.6, 108.6, 84.0, 74.8, 52.9, 27.9, 18.7. GC-MS (*m/z*): $[M]^+$ calculated for $C_{10}H_{10}O_3S$, 210.0; found, 210.0.

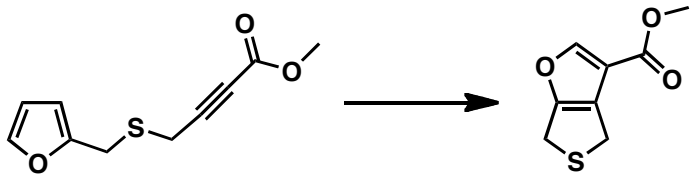

3 4

*Methyl 4,6-dihydrothieno[3,4-b]furan-3-carboxylate (**4**).* Compound **3** (10.5 g, 49.9 mmol) was combined with 3,6-di(pyridin-2-yl)-1,2,4,5-tetrazine (13.0 g, 55.0 mmol) in a 1 L flask. After purging the reaction vessel with three vacuum/nitrogen cycles, the reaction contents were refluxed in toluene (450 mL) for 16 h. When the reaction mixture returned to room temperature, the reaction contents were filtered and washed with ether. Volatiles in the filtrate were removed under reduced pressure, and the crude material was extracted with diethyl ether, washed with a solution of 1 M hydrochloric acid and water, dried over $MgSO_4$, and filtered. Volatiles were removed under reduced pressure to yield 5.52 g of beige solid (60 %). The crude product was used without any further purification. ^{1}H NMR (600 MHz, $CDCl_3$, δ): 7.94 (s, 1 H), 3.99-3.92 (m, 4 H), 3.81 (s, 3 H). ^{13}C (150 MHz, $CDCl_3$, δ): 163.1, 155.7, 151.8, 124.4, 117.1, 51.6, 28.4, 28.0. GC-MS (*m/z*): $[M]^+$ calculated for $C_8H_8O_3S$, 184.0; found, 184.0.

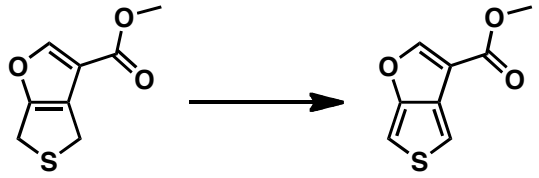

4 5

*Methyl thieno[3,4-b]furan-3-carboxylate (**5**).* Compound **4** (5.39 g, 29.3 mmol) was dissolved in DCM (210 mL) in a 500 mL flask and chilled to 0 °C. 2,3-Dichloro-5,6-dicyano-1,4-benzoquinone (8.30 g, 36.6 mmol) was added to the reaction mixture in one portion, and the reaction mixture was stirred for 16 h at room temperature. The reaction contents were filtered and washed with DCM, and volatiles in the filtrate were removed under reduced pressure. The crude material was passed through a plug of silica (DCM), then purified by flash chromatography (4:1 hexanes:DCM) to yield 3.67 g of yellow solid (69 %). ^{1}H NMR (400 MHz, $CHCl_3$, δ): 8.21 (s, 1 H), 7.25 (d, *J* = 2.60 Hz, 1 H), 6.84 (d, *J* = 2.58 Hz, 1 H), 3.89 (s, 3 H). ^{13}C (100 MHz, $CHCl_3$, δ): 163.4, 158.7, 156.6, 131.2, 112.4, 109.9, 97.1, 51.9. GC-MS (*m/z*): $[M]^+$ calculated for $C_8H_6O_3S$, 182.0; found, 182.0.

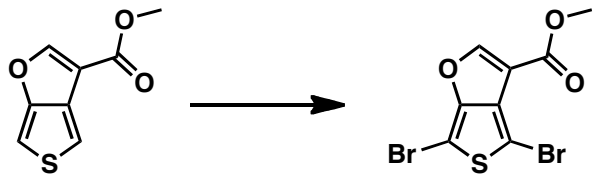

5 6

*Methyl 4,6-dibromothieno[3,4-b]furan-3-carboxylate (**6**).* Compound **5** (1.50 g, 8.23 mmol) was dissolved in $CHCl_3$ (50 mL) in a 100 mL flask and chilled to 0 °C. *N*-Bromosuccinimide (NBS) (2.21 g, 12.4 mmol) was added to the reaction mixture in one portion, and the reaction mixture was stirred for 2 h at room temperature. The reaction contents were quenched with a solution of 10 % sodium hydroxide, extracted with $CHCl_3$, washed with water, dried over $MgSO_4$, and filtered. Volatiles were removed under reduced pressure to yield 2.61 g of white solid (93 %). The crude product was used without any further purification. ^{1}H NMR (400 MHz, $CHCl_3$, δ): 8.18 (s, 1 H), 3.88 (s, 3 H). ^{13}C (100 MHz, $CHCl_3$, δ): 162.1, 159.8, 153.9, 130.2, 113.3, 96.1, 82.7, 52.0. GC-MS (*m/z*): $[M]^+$ calculated for $C_8H_4Br_2O_3S$, 339.8; found, 339.8.

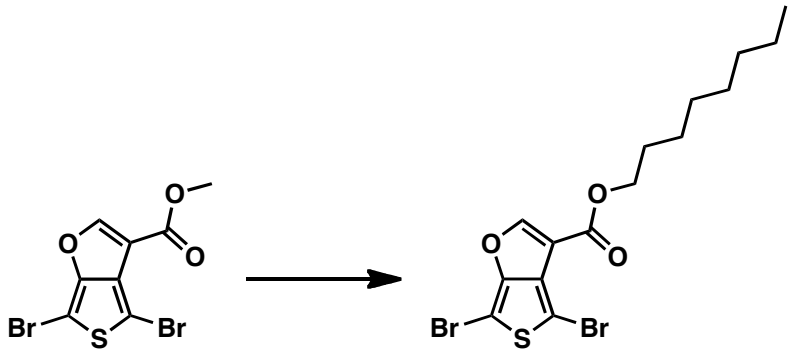

6 7

Octyl 4,6-dibromothieno[3,4-b]furan-3-carboxylate (7). Compound **6** (1.00 g, 2.94 mmol) was dissolved in 1-octanol (4.60 g, 35.3 mmol) in a 15 mL flask at 100 °C. Sulfuric acid (10 drops) was added to the reaction mixture dropwise, and the reaction contents were stirred for 16 h at 100 °C. The reaction contents were quenched with a solution of saturated sodium bicarbonate, extracted with ether, washed with water, dried over $MgSO_4$, and filtered. Volatiles were removed under reduced pressure. The crude material was purified by flash chromatography (4:1 hexanes:$CHCl_3$) and the resulting white solid was washed with methanol to yield 664 mg of white solid (52%). ^{1}H NMR (600 MHz, $CHCl_3$, δ): 8.19 (s, 1 H), 4.30 (t, J = 6.80 Hz, 2 H), 1.78-1.73 (m, 2 H), 1.43-1.38 (m, 2 H), 1.35-1.23 (m, 8 H), 0.88 (t, J = 7.03 Hz, 3 H). ^{13}C (100 MHz, $CHCl_3$, δ): 161.8, 159.8, 154.0, 130.3, 113.8, 96.1, 82.6, 65.5, 31.9, 29.4, 29.3, 28.8, 26.1, 22.8, 14.2. EI-MS (*m/z*): $[M]^+$ calculated for $C_{15}H_{18}Br_2O_3S$, 437.9323; found, 427.9330. Anal. calculated for $C_{15}H_{18}Br_2O_3S$: C, 41.12; H, 4.14; found: C, 41.28; H, 4.06.

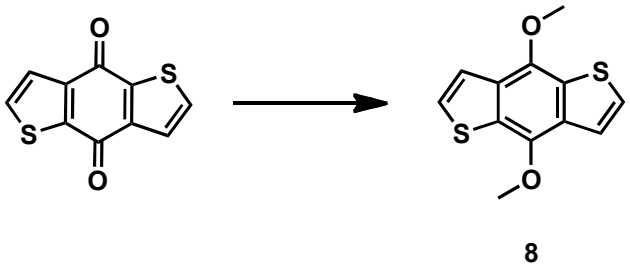

8

*4,8-Dimethoxybenzo[1,2-b:4,5-b']dithiophene (**8**).* Benzo[1,2-*b*:4,5-*b*']dithiophene-4,8-dione (2.00 g, 9.08 mmol), zinc powder (2.08 g, 31.8 mmol) and water (50 mL) were combined in a 100 mL flask. Sodium hydroxide (5.48 g, 137 mmol) was added to the reaction mixture and the reaction contents were heated at reflux for 2 h. Once the reaction turned bright yellow, the reaction mixture was cooled to room temperature, and methyl tosylate (6.76 g, 36.3 mmol) was added to the flask. The reaction contents were heated again at 50 °C for 12 h before being cooled to room temperature. The reaction mixture was extracted with diethyl ether, washed with water, dried over $MgSO_4$, and volatiles were removed under reduced pressure. The crude material was purified by flash chromatography (90:10 $CHCl_3$:hexanes) to yield 1.65 g of a colorless solid (73 %). ^{1}H NMR (400 MHz $CDCl_3$, δ): 7.51 (d, J = 5.54 Hz, 2H), 7.40 (d, J = 5.53 Hz, 2H), 4.14 (s, 6H). ^{13}C NMR (150 MHz, $CDCl_3$, δ): 145.47, 131.40, 129.92, 126.41, 120.22, 61.14. EI-MS (*m/z*): $[M]^+$ calculated for $C_{12}H_{10}O_2S_2$, 250.0122; found, 250.0128. Anal. calculated for $C_{12}H_{10}O_2S_2$: C, 57.57; H, 4.03; found: C, 57.31; H, 3.90.

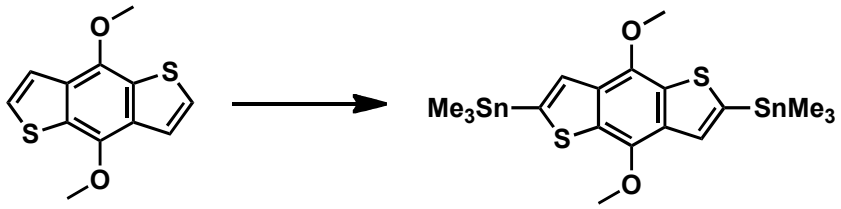

8 **9**

*(4,8-Dimethoxybenzo[1,2-b:4,5-b']dithiophene-2,6-diyl)bis(trimethylstannane) (**9** = **BDT-Me**)*. Compound **8** (976 mg, 3.90 mmol), tetramethylethylenediamine (dried over CaH_2 and vacuum distilled, 1.36 g, 11.70 mmol) and THF (20 mL) were combined in a 50 mL flame-dried flask. The reaction contents were cooled to 0 °C and *n*-butyllithium (3.28 mL of a 2.5 M solution in hexanes, 8.19 mmol) was added to the reaction mixture dropwise. After stirring for 2 h on the melting ice bath, the reaction mixture was cooled to 0 °C and trimethyltin chloride (2.33 g, 11.70 mmol) was added. The reaction contents were stirred for another 12 h at room temperature before being quenched with water (10 mL). The reaction mixture was then extracted with diethyl ether, washed with water, dried over $MgSO_4$, and filtered. Volatiles were removed under reduced pressure, and the crude product was recrystallized (5:1 isopropyl alcohol:acetone) to yield 1.31 g of pale yellow crystals (58 %). ^{1}H NMR (500 MHz, $CDCl_3$, δ): 7.55 (s, 2 H), 4.15 (s, 6 H), 0.45 (s, 18 H). ^{13}C NMR (150 MHz, $CDCl_3$, δ): 144.1, 141.1, 133.7, 132.8, 127.9, 61.0, -8.2. EI-MS (*m/z*): $[M]^+$ calculated for $C_{18}H_{26}O_2S_2Sn_2$, 575.9412; found, 575.9420.

Polymer Synthesis.

Copolymer PTFF. Compound **7** (154 mg, 351 μmol), **F** (135 mg, 343 μmol) and chlorobenzene (4.5 mL) were combined in a 25 mL Schlenk flask and degassed with nitrogen for 25 min. Tris(dibenzylideneacetone)dipalladium(0) (9.68 mg, 10.6 μmol), and tri-*o*-tolylphosphine (12.9 mg, 42.4 μmol) were added to the flask and the reaction mixture was stirred for 36 h at 110 °C. A strong complexing ligand (*N*,*N*-diethyl-2-phenyldiazenecarbothioamide) was added to the reaction mixture to remove residual catalyst before precipitating the reaction contents into methanol (150 mL). The precipitate was filtered through a Soxhlet thimble and purified via Soxhlet extraction for 2 h with methanol, 15 h with hexanes, and was finally collected in chloroform. The chloroform solution was then concentrated under reduced pressure, precipitated into methanol (110 mL) and filtered to yield 105 mg of a dark solid (87 %). SEC analysis: M_n = 1.6 kDa, M_w = 3.1 kDa, PDI = 1.9.

Copolymer PTF2T. Synthesized with the same procedure that was used for **PTFF** except Compound **7** (80.0 mg, 183 μmol) and 2T (87.1 mg, 177 μmol) were copolymerized to yield 37.2 mg of a dark solid (46 %). SEC analysis: M_n = 2.6 kDa, M_w = 3.6 kDa, PDI = 1.4.

Copolymer PTFBDT-Me. Synthesized with the same procedure that was used for **PTFF** except Compound **7** (80.0 mg, 183 μmol) and BDT-Me (102 mg, 177 μmol) were copolymerized to yield 56.1 mg of a dark solid (58 %). Too insoluble in $CHCl_3$ for SEC analysis.

Copolymer PTFBDT-EH. Synthesized with the same procedure that was used for **PTFF** except Compound **7** (8.00 mg, 183 μmol) and BDT-EH (137 mg, 177 μmol) were copolymerized to yield 114 mg of a dark solid (86 %). SEC analysis: M_n = 17 kDa, M_w = 33 kDa, PDI = 2.0.

Copolymer PTFBDT-EHT. Synthesized with the same procedure that was used for **PTFF** except Compound **7** (8.00 mg, 211 μmol) and BDT-EHT (160 mg, 177 μmol) were copolymerized to yield 140 mg of a dark solid (86 %). SEC analysis: M_n = 19 kDa, M_w = 34 kDa, PDI = 1.9.

References

(1) Roncali, J. *Chem. Rev.* **1997**, *97*, 173–205.
(2) Cheng, Y.-J.; Yang, S.-H.; Hsu, C.-S. *Chem. Rev.* **2009**, *109*, 5868–5923.
(3) Douglas, J. D.; Griffini, G.; Holcombe, T. W.; Young, E. P.; Lee, O. P.; Chen, M. S.; Fréchet, J. M. J. *Macromolecules* **2012**, *45*, 4069–4074.
(4) Wudl, F.; Kobayashi, M.; Heeger, A. J. *J. Org. Chem.* **1984**, *49*, 3382–3384.
(5) Brédas, J. L.; Heeger, A. J.; Wudl, F. *J. Chem. Phys.* **1986**, *85*, 4673–4678.
(6) Pomerantz, M.; Gu, X. *Synt. Met.* **1997**, *84*, 243–244.
(7) Neef, C. J.; Brotherston, I. D.; Ferraris, J. P. *Chem. Mater.* **1999**, *11*, 1957–1958.
(8) Lee, K.; Sotzing, G. A. *Macromolecules* **2001**, *34*, 5746–5747.
(9) Chen, H.-Y.; Hou, J.; Zhang, S.; Liang, Y.; Yang, G.; Yang, Y.; Yu, L.; Wu, Y.; Li, G. *Nat. Photon.* **2009**, *3*, 649–653.
(10) He, Z.; Zhong, C.; Huang, X.; Wong, W.-Y.; Wu, H.; Chen, L.; Su, S.; Cao, Y. *Adv. Mater.* **2011**, *23*, 4636–4643.
(11) He, Z.; Zhong, C.; Su, S.; Xu, M.; Wu, H.; Cao, Y. *Nat. Photon.* **2012**, *6*, 591–595.
(12) Lu, L.; Luo, Z.; Xu, T.; Yu, L. *Nano Lett.* **2013**, *13*, 59–64.
(13) Piliego, C.; Holcombe, T. W.; Douglas, J. D.; Woo, C. H.; Beaujuge, P. M.; Fréchet, J. M. J. *J. Am. Chem. Soc.* **2010**, *132*, 7595–7597.
(14) Szarko, J. M.; Guo, J.; Liang, Y.; Lee, B.; Rolczynski, B. S.; Strzalka, J.; Xu, T.; Loser, S.; Marks, T. J.; Yu, L.; Chen, L. X. *Adv. Mater.* **2010**, *22*, 5468–5472.
(15) Woo, C. H.; Beaujuge, P. M.; Holcombe, T. W.; Lee, O. P.; Fréchet, J. M. J. *J. Am. Chem. Soc.* **2010**, *132*, 15547–15549.
(16) Li, Y.; Sonar, P.; Singh, S. P.; Ooi, Z. E.; Lek, E. S. H.; Loh, M. Q. Y. *Phys. Chem. Chem. Phys.* **2012**, *14*, 7162–7169.
(17) Kobilka, B. M.; Hale, B. J.; Ewan, M. D.; Dubrovskiy, A. V.; Nelson, T. L.; Duzhko, V.; Jeffries-EL, M. *Polym. Chem.* **2013**, DOI: 10.1039/c3py00138e.
(18) Yiu, A. T.; Beaujuge, P. M.; Lee, O. P.; Woo, C. H.; Toney, M. F.; Fréchet, J. M. J. *J. Am. Chem. Soc.* **2012**, *134*, 2180–2185.
(19) Peart, P. A.; Repka, L. M.; Tovar, J. D. *Eur. J. Org. Chem.* **2008**, 2193–2206.
(20) Bunz, U. H. F. *Angew. Chem. Int. Ed.* **2010**, *49*, 5037–5040.
(21) Liang, Y.; Feng, D.; Wu, Y.; Tsai, S.-T.; Li, G.; Ray, C.; Yu, L. *J. Am. Chem. Soc.* **2009**, *131*, 7792–7799.
(22) Kumar, A.; Buyukmumcu, Z.; Sotzing, G. A. *Macromolecules* **2006**, *39*, 2723–2725.
(23) Ha, J. S.; Kim, K. H.; Choi, D. H. *J. Am. Chem. Soc.* **2011**, *133*, 10364–10367.
(24) Kumar, A.; Bokria, J. G.; Buyukmumcu, Z.; Dey, T.; Sotzing, G. A. *Macromolecules* **2008**, *41*, 7098–7108.